

**MICROSTRUCTURAL CHARACTERISTICS AND MECHANICAL  
PROPERTIES OF Sn-Ag-Cu SOLDERS WITH MINOR ADDITIONS OF  
Al AND Zn**

**LEONG YEE MEI**

**FACULTY OF ENGINEERING  
UNIVERSITY OF MALAYA  
KUALA LUMPUR**

**2020**

**MICROSTRUCTURAL CHARACTERISTICS AND MECHANICAL  
PROPERTIES OF Sn-Ag-Cu SOLDERS WITH MINOR ADDITIONS OF  
Al AND Zn**

**LEONG YEE MEI**

**THESIS SUBMITTED IN FULFILMENT OF THE  
REQUIREMENTS FOR THE DEGREE OF DOCTOR OF  
PHILOSOPHY**

**FACULTY OF ENGINEERING  
UNIVERSITY OF MALAYA  
KUALA LUMPUR**

**2020**

**UNIVERSITI MALAYA**

**ORIGINAL LITERARY WORK DECLARATION**

Name of Candidate: **LEONG YEE MEI**

Registration/Matric No: **KHA120023**

Name of Degree: **DOCTOR OF PHILOSOPHY**

Title of Project Paper/Research Report/Dissertation/Thesis (“this Work”):

**MICROSTRUCTURAL CHARACTERISTICS AND MECHANICAL  
PROPERTIES OF Sn-Ag-Cu SOLDERS WITH MINOR ADDITIONS OF Al  
AND Zn**

Field of Study: **SOLDER MATERIALS**

I do solemnly and sincerely declare that:

- (1) I am the sole author/writer of this Work;
- (2) This Work is original;
- (3) Any use of any work in which copyright exists was done by way of fair dealing and for permitted purposes and any excerpt or extract from, or reference to or reproduction of any copyright work has been disclosed expressly and sufficiently and the title of the Work and its authorship have been acknowledged in this Work;
- (4) I do not have any actual knowledge nor do I ought reasonably to know that the making of this work constitutes an infringement of any copyright work;
- (5) I hereby assign all and every rights in the copyright to this Work to the University of Malaya (“UM”), who henceforth shall be owner of the copyright in this Work and that any reproduction or use in any form or by any means whatsoever is prohibited without the written consent of UM having been first had and obtained;
- (6) I am fully aware that if in the course of making this Work I have infringed any copyright whether intentionally or otherwise, I may be subject to legal action or any other action as may be determined by UM.

Candidate’s Signature

Date

Subscribed and solemnly declared before,

Witness’s Signature

Date

Name:

Designation:

# MICROSTRUCTURAL CHARACTERISTICS AND MECHANICAL PROPERTIES OF Sn-Ag-Cu SOLDERS WITH MINOR ADDITIONS OF Al AND Zn

## ABSTRACT

Driven by the recent trend towards miniaturization of lead free electronic products, researchers are putting immense efforts to improve the properties and reliability of Sn based solders. Recently, much interest has been shown on low silver (Ag) content solder SAC 105 (Sn-1.0Ag-0.5Cu) solder because of economic reasons and improvement of impact resistance as compared to SAC387(Sn-3.8Ag-0.7Ag). The present work investigates the effect of minor (0.1-0.5wt.%) Aluminium (Al) and Zinc (Zn) addition to SAC105 on the bulk and interfacial structure between solder and copper substrate during reflow and after thermal aging, the mechanical properties of the solder joint and the nano-mechanical properties of IMC formed. Al and Zn have been chosen as they have shown promising results in improving the solder microstructure and mechanical properties from the previous studies. DSC was used to determine the effect of melting characteristics of SAC105 with addition of minor Al or Zn solder. XRD, FESEM, EPMA were used to evaluate the IMC phases and concentration of minor alloying element prior to the shear test and nanoindentation test. Nanoindentation was used to evaluate the mechanical properties of bulk and IMC formed in the solder. Minor addition of Al up to 0.5% promoted formation of small, equiaxed  $\text{Cu}_3\text{Al}$  intermetallic particle in the bulk microstructure, which exhibited much higher hardness and modulus as compared to  $\text{Cu}_6\text{Sn}_5$  and  $\beta\text{-Sn}$ . On the other hand, minor addition of Zn up to 0.5 % did not lead to the formation Cu-Zn compound, but Zn dissolved in Cu-Sn IMC and formed  $\text{Cu}_6(\text{Sn,Zn})_5$ . It was found that Zn tends to accumulate at the edge of solder/

IMC and especially at the IMC/ Cu interface. Results show that the minor addition of Al and Zn does not alter the morphology of the interfacial intermetallic compounds, but they substantially suppress the growth of the interfacial IMC during reflow and after aging. It is suggested that both Al and Zn exert their influence with different mechanism. Al exerts its influence by lowering the activity of reacting species by its presence at the solder/IMC interface. It was suggested Zn exerts its influence the synergy effect of stabilizing  $\text{Cu}_6(\text{Sn,Zn})_5$  and hindering the flow of reacting species at the solder/IMC and IMC/Cu interface. Nanoindentation results showed that with the addition of Zn, the hardness value  $\text{Cu}_6(\text{Sn,Zn})_5$  of has increased and creep performance of SAC+ Zn in the bulk has improved in comparison to SAC105. Shear strengths for samples with addition of Al and Zn have decreased in comparison to SAC 105 after reflow. Failure mode and mechanisms of SAC 105 and SAC + X (X= Al or Zn) are discussed and compared.

# MIKROSTRUKTUR DAN SIFAT MEKANIKAL Sn-Ag-Cu DENGAN PENAMBAHAN KECIL Al DAN Zn

## ABSTRAK

Didorong oleh trend ke arah pengecilan produk elektronik yang tidak mengandungi plumbum (Pb), para penyelidik telah berusaha untuk meningkatkan sifat-sifat dan kebolehpercayaan semua pateri berasaskan tin (Sn). Baru-baru ini, trend pateri telah ditunjukkan pada pateri yang mengandungi kandungan perak (Ag) yang rendah, contohnya, pateri SAC105 (Sn-1.0Ag-0.5Cu) pateri kerana disebabkan harga perak yang mahal dan perendahan perak juga meningkatkan ketahanan impak berbanding dengan pateri SAC387 (Sn-3.8Ag-0.7Ag). Kajian ini menyiasatkan kesan penambahan sedikit aluminium (Al) dan zink (Zn) terhadap nano-mekanik IMC dan struktur antara muka pateri SAC dan Cu substrat tembaga semasa reflow. Al dan Zn telah dipilih kerana ia telah menunjukkan hasil yang memberangsangkan dalam meningkatkan mikrostruktur pateri dan sifat-sifat mekanik dari kajian sebelum ini. DSC telah digunakan untuk menentukan kesan elemen elemen yang ditambah terhadap ciri-ciri peleburan SAC105 pateri. XRD, FESEM, FE-EPMA digunakan untuk menilai fasa IMC dan kepekatan unsur pengalioian kecil di IMC sebelum ujian nanoindentation itu. Nanoindenter telah digunakan untuk menilai sifat-sifat mekanik IMC ditubuhkan pada pateri. Wujudnya partikel Cu-Al baru di SAC+Al dan ia dikenal pasti sebagai  $\text{Cu}_3\text{Al}$ .  $\text{Cu}_3\text{Al}$  terbentuk dekat permukaan / tepi pateri dan mempamerkan kekerasan dan modulus yang lebih tinggi berbanding dengan  $\text{Cu}_6\text{Sn}_5$  dan  $\beta\text{-Sn}$ . Sebaliknya, penambahan kecil Zn sehingga 0.5% tidak menunjukkan pembentukan sebatian Cu-Zn, tetapi Zn dilarutkan dalam Cu-Sn IMC dan membentuk  $\text{Cu}_6(\text{Sn}, \text{Zn})_5$ . Selain itu, Zn atom di dalam  $\text{Cu}_6(\text{Sn}, \text{Zn})_5$  jugak cenderung untuk mengumpul di pinggir solder / IMC

dan terutamanya di antara muka IMC/Cu. Keputusan menunjukkan bahawa penambahan kecil Al dan Zn tidak mengubah morfologi IMC yang terbentuk di antara pateri dengan substrat, tetapi berkesan dalam menghalang pertumbuhan IMC di antara muka. Adalah dicadangkan bahawa Al dan Zn menggunakan pengaruh mereka dengan mekanism yang berbeza. Al menguatkan pengaruhnya dengan menurunkan aktiviti spesies yang bertindak balas dengan kehadirannya di antara muka pateri / IMC. Zn mengenakan pengaruhnya dengan menstabilkan  $\text{Cu}_6(\text{Sn}, \text{Zn})_5$  dan menghalang aliran spesies yang bertindak balas pada pateri/IMC dan IMC/Cu antaramuka. Hasil nano-indentasi menunjukkan bahawa dengan penambahan Zn, nilai kekerasan  $\text{Cu}_6(\text{Sn}, \text{Zn})_5$  telah meningkat dan prestasi 'creep' SAC+ Zn di pateri telah bertambah baik berbanding dengan SAC105. Kekuatan 'Shear' untuk sampel dengan penambahan Al dan Zn telah berkurang berbanding dengan SAC105 selepas reflow. Mod kegagalan dan mekanisme SAC 105 dan SAC + X dibincangkan dan dibandingkan.

## ACKNOWLEDGEMENTS

This thesis becomes a reality with the kind supports and help from many individuals. I would like to extend my sincere thanks to all of them.

First and foremost, I would like to express my deepest appreciation and gratitude to my supervisor, Prof. Dr. A. S. M. A. Haseeb from Department of Mechanical Engineering, University of Malaya. I deeply appreciate his precious time to supervise, his guidance and supports throughout my study. It was my honour and it has been a great pleasure working under his research group. I would like to give special thanks to Prof. Dr. Hiroshi Nishikawa and Dr. Omid Mokhtari from Joining and Welding Research Institutes, Osaka University, Japan for providing electron probe micro-analyzer and transmission electron microscope facility. I greatly appreciate their warm welcome and useful insights during my short visit in Japan.

I would like to thank my fellow research group members, Dr. Arafat Mahmood, Dr. Tharsika Thabothanayakam, Dr. Goh Yingxin, Ms. Chia Pay Ying and Mr. Sujan Kumer Ghosh for helping in miscellaneous research works. I am grateful for their kind assistance and valuable input into my research. Special thanks to all science officers and lab technicians who helped to perform tests and analyses, particularly Mr. Mohd Nazarul Zaman for FESEM and EDX analysis.

I would also like to thank the Malaysian Ministry of Higher Education and University of Malaya for the funding for this project and providing financial support throughout the period of my study. Last but not least, I wish to thank my family members and friends for their unconditional love and encouragement to complete my study.

## TABLE OF CONTENT

Title Page.....	i
Original Literacy Work Declaration Form.....	ii
Abstract.....	iii
Abstrak.....	v
Acknowledgement.....	vii
Table of Contents.....	viii
List of Figures.....	xii
Lists of Tables.....	xvi
List of Symbols and Abbreviations.....	xvii
CHAPTER 1: INTRODUCTION.....	1
1.1    Introduction.....	1
1.2    Objectives.....	5
1.3    Scope and outline of work.....	5
CHAPTER 2: LITERATURE REVIEW.....	6
2.1    Introduction.....	6
2.2    Main drawbacks of Sn-Ag-Cu based lead free solders.....	8
2.3    Thermodynamics properties of SAC solder.....	13
2.3.1 $\beta$ Sn.....	13
2.3.2 Cu.....	14

2.3.3	Sn-Ag.....	16
2.3.4	Sn-Ag-Cu.....	17
2.3.5	Nucleation and Solidification Behavior.....	20
2.4	Interfacial reaction between Sn and Cu.....	22
2.4.1	Liquid state reaction.....	22
2.4.2	Solid State Reaction.....	24
2.5	Effect of fourth alloying element on lead-free solder.....	25
2.5.1	Al.....	30
2.5.2	Zn.....	34
2.6	Mechanical Properties.....	36
2.6.1	Effect of fourth alloying element on mechanical properties of SAC/Cu solder joints.....	37
2.6.2	Nanomechanical properties.....	39
2.6.3	Effect of additional element on the nanomechanical properties of Cu- Sn intermettalic.....	41
2.7	Summary.....	44
CHAPTER 3: RESEARCH METHODOLOGY.....		46
3.1	Introduction.....	46
3.2	Solder joint sample preparation.....	47
3.3	Sample characterization.....	51
3.3.1	Differential scanning calorimeter (DSC).....	51
3.3.2	X-ray diffraction (XRD).....	53

3.3.3	Field-emission Scanning Electron Microscopy (FESEM) equipped with Energy dispersive X-ray spectroscope (EDS).....	53
3.3.4	Field emission electron probe for micro-analysis (FE-EPMA).....	54
3.4	Nanoindentation.....	55
3.4.1	Hardness and Modulus.....	55
3.4.2	Creep.....	57
3.5	Shear test.....	57
CHAPTER 4: RESULTS AND DISCUSSIONS.....		59
4.1	Thermal Analysis.....	59
4.1.1	Melting and Solidification Behaviour of SAC +X.....	59
4.2	Microstructure Analysis.....	64
4.2.1	Microstructure Characterization of As-received Solder.....	65
4.2.2	Microstructure of Bulk Solder After Reflow and Thermal Aging for 1 Month.....	65
	(a) Field Emission Scanning Electron Microscope (FESEM)- Energy dispersive X-ray (EDX) spectroscopy.....	67
	(b) XRD (X- Ray Diffraction).....	74
	(c) TEM-EDS.....	76
4.2.3	Microstructure of Interfacial IMC (After Reflow and After Thermal Aging).....	77
	(a) FESEM.....	
	(b) Wavelength-Dispersive X-Ray Spectroscopy (WDS).....	83

4.2.4	Top View of Interfacial IMC .....	85
4.2.5	Discussions of Thermal and Microstructure Properties of SAC + X...89	
	(a) Thermal Properties.....	89
	(b) Bulk microstructure .....	91
	(c) Interfacial reaction .....	92
4.2.6	Summary of Thermal Properties and Microstructure of SAC+X.....	96
4.3	Mechanical Properties .....	97
4.3.1	Vickers Hardness Test .....	97
4.3.2	Nanoindentation on Bulk solder and IMC.....	98
4.3.3	Nanoindentation Creep on Bulk solder and IMC.....	104
4.3.4	Shear strength .....	107
	4.3.4.1 Shear Fracture Analysis (as -reflowed sample).....	108
	4.3.4.2 Shear Fracture Analysis (Aging at 150 °C up to 1 month) .....	114
4.3.5	Discussions of Mechanical Properties of SAC + X .....	118
CHAPTER 5: CONCLUSION AND RECOMMENDATION.....		127
5.1	Conclusion.....	127
	5.1.1 Effect of minor addition of Al on SAC105.....	127
	5.1.2 Effect of minor addition of Zn on SAC105 .....	128
5.2	Recommendation.....	129
REFERENCES.....		131
List of Publications and Papers Presented .....		142

## LIST OF FIGURES

### CHAPTER 2

Figure 2.1 shows large $\text{Cu}_6\text{Sn}_5$ and plate-like $\text{Ag}_3\text{Sn}$ IMC found in SAC alloy.....	10
Figure 2.2 shows that SnPb perform better in drop impact test than SAC solder after 250 thermal cycle.....	11
Figure 2.3 Sn-Cu phase diagram.....	15
Figure 2.4 The Sn- rich portion of Sn-Cu phase diagram.....	15
Figure 2.5 Phase diagram of Sn-Ag system.....	17
Figure 2.6 Calculated liquid surface at high Sn region of SAC ternary phase diagram..	18
Figure 2.7 Comparison of calculated fraction solid as a function of temperature for five different Sn-Ag-Cu alloys.....	19
Figure 2.8 A Darken–Gurry ellipse plot with Cu as the central atom, and electronegativity elements were plotted against the element atomic radius. The elements within the ellipse are likely to have high solubility in Cu (up to 5 at.%).....	20

### CHAPTER 3

Figure 3.1 Flow Chart of experimental work.....	46
Figure 3.2 Schematic diagram of SAC+X solder joint before it was subjected to reflow.....	50
Figure 3.3 Reflow soldering profile.....	50
Figure 3.4 Schematic DSC plots showing error induced by using extrapolation method for onset determination.....	52
Figure 3.5 Image and schematic diagram of the shear test setup.....	58

### CHAPTER 4

Figure 4.1 shows the (a) endothermic and (b) exothermic DSC curves of SAC105, SAC +0.1Al, SAC +0.3Al and SAC +0.5Al.....	61
Figure 4.2 shows the (a) endothermic and (b) exothermic DSC curve of SAC105, SAC +0.1Zn, SAC +0.3Zn and SAC +0.5Zn.....	63

Figure 4.3 Cross sectioned SEM micrographs of as-received SAC +X.....	66
Figure 4.4 Cross-sectioned FESEM image of SAC +X after 1 x reflow.....	68
Figure 4.5 (a) Optical microscope cross sectional images SAC105+0.5Al near top surface of the solder after 1 × reflow and (b) FESEM images of equiaxed but faceted IMCs found at cross-sectioned of SAC105+0.5Al.....	69
Figure 4.6 Cross-sectioned image of SAC +X after 1 month aging.....	70
Figure 4.7 The ‘needle-like’ IMC found in bulk microstructure of SAC + 0.5 Al under high magnification.....	71
Figure 4.8 Crossed sectional FESEM images of (a) equiaxed IMC and (b) needle-like IMC found in SAC+0.5Al after 1 month aging. (c) EDX spectrum of equiaxed and needle-like IMC.....	72
Figure 4.9 EDS line scan across equiaxed IMCs in SAC105+0.5Al after reflow.....	73
Figure 4.10 (a) Cross-sectioned FESEM image of SAC105+0.5Al after reflow. Elemental maps for the constituent elements: (b) Al; (c) Cu; (d) Sn; and (e) Ag.....	73
Figure 4.11 (a) Cross-sectioned FESEM image of SAC105+0.5Al after 1 month thermal aging. Elemental maps for the constituent elements: (b) Al; (c) Cu; (d) Sn and (e) Ag.....	74
Figure 4.12 XRD diffractogram of SAC and SAC+0.5Al.....	75
Figure 4.13 Cu-Al phase diagram.....	76
Figure 4.14 (a) TEM image of FIB sliced Cu-Al IMC. Elemental maps for the constituent elements: (b) Al, (c) Cu, (d) Sn.....	78
Figure 4.15 Cross-sectioned image at interfacial of SAC+X/Cu after 1 x reflow. ....	79
Figure 4.16 Variation of Cu <sub>6</sub> Sn <sub>5</sub> thickness with SAC + X samples after reflow.....	79
Figure 4.17 FESEM and EDX spectrum of interfacial Cu <sub>6</sub> Sn <sub>5</sub> of (a) SAC+Al and (b) SAC+Zn samples.....	80
Figure 4.18 Cross-sectioned image at interfacial of SAC+X/Cu after 1 month aging... ..	82
Figure 4.19 Variation of Cu <sub>6</sub> Sn <sub>5</sub> and Cu <sub>3</sub> Sn thickness with SAC + X samples after 1 month aging.....	83
Figure 4.20 Zn distribution maps at the solder/ Cu interface in SAC +0.1Zn, SAC+0.3Zn and SAC+0.5Zn after aging 0hr, 168hr and 720 hr .....	84

Figure 4.21 Variation of Zn composition in $\text{Cu}_6(\text{Zn, Sn})_5$ in SAC +0.1Zn, SAC+0.3Zn and SAC+0.5Zn after aging at 0hr, 168hr and 720 hr.....	85
Figure 4.22 (a) Top view image of deeply etched SAC and SAC105+0.5Al after 1x reflow.....	86
Figure 4.23 (a) Top view image of deeply etched SAC105+0.5Al after 1x reflow. Elemental maps for the constituent elements: (b) Al, (c) Cu and (d) Ag.....	87
Figure 4.24 FESEM top view image of IMC a) SAC105, b) SAC +0.1Zn, c) SAC+0.3Zn and d) SAC+0.5Zn after reflow. ....	88
Figure 4.25 Number of top $\text{Cu}_6\text{Sn}_5$ grains in $10,000\mu\text{m}^2$ in SAC105, SAC+0.1Zn, SAC+0.3Zn and SAC+0.5Zn.....	88
Figure 4.26 Variation of Vickers hardness in as received SAC+solders.....	98
Figure 4.27 (a) Optical micrograph of the indentation arrays on the Sn an eutectic region of bulk solder; (b) Scanning probe microscopy image of $\text{Cu}_6\text{Sn}_5$ at the solder/Cu interface after indentation; (c) Scanning probe microscopy image of $\text{Cu}_3\text{Al}$ in the bulk solder after indentati.....	100
Figure 4.28 Load vs displacement plot for indentations performed on bulk solder, $\text{Cu}_6\text{Sn}_5$ and $\text{Cu}_3\text{Al}$ in SAC +X.....	102
Figure 4.29 SPM images of residual indents and the measured height profile for (a) Sn and (b) $\text{Cu}_6\text{Sn}_5$ .....	102
Figure 4.30 Average time-displacement curves for SAC, SAC+0.1Zn and SAC+0.5Zn.....	106
Figure 4.31 Shear strength of SAC+ X after thermal aging at 150 °C at 0hr(as reflow), 168hr(1 week aging) and 720 hr(1 month aging).....	107
Figure 4.32 (a) Top view FESEM micrograph of shear fracture of (a,b)as reflowed SAC; (c) Cross sectional FESEM micrograph of shear fracture of as reflowed SAC105.....	109
Figure 4.33 Top view FESEM micrograph of shear fracture of (a) top sample, (b) bottom sample;(c) shear fracture on Sn region; (d) fracture region exposing interfacial IMC region and (e) Cross sectional FESEM micrograph of shear fracture of as-reflowed SAC+0.1Al.....	111
Figure 4.34 EDX analysis on the flux residue at the boundary of SAC +0.5Al solders joints.....	112
Figure 4.35 Top view FESEM micrograph of shear fracture of SAC+0.5Al.....	112
Figure 4.36 Cross sectional FESEM micrograph of shear fracture of as-reflowed SAC+0.1Zn.....	113

Figure 4.37 Top view FESEM micrograph of shear fracture of (a)Sn region and b)voids after 1 month aging.....	114
Figure 4.38 (a,b) Top view FESEM micrograph of shear fracture of SAC+0.5Al after 1 month aging. (c) Magnified FESEM image of red circled area and elemental maps for the constituent elements: (d) Al; (e) Cu; (f) Sn.....	116
Figure 4.39 Top view FESEM micrograph of shear fracture of (a) $Cu_6(Sn, Zn)_5$ , (b) $Cu_3(Sn,Zn)$ , (c)Sn region and (d) Cross sectional FESEM micrograph of shear fracture SAC+0.1Zn after aging for 720hr.....	118
Figure 4.40 Illustration of Vickers hardness indentation on (a) SAC, (b) SAC+0.5Al and (c)SAC+0.5Zn.....	121
Figure 4.41 Illustration of microhardness indentation on (a) SAC and (b) SAC+0.5Zn.....	122

University of Malaya

## LIST OF TABLES

### CHAPTER 2

Table 2.1 Criteria for acceptable Pb free solders.....	7
Table 2.2 Advantages and disadvantages / problem of SAC solder.....	12
Table 2.3 Summary of lead free solders with addition of Al as minor alloying element that have been studied so far.....	31
Table 2.4 Effects of minor alloying element on the mechanical properties of SAC solder matrix.....	37
Table 2.5 Elastic modulus and hardness of Sn, eutectic, Cu, Cu <sub>6</sub> Sn <sub>5</sub> , and Cu <sub>3</sub> Sn phase in SAC/Cu or SA/Cu.....	40
Table 2.6 Average values of elastic modulus and hardness of Cu-Sn IMC with and without addition of the fourth alloying element under various condition solder/Cu (after reflow, after aging, (001) and (100) crystal plane).....	43
Table 2.7 Summary of effect of fourth alloying element on Cu-Sn IMC.....	44

### CHAPTER 3

Table 3.1 Alloy Compositions.....	48
-----------------------------------	----

### CHAPTER 4

Table 4.1 shows the onset of melting, onset of solidification and undercooling of SAC 105, and SAC +X(X= 0.1, 0.3, 0.5 % Al or Zn).....	64
Table 4.2 Hardness and modulus of bulk solder and Cu <sub>6</sub> Sn <sub>5</sub> IMC in SAC105, SAC +0.1Zn, SAC+0.3Zn and SAC+0.5Zn after 1x reflow.....	103
Table 4.3 Instantaneous, total, time-dependent displacement of bulk solder in SAC, SAC+0.1Zn and SAC+0.5Zn.....	106
Table 4.4 Hardness testing scales defined by ISO 145771.....	119
Table 4.5 Summary of the shear fracture analysis of SAC+ X after reflow and after 1 month aging.....	124

## LIST OF SYMBOLS AND ABBREVIATIONS

Symbol/Abbreviation	Description
%	Percentage
Ag	Silver
Al	Aluminium
Bi	Bismuth
Cm	Centimeter
Ce	Cerium
Cu	Copper
g	Gram
h	Hour
IMC	Intermetallic Compounds
In	Indium
iNEMI	International Electronics Manufacturing Initiative
kg	Kilogram
M	Metal/ Molar concentration
o	Degree
Pb	Lead
Pb-free	Lead-free
Pt	Platinum
RoHS	Restriction of Hazardous Substances
Sn	Tin
Ti	Titanium
US\$	United States Dollar
wt.%	Weight Percentage
Zn	Zinc
µm	Micrometer
FESEM	Field-emission scanning electron microscope
EDX	Energy dispersive X-ray spectroscopy
DSC	Differential scanning calorimetry
XRD	X-Ray Diffraction

## CHAPTER 1: INTRODUCTION

### 1.1 Introduction

Electronics devices are constantly advancing towards miniaturization, high integration and being multifunctional. This puts forward higher requirement on solder joints in electronic packaging. Solder joint reliability issues are mainly due to geometry factor and microstructure factor (Qin et al., 2015). Thus, studies on materials development to address these issues are constantly facing changing targets. Especially when lead (Pb) free-concept came into the picture in early 1990, owing to the toxicity of lead which can lead to health and environment hazards, studies on lead free solders have been booming since then. At that time, SnPb solders were widely used in the electronic industry, thus limitation on lead usage has led to a massive search for suitable replacement. Sn-Ag-Cu (SAC) solder alloy is recommended as one of the favorable lead-free replacement for SnPb by the International Electronics Manufacturing Initiative (iNEMI) (Bradle et al., 2007).

Extensive research and development have been done on the SAC solder and a number of reliability issues of SAC have been reported. In comparison with conventional tin-lead solder, SAC solder exhibits characteristics, like large Sn undercooling during solidification, large  $\text{Ag}_3\text{Sn}$  plate formation, rapid interfacial reaction during reflow or thermal aging and fast diffusion of nickel (Ni), copper (Cu), silver (Ag) solute atoms along the c-axis of  $\beta$ -Sn and etc. (Subramaniam, 2007). These characteristics have implications on the solder reliability issues, such as, fatigue crack growth along large  $\text{Ag}_3\text{Sn}$  plate, excessive Cu consumption, void formation, lower drop impact resistance failure, electromigration etc. (Subramaniam, 2007). As an attempt to improve the reliability of SAC solder, researchers

have tried to modify the composition of SAC based solders by adding a minor alloying element.

By about 2005, SAC305 (Sn-3.0Ag-0.5Cu) was largely used in the electronic industry because of its off eutectic composition and has a wider “pasty range.” Due to its wider pasty range compared to SAC387, it contains higher solid mass fraction during melting and this creates slower wetting speed, and hence reducing tombstoning (Bastow & Jensen, 2009). SAC305 also saved costs by involving less Ag (as compared to eutectic Sn-3.8Ag-0.7Cu (SAC387)). But by the year 2011, silver price has increased up to \$40/oz., four times its price as of year 2005. As a logical result, prices of solder rose as well. Although silver comprises a small percentage of alloy composition in solder alloy, however, its value comprises a significant percentage of the value of solder alloy. Researchers then had to look for alternatives, low or no silver solder alloys.

Therefore, Sn-1.0Ag-0.5Cu (SAC105) has drawn much attention in recent years not only due to its low Ag-content, but also due to its excellent drop performance as compared to SAC305 and SAC387 (Kang et. al, 2004; Brook & Lasky, 2012). However, despite its cost saving and excellence drop performance, it has some drawbacks as well. Due to its non-eutectic composition, its liquidus temperature is rather high, thus need to be reflow at higher temperature (Kang et. al; 2004). It also has lower shear strength and poor thermal cycling performance as compared to SAC305 and SAC387 (Subramaniam 2007). These drawbacks have prompted an exploration in modifying the solder content by adding fourth micro-alloying elements.

There are numerous studies on the minor fourth alloying element into SAC solders, such as Ni (Nogita et al. 2010), Co (Anderson et al., 2006), Mn (Szurdan, 2019), Zn (Kang et al. 2005) , Ti (Chuang et al., 2012), Ce (Zhao et al. 2007), In (Fallahi et al., 2012), Al

(Anderson et al., 2009), Fe (Fallahi et al., 2012), Bi (Hodulova et al., 2018). It has been reported that these dopants can improve properties like wetting, mechanical properties, and reliability of the SAC solder, and yet maintain similar reflow profile (Brook & Lasky, 2012).

Among all the minor fourth alloying elements, additions of Al and Zn were reported to reduce undercooling and enhance microstructure and mechanical properties of SAC solder (SAC solders with Ag  $\geq$  3 %). The addition of Al was found to reduce the undercooling of Sn-3.5Ag-0.95Cu (SAC3595) solder (Anderson et al. 2009). With Al additions, ambiguous new Cu-Al IMC were found in the solder and no comprehensive research has been done on the effect of minor Al addition on the interfacial reaction of SAC solder. Study shows that the addition of 0.1 % Al improved the tensile strength and exhibit ductile failure. However, higher Al content e.g., up to 0.5 % reduced the tensile strength and exhibit intergranular fracture. On the other hand, addition of Zn was reported to reduce the undercooling of SAC 305 (Kang et al., 2006). Zn was reported to hinder the growth of interfacial IMC significantly after isothermal aging (Kotadia et al., 2012; Kang et al., 2012). Zn was also reported to reduce void formations at the IMC/Cu interface (Kang et. al, 2012). Anderson et al. (2009) reported that the addition of 0.1 % Zn to SAC3595 improved the impact strength after reflow. Besides, SAC3595+0.1Zn only lost 3 % of the impact strength after isothermal aging for 1000 hr at 150 °C.

So far, most of the studies on the additions of fourth alloying elements have used SAC 305 or SAC with higher Ag % ( $\geq$ 3). Hence, this study aims at investigating the additions of Al or Zn as minor alloying element into SAC105. SAC105 was selected due to its lower silver content which provides lower cost and good impact resistance. Al and Zn were selected due to their reports as mentioned above. In this study, thermal analysis,

microstructure and mechanical properties were studied upon additions of Al and Zn as minor alloying element into SAC105. The microstructure study was divided into bulk microstructure and interfacial reaction at the solder/ Cu interface. Al and Zn were expected to exert their influence on SAC microstructure in a different mechanism as they were both very different in terms of solubility in Cu-Sn IMC ( $\text{Cu}_6\text{Sn}_5$ ,  $\text{Cu}_3\text{Sn}$ ). Al has no solubility in both Cu-Sn IMC, while Zn was reported to have significant solubility in both Cu-Sn IMCs (Chou & Chen, 2006). Mechanical properties of the solder were characterized in bulk microstructure (shear, hardness, Young's modulus creep) and IMC (hardness, Young's Modulus, creep) at the solder/substrate interface. Shear properties were investigated in this study because shear test is one of the important mechanical reliability tests to be considered in electronic packaging due to electronic devices being subjected to vibrations, shocks and loading from different directions. Besides that, in the studies of mechanical properties of SAC, fractures were occurred either at the (i) bulk microstructure, (ii) solder/IMC interface (iii) across the IMC, or (iv) combinations of the 3 above (Huang et. al, 2013). Thus, in order to have a better understanding in the elastic–plastic properties and creep behaviour of SAC solders at microscale, it is vital to characterize the hardness, modulus and creep properties of the solder matrix and IMC. Moreover, the interrelationships between the mechanical properties of bulk solder and IMC with the fracture mode for SAC+X (X= Al, Zn) joints are yet to be reported in the literature. Thus, in this study, the effects of fourth alloying element (Al, Zn) on the microstructure of SAC105, mechanical properties in the bulk and IMC, shear deformation behavior of the joints and those interrelationships mentioned above were investigated.

## 1.2 Objectives

The objectives for this works are as follow:

1. To characterize the microstructure of SAC105+X (X= 0.1-0.5wt % Al, Zn) solder joints on Cu substrate after reflow and after thermal aging.
2. To investigate the mechanical properties (hardness, modulus, creep) of bulk solder and interfacial IMC formed at the solder joints in SAC105+X (X= 0.1-0.5wt % Al, Zn).
3. To study the shear behaviour of SAC+X (X= 0.1-0.5wt % Al, Zn) solder joints.
4. To correlate the microstructure of solder joints and their mechanical behavior.

## 1.3 Scope and outline of work

The thesis contains five chapters. Chapter 1 provides a brief introduction and objectives of the study. Chapter 2 provides a comprehensive literature review on drawbacks of SAC based lead free solders, thermodynamic properties of SAC solder, interfacial reaction between Sn and Cu and effect of fourth alloying element on SAC solder. Chapter 3 provides detailed procedures in sample preparation and tests carried out in this study.

Chapter 4 presents the main findings of this work. This chapter is divided into 3 main subchapters which are i) Thermal Analysis, ii) Microstructure Analysis, and iii) Mechanical Properties. Melting and solidification behavior of SAC+X solders are studied. Effects of Al and Zn on the microstructure of SAC after reflow and aging are investigated. Lastly, the effects of Al and Zn on the bulk and interfacial IMC are studied. The interrelationship between solder microstructure, mechanical properties and fracture mode is investigated. Finally, Chapter 5 summarizes the result of this thesis work and recommends future work that can be carried out to bring the research on effect of Al and Zn on SAC105 to the fore.

## CHAPTER 2: LITERATURE REVIEW

### 2.1 Introduction

Solders play a very crucial role in the electronic assemblies. They are interconnect materials in electronic packaging, where they are used to join chips and components together electrically and mechanically to provide functional circuit. For decades, leads (Pb) have been a key element in solder and solder pastes, though its toxicity has been long known. Over the years before the bans of lead in 2006, industrial and academics researchers have started research on the lead free solder performance and reliability measures of lead free solders. When RoHS, (Restriction of Hazardous Substances Directive) took effect in 2006 restricting the toxic material usage in electrical or electronic products, the exploration for a Pb free replacement for lead based solders has turn into reality, and research on lead free solder has instantly turned into an important topic in electronic packaging.

In order to remove Pb from solder, we must first understand the role played by Pb in Sn-Pb solder. There are a few main aspects on why Pb played an important role in soldering. First, eutectic temperature of Sn-Pb solder is low ( $T_m=183\text{ }^\circ\text{C}$ ), so the reflow temperature used is low ( $200\text{ }^\circ\text{C}$ ) (Fecht et al., 1989). Secondly, Pb provide ductility to Sn-Pb solder (Zeng & Tu, 2002). Thirdly, Pb lowered the interfacial and surface energy of the solder, and thus has a very good wettability on Cu substrate (wetting angle =  $11\text{ }^\circ$ ). In summary, lead containing solders have been historically widely used because of its low melting point, ease of manufacture and good wetting properties which offered good and reliable joints (Noor, 2016; Dusek et. al, 2011). Thus, during the initial transition to lead free solder, finding a lead free solder replacement is a problem face by many manufacturers, as not only the solders need to be identified, tested and suitable for used, but also the well-established manufacturing process, for examples, manufacturing temperature need to be changed and

the equipment for a lead-free process needs to be purchased. Since the use of Sn-Pb solder was very well established, thus during the search for lead free replacement for Sn-Pb solder, properties of Sn-Pb eutectic solder is used as the guideline for the main design alloy criteria. Some of the few primary criteria based on National Center for Manufacturing Sciences (NCMS) Pb-Free Solder Project in developing acceptable Pb free solders are shown in the table below:

**Table 2.1** Criteria for acceptable Pb free solders (NCMS Lead-free Solder Project Final Report, 1997)

<b>Property</b>	<b>Acceptable level</b>
Toxicity	Considerably lower than that of Pb
Supply	Sufficient supply for 80% conversion
Liquidus Temperature	< 225 °C. During assembly, 240 °C is the maximum acceptable component temperature.
Pastry range	< 30 C
Wettability	$F_{\max} > 300 \mu\text{N}$ $t_0 < 0.6 \text{ s}$ $t_{2/3} < 1 \text{ s}$
Thermomechanical fatigue	Usually > 50 %
Coefficient of Thermal Expansion (CTE)	< $2.9 \times 10^{-5} \text{ }^\circ\text{C}$
Creep	> 3.4 MPa
Elongation	>> 10 %

Based on those criteria mentioned above, iNEMI has recommend SAC alloys as the most promising lead free replacement for Sn-Pb. After more than a decade since the

RoHS's restriction guide, many tin-based lead free solders are commercially available in the market now, SAC solder have been developed as a world widely used general-purpose lead-free alloy. The transition of lead free solder is not a smooth ride. Many challenges surfaced along the way in difference aspects, and reliability issues are one of the challenges that faced by the researchers. Thus, in recent years, a great deal of research has been done to optimize and improve the properties of SAC solders by adding minor alloying element. In the following sections, problems encountered in lead solders and reported findings of 4<sup>th</sup> alloying elements are discussed.

## **2.2 Main drawbacks of Sn-Ag-Cu based lead free solders**

As mentioned previously, Pb has played an important role on the conventional Sn-Pb solder. Thus, it is important to make sure that the properties of the lead free solder are comparable or better than Sn-Pb solder. The perfect drop-in replacement for SnPb research is still on the search. Many eutectics Sn-based alloys have been tried, and Sn-Ag-Cu solder has emerged as the primary lead free solder. Eutectic SAC solder has proved to be a favored replacement for Sn-Pb solders due to its relatively low melting point (as compared to other lead free solder), wetting ability and adequate mechanical properties. Wettability is an important criteria in evaluating a solder because it affects the bonding quality between solder and substrate, and in turn affect the electrical properties, thermal and mechanical properties of solder. The eutectic SAC alloy has been reported to wet and form good quality joint on Cu substrate (Bath, 2007). In terms of mechanical properties, though eutectic SAC solder has lower bending test reliability than SnPb solder, it has been reported that SAC solder perform better than SnPb in other tests, such as tensile strength, shear test, and creep

(Subramaniam, 2012). Although there are many aspects of SAC solders that are acceptable or better than Sn-Pb solders, these solders still have a number of drawbacks.

One of the problems associated with lead free solder is its melting profile as compared to Sn-Pb. The melting temperature ternary eutectic SAC solder ( $T_m=217\text{ }^\circ\text{C}$ ), is about  $30\text{ }^\circ\text{C}$  higher than the conventional Sn60/Pb40 and Sn63/Pb37 ( $T_m=183\text{ }^\circ\text{C}$ ) (Moon et al., 2000, Fecht et al., 1989). As seen in table 2.1, solder with recommended liquidus temperature less than  $225\text{ }^\circ\text{C}$  and a narrow pasty range of no more than  $30\text{ }^\circ\text{C}$  were the criteria recommended by manufacturers due to constraints on processing and materials (Zeng & Tu, 2002). Though the melting characteristics of eutectic or some near eutectic SAC solder could full fill the maximum liquidus temperature and narrow liquid + solid melting criteria, it is undeniable that the increase of reflow processing temperature could damage other electronic component, increase the dissolution rate and solubility of substrate and the rate of intermetallic compound (IMC) formation. Besides, SAC solders were reported to have higher undercooling ( $10\text{-}30\text{ }^\circ\text{C}$ ) as compared to SnPb solders. It was due to the higher Sn content in SAC solders (more than 90 % of Sn), as  $\beta$ -Sn required large undercooling during solidification. This large undercooling promoted undesirable microstructures such as, formation of large  $\text{Ag}_3\text{Sn}$  blades and  $\text{Cu}_6\text{Sn}_5$  rods which were reported to cause joint embrittlement and reliability issue (Kang et al., 2004). Thus, researchers are still looking for lead free solder which have lower melting point and smaller undercooling. The nucleation and solidification behaviour of SAC will be discussed in detail in the following section.

Another serious problem is that the microstructure of Sn-Ag-Cu alloy is more complex than that of Sn-Pb solders. Unlike SnPb which has no IMC in the bulk microstructure after reflow, lead free solder such as eutectic SAC consists of Sn and mixture of IMC in their bulk microstructure. The IMC that formed from the constituent elements of SAC solder are

$\text{Cu}_6\text{Sn}_5$  and  $\text{Ag}_3\text{Sn}$  (Subramaniam, 2012). It was reported that SAC solder has small discrete  $\text{Cu}_6\text{Sn}_5$  and large plate-like  $\text{Ag}_3\text{Sn}$  that precipitate throughout the solder (Figure 2.1) (Subramaniam, 2012; Keller et al. 2011). Large  $\text{Ag}_3\text{Sn}$  plate or  $\text{Cu}_6\text{Sn}_5$  rod are brittle in nature and are undesirable for solder alloys because they may lead to serious reliability issues. Besides, with the formation of these IMC in the bulk solder, SAC has a higher Young's modulus than SnPb, making it more susceptible to embrittlement (Zeng & Tu, 2012). Hence, solder joints will deteriorate and fractures can occur when the electronic components are subjected to stress. Thus, many researchers have doped SAC with another minor alloying element to improve the bulk microstructure of solders. Besides that, it was observed that there is a significant difference in microstructure of SAC at room temperature  $25\text{ }^\circ\text{C}$  and at elevated temperature  $125\text{ }^\circ\text{C}$  (Choi et. al, 1999). There is a larger microstructure coarsening in SAC solder compared SnPb at elevated temperature, which is detrimental to the reliability (Choi et. al, 1999). This large brittle IMC and microstructure coarsening of SAC have deteriorated the reliability of SAC solder in drop impact test. Figure 2.2 shows the drop impact test of as reflow sample, 100 thermal cycles and 250 thermal cycles of SnPb and SAC solders (Liu et. al, 2009).

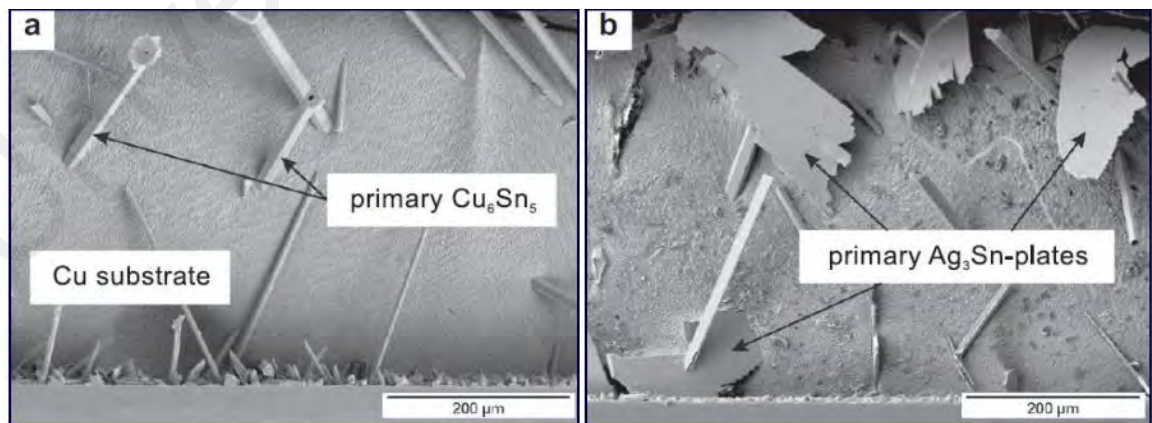


**Figure 2.1** shows large  $\text{Cu}_6\text{Sn}_5$  and plate-like  $\text{Ag}_3\text{Sn}$  IMC found in SAC alloy.

(Keller et. al., 2011)

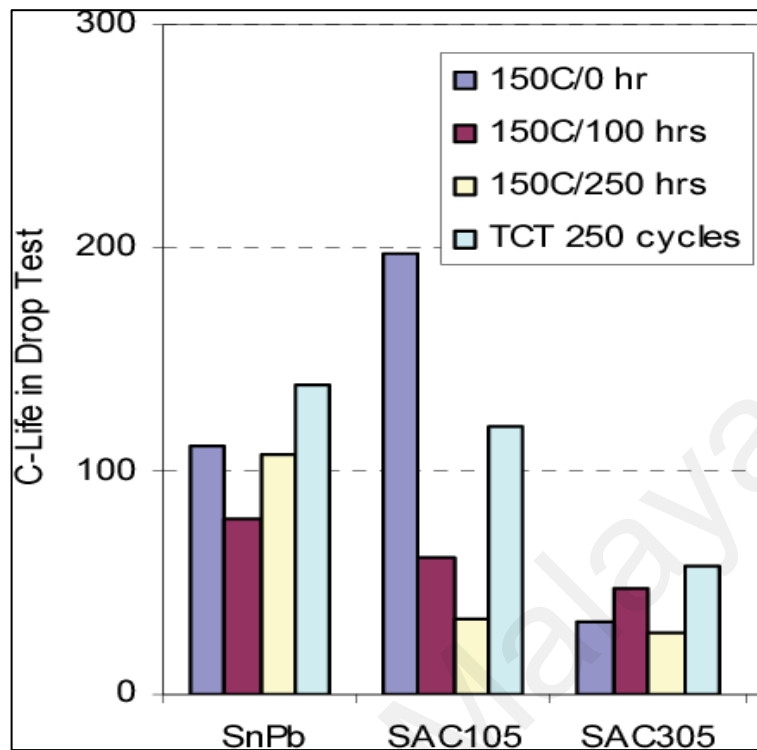


**Figure 2.2** shows that SnPb perform better in drop impact test than SAC solder after 250 thermal cycle (Liu et. al, 2009).

As the trends of electronic packaging going towards miniaturization, another reliability challenge has risen for the lead free solder. This challenge is associated with intermetallic compounds (IMCs) that formed between solder and Cu substrates. Cu-Sn IMC layers are formed at the interface when Sn-based solder react with Cu substrate during reflow. The formation of the interfacial IMCs are essential to ensure good bonding and reliable joint. For SAC solder and SnPb solder on Cu substrate, two types of Cu-Sn IMC will formed at the interface upon reflow. Scallop-shaped  $\text{Cu}_6\text{Sn}_5$  IMC layer and a planar, thin layer of  $\text{Cu}_3\text{Sn}$  will formed at the interface, with  $\text{Cu}_6\text{Sn}_5$  IMC adjacent to solder and  $\text{Cu}_3\text{Sn}$  adjacent to Cu substrate. It was reported that the IMC formed at the interface of both SAC and SnPb has the same morphology and the growth of the IMC are similar (Biocca, 2011; Subramaniam, 2012). During the mechanical testing, it was found that the failure mostly

occurred with crack initiation and propagation at the highest strain region of the solder joint and then cracks can propagate through the intermetallic and at the intermetallic/solder interface (Frear et. al, 2002). Thus, the reliability of the solder is highly relying on the bulk microstructure as it is usually where the crack initiated. However, as the trend of miniaturization continues, the ratio of volume fraction of IMC to the volume of solder joint will increase. As a result, the reliability of a solder joint will be highly dependent on mechanical properties of IMCs rather than the bulk solder alloys. With brittle nature of Cu-Sn IMCs, formation of thick IMC in a small solder joints will deteriorate the reliability of the solder. In summary, the advantages and disadvantages/ problems of SAC is listed as the table shown below :

**Table 2.2** Advantages and disadvantages / problem of SAC solder.

<b>Advantages</b>	<b>Disadvantages / Problems</b>
RoHS Compliant	Relatively higher melting temperature( $\sim 217$ °C),
Acceptable Reliability	Large undercooling ( $\sim 10-30$ °C), which cause microstructure coarsening (brittle IMC)
Good soldering and Wettability	Equipment Compatibility
	High cost due to high Ag price
	Relatively poor drop shock- thermal cycling (due to brittle and coarse IMC in bulk microstructure/ interface)

It could be seen that the reliability issues faced by the SAC solders are mainly due to its complex and brittle IMC growth in the bulk microstructure and interface. Thus, the quest to control the IMC growth at the interface and to improve the mechanical properties of the

IMC has been one of the challenges for researchers. To have a better understanding of the formation and the properties of Cu-Sn IMC, interfacial reaction between Sn and Cu is discussed in the next section.

### **2.3 Thermodynamics properties of SAC solder**

The microstructure of solders joints is greatly influenced by the melting and solidification behaviour during soldering. The microstructure of solder joints plays an important role in the performance and durability of solder joints. A comprehensive understanding on the phase equilibrium in the intermetallic system generated by soldering are crucial, and this should be supported by the relevant information on thermodynamics (Ipser et.al, 2006).

As mentioned above, SAC solder is currently one of the viable replacements for SnPb solder used in the industry. However, its high melting temperature and its large undercooling as compared to SAC has caused some reliability issues. Therefore, adding other alloying element to SAC is needed to reduce the liquidus temperature and the large undercooling of SAC solders. With Sn, Ag and Cu as the main element in the SAC based solder, we will discuss on the main phases and IMCs formed in SAC solder.

#### **2.3.1 $\beta$ Sn**

Sn was a soft, ductile and conductive element with a melting temperature of 231°C. Due to its unique properties, it was used for solders, corosions resistant alloys, and easily machinable parts. Sn has a body centered tetragonal (BCT) crystal structure at room temperature. This structure known as  $\beta$ -Sn and was anisotropic, where it could have different property responses in different crystallographic directions.  $\beta$ -Sn was also commonly known as white tin which was malleable and it exhibited excellent corrosion

resistance. As the temperature drops below 13°C, Sn underwent phase transformation. It transformed from  $\beta$ -Sn to  $\alpha$ -Sn which has a diamond cubic crystal structure.  $\alpha$ -Sn known as grey tin, was brittle and has no metallic properties as its atoms form a covalent structure in which electrons cannot move freely. Besides that, there was a drastic change in density during the  $\beta \rightarrow \alpha$  transformation where the density drops from 7.29 g/cm<sup>3</sup> to 5.76 g/cm<sup>3</sup>. This caused great volume expansion during the transformation, and lead to crumbling (Nogita et. al, 2013, Karlya et al., 2000). This phenomenon was commonly known as tin pest. There were a few alloying metals which could retard or eliminate the formation of tin pest. It was found that alloying elements with high solubility in tin were capable of suppressing tin pest. Alloying elements suppressed tin pest by inhibiting lattice expansion with dislocations or other defect sites (Lasky, 2005). Examples of these were Bi, Sb and Pb, which were most effective in retarding tin pest. On the other hand, commonly used element in solder such as Cu and Ag were insoluble in tin and form intermetallics with tin were less likely to suppress tin pest (Lasky, 2005). Thus, it should be a practical concern for lead free solder which operates in cold environments without tin pest inhibitors.

### 2.3.2 Sn-Cu

Sn-Cu system (Figure 2.3), consists of two intermetallic compounds (IMCs) at room temperature which are Cu<sub>6</sub>Sn<sub>5</sub> ( $\eta$ ) and Cu<sub>3</sub>Sn ( $\epsilon$ ). Sn and Cu are not soluble with each other at room temperature (Shim et.al, 1996). Cu<sub>6</sub>Sn<sub>5</sub> melts at 415°C and Cu<sub>3</sub>Sn melts at 676 °C. Figure 2.4 shows the Sn-rich side of the Sn-Cu phase diagram, it could be seen that eutectic reaction,  $L \rightarrow \text{Cu}_6\text{Sn}_5 + \text{Sn}$  occur at 227 °C, at Sn-0.7Cu composition. Cu<sub>6</sub>Sn<sub>5</sub> phase was often seen in the bulk microstructure of SAC solder while both Cu<sub>3</sub>Sn and Cu<sub>6</sub>Sn<sub>5</sub> phase were seen at the interface when SAC solder was reflowed on a Cu substrate. It is often seen

that  $\text{Cu}_6\text{Sn}_5$  forms at the solder matrix and solder/ Cu interface upon initial solidification after reflow, while  $\text{Cu}_3\text{Sn}$  appears between  $\text{Cu}_6\text{Sn}_5$  and Cu substrate upon thermal aging.

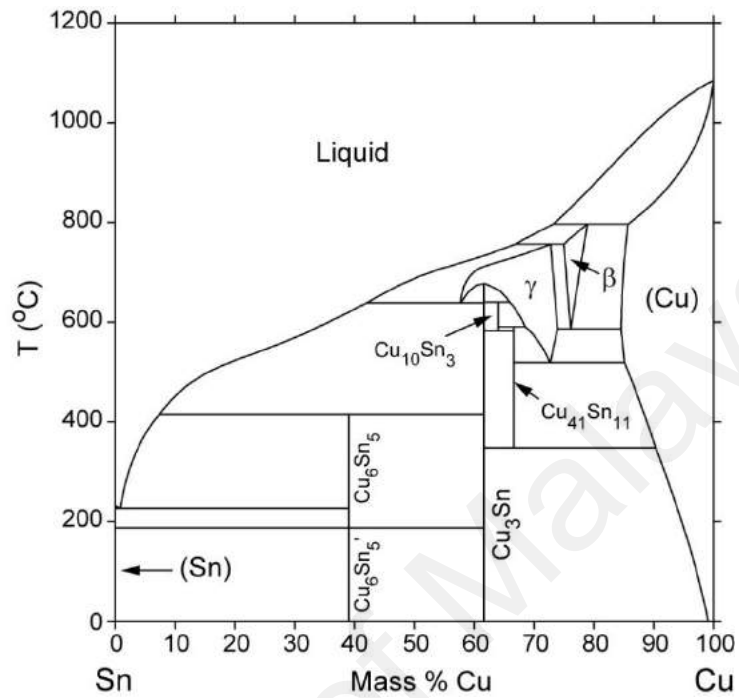


Figure 2.3 Sn-Cu phase diagram.

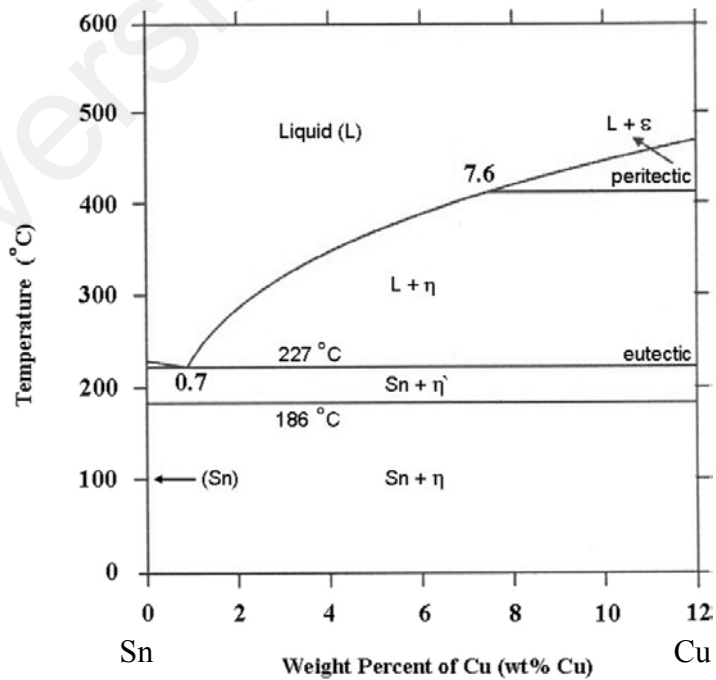


Figure 2.4 The Sn- rich portion of Sn-Cu phase diagram.

### 2.3.3 Sn-Ag

From the binary Sn-Ag phase diagram, it was seen that the eutectic reaction occurs at Sn-3.5wt. % Ag at 221 °C (Figure 2.5). The Sn-Ag IMC that formed during SA or SAC soldering is  $\text{Ag}_3\text{Sn}$  ( $\gamma$ ). It was usually seen as a rod-like eutectic phase or occasionally seen as a pro-eutectic blade-like phase (detrimental to solder joint). Fine rod-like  $\text{Ag}_3\text{Sn}$  formed in the ternary eutectic could strengthen the microstructure. However, large  $\text{Ag}_3\text{Sn}$  blade could be a weak point for the joint. During thermomechanical testing, cracking was often seen in solder joints with large blade-like  $\text{Ag}_3\text{Sn}$ . Cracks were found to occur between Sn and  $\text{Ag}_3\text{Sn}$  blades (Boesenberg et al., 2011). Formation of  $\text{Ag}_3\text{Sn}$  blade could be controlled by reducing Ag content in SAC solder and increasing cooling rate of SAC solder during reflow (Song et al., 2007). Cooling rate has been found to be a crucial factor in the shape of  $\text{Ag}_3\text{Sn}$  formation. Depends on the cooling rate,  $\text{Ag}_3\text{Sn}$  could appeared in rod-like, plate-like, sphere and even fiber morphology in SAC alloys (Garcia et al., 2011). Thus, it is critical to control the composition of Ag and cooling rate of solder joints in order to eliminate the detrimental  $\text{Ag}_3\text{Sn}$  blades.

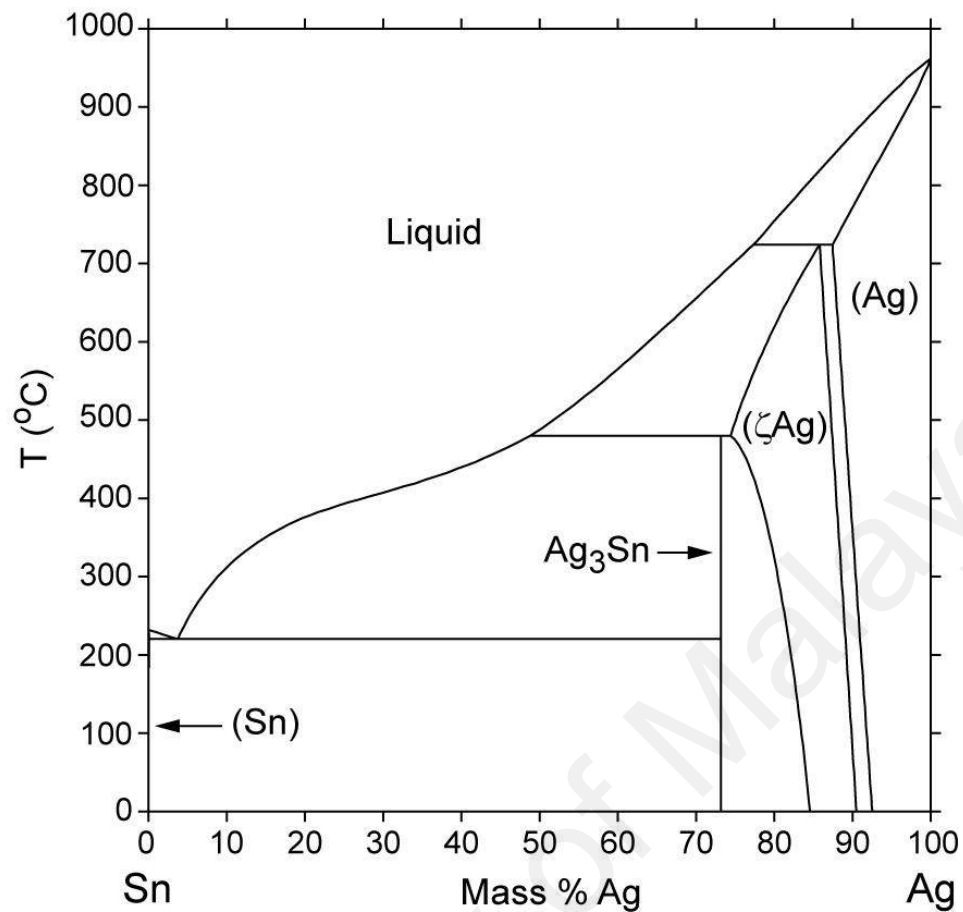
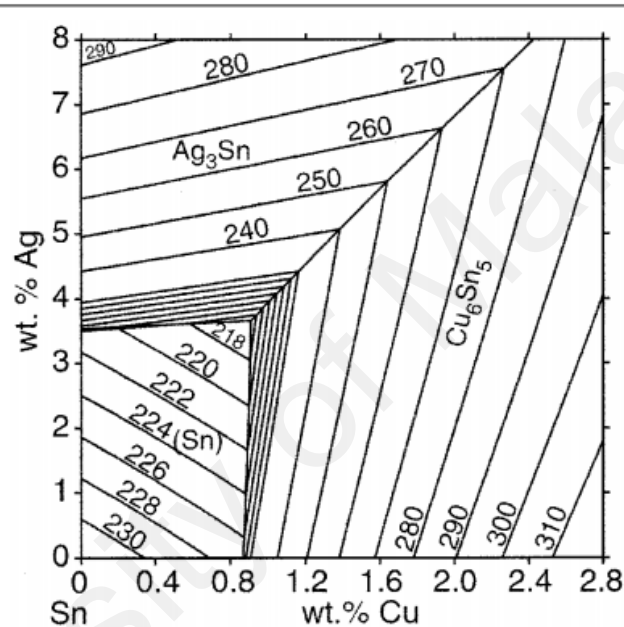


Figure 2.5 Phase diagram of Sn-Ag system (Oh et. al. 1996).

### 2.3.4 Sn-Ag-Cu

The first ternary phase diagram of Sn-Ag-Cu was experimentally determined by Gebhardt and Petzow (1959). It was reported that the solid phases have rather small ternary homogeneity ranges, and there is no ternary intermetallic compound. A few studies have reported the invariant reaction in the tin-rich corner is eutectic with a temperature of  $\sim 217$  °C, and the liquid decomposes into Sn and two binary intermediate compounds ( $Ag_3Sn$  and  $Cu_6Sn_5$ ),  $L \rightarrow Ag_3Sn + Cu_6Sn_5 + Sn$  (Miller et.al, 1984 ; Looman and Fine,2000). However, there was disagreement on the ternary eutectic composition of the liquid phase at the eutectic temperature,  $\sim 217$  °C. Miller et al. (1984) reported an eutectic composition of Sn-4.7Ag-1.7Cu (wt. %) with eutectic temperature of 216.8 °C while Looman and Fine

(2000) reported an eutectic composition of Sn-3.5Ag-0.9Cu and eutectic temperature of 217.2°C. Moon et al. (2000) later confirmed the composition of the liquid phase as 3.5 % Ag and 0.9 % Cu, and the temperature as 217.2°C, where their results are consistent with Looman and Fine's finding. Figure 2.6 shows the calculated tin-rich part of the liquidus projection and it could be seen that the eutectic composition is at Sn-3.5Ag-0.9Cu.



**Figure 2.6** Calculated liquid surface at high Sn region of SAC ternary phase diagram

(Moon et al., 2000)

The effect of Ag content and Cu content on the equilibrium melting behavior of SAC system have been studied as well (Figure 2.7). Five SAC composition (Sn-3.0Ag-0.5Cu, Sn-1.0Ag-0.5Cu, Sn-3.9Ag-0.6Cu, Sn-3.5Ag-0.9Cu, Sn-4.7Ag-1.7Ag) were shown as comparison. Figure 2.7 shows the total solid functions vs heating temperature of these 5 solder alloys. There are a few important points on the sensitivity of melting behavior

regarding the change of Ag and Cu content. For all the tested alloys, they have a high fraction of Sn, >90 % in the solid phase, and all of them melts very close to 217 °C. For near eutectic alloys such as Sn-3.9Ag-0.6Cu, liquidus temperatures measured will be 217 °C as well, as its total fraction of intermetallic phases over the wide composition ranges is small. During reflow, it is likely that this small fraction of IMC phase will have minimal effect on solder flow and wetting. On the other hand, by altering the Ag to a lower content as compared to the eutectic SAC (Ag = 3.5 %), SAC 305 and SAC 105 has a liquidus temperatures of 220 °C and 226 °C respectively. Since the fraction of Sn remaining between 217 °C and the liquidus temperature is significant, the alloys must reach their liquidus temperature during assembly to ensure it was melted completely.

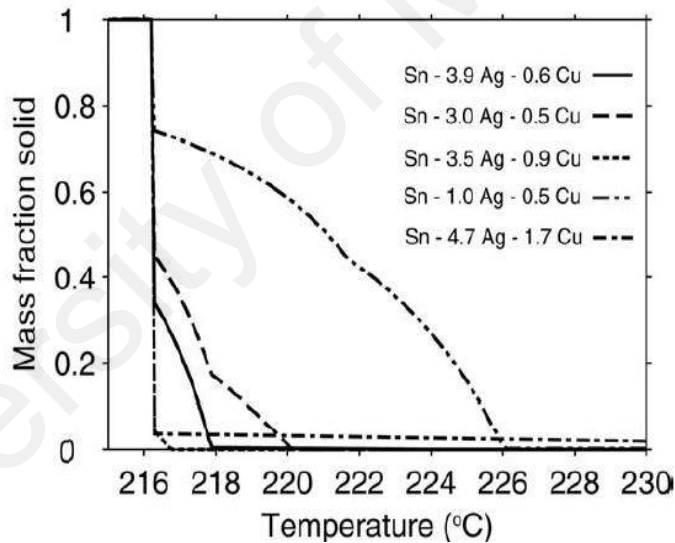


**Figure 2.7** Comparison of calculated mass fraction solid as a function of temperature for five different Sn-Ag-Cu alloys (Handwerker, 2003).

As mentioned in table 2.4, during assembly, 240 °C is usually considered the maximum acceptable component temperature. Since soldering temperature is typically at least 15 °C above liquidus temperature, thus the maximum acceptable liquidus temperature should be ~ 225 °C. Based on the analyses described above, SAC system is quite forgiving in terms of

its insensitivity of melting behavior to solder composition, where the Ag content could be lower to 1%wt. Besides that, there are studies that showed that for a fixed Ag concentration, low Cu content in solder encouraged fast dissolution from the boards and the components, while high Cu content in the solder promoted intermetallic formation in colder sections of the bath (Bath, 2007). This tradeoff has led researchers to suggest a balance copper concentration limit to the range 0.5 to 0.6wt. % for solder alloys used in electronic assemblies. Therefore, the effect of solder composition on reflow behavior should be minimal for solder composition within this silver and range.

### **2.3.5 Nucleation and Solidification Behavior**

Solidification of SAC system has plays an important role in affecting its microstructural evolution. One of the main effects of solidification on the bulk microstructure of a solder is due to the difficulty of  $\beta$ -Sn nucleation.

The eutectic temperature of SAC system is 217 °C, this is often referred as the onset melting temperature of SAC. However, during solidification, SAC solder could still remain in liquid even below 217 °C. This is due to the microstructure of SAC which is predominantly  $\beta$ -Sn (>90 %) with minimal amount of  $\text{Cu}_6\text{Sn}_5$  and  $\text{Ag}_3\text{Sn}$ .  $\beta$ -Sn is well known to have difficulties in nucleating during cooling which leads to Sn dendrites nucleation below its melting temperature. Solidification is the result of two successive steps: nucleation and growth of solid phase. In nucleation, the solder system has to overcome an energy barrier, and the liquid solder must supercool down to the so-called solidification temperature at which the solid phase first starts to form. The two energies involved in the solidification of a pure metal are surface free energy and volume free energy (Yu, H. & Kivilatih, J.K., 2006). These energies contribute to the total free energy,  $\Delta G = \Delta G_V + \Delta G_S$ .

Thus, for solidification of  $\beta$ -Sn to occur, undercooling must arise to create the thermodynamic driving force for phase change (Yu, H. & Kivilatih, J.K., 2006). The difference between the onset of melting and onset of solidification is known as undercooling temperature ( $\Delta T$ ). Pure Sn ( $T_m = 231\text{ }^\circ\text{C}$ ) has a large undercooling ( $\sim 40\text{ }^\circ\text{C}$ ), and has been found to be solidified at  $190\text{ }^\circ\text{C}$  under a controlled environment (Swenson, 2007), SAC solder is often reported to have an undercooling of  $15\text{-}30\text{ }^\circ\text{C}$ .

During cooling from the molten SAC liquid, the first phase to solidify depends on the composition of SAC. For eutectic Sn-3.5Ag-0.9Cu solder (SAC359),  $\text{Ag}_3\text{Sn}$  is the first phase to form, and  $\beta$ -Sn should be the next to solidify. However, if  $\beta$ -Sn does not nucleate,  $\text{Ag}_3\text{Sn}$  continues to form, and the supercooled liquid becomes depleted in Ag.  $\text{Cu}_6\text{Sn}_5$  is the next stable phase to form, and it will form when the liquid composition reaches the metastable liquidus “valley” (Handwerker et al., 2007). As  $\text{Ag}_3\text{Sn}$  and  $\text{Cu}_6\text{Sn}_5$  IMC continue to form, the supercooled liquid continues with Ag and Cu depletion. For the  $\text{Ag}_3\text{Sn}$  which formed during the initial solidification, they continue to grow from the supercooled liquid below eutectic temperature and thus eventually become the large  $\text{Ag}_3\text{Sn}$  plates we usually observed in the solder matrix. As the temperature continues to drop, the supercooled liquid eventually becomes supersaturated with  $\beta$ -Sn and  $\beta$ -Sn starts to nucleate in the presence of local heterogeneous nucleation sites (eg. Solidify IMC) in the solder. From a small number of nuclei,  $\beta$ -Sn forms dendrites that eventually solidify completely with the remaining ternary alloy liquid forming regions with different phases and morphologies as discussed by Moon et al. (2000).

Researchers have tried many ways in attempt to modify the microstructure of SAC with large brittle IMCs in the bulk solder. One of the ways to affect the nucleation of  $\text{Ag}_3\text{Sn}$  is by controlling the cooling rate, however, this is not feasible in a practical way for electronic assemblies with different cooling rates. Another method is by lowering Ag content in SAC

solder. Henderson et al. (2002) showed that the formation of  $\text{Ag}_3\text{Sn}$  could be suppressed by using substantially lower Ag content. They estimated the Ag content in SAC solder must be less than 2.7 % in order to avoid the formation of  $\text{Ag}_3\text{Sn}$  plates. Thus, one of the reasons that SAC105 has attracted much attention was due to the suppression of  $\text{Ag}_3\text{Sn}$  plate formation. Besides that,  $\text{Ag}_3\text{Sn}$  plate formation could be suppressed by promoting  $\beta$ -Sn nucleation with minor alloying element additions (Anderson et. al, 2009).

## **2.4 Interfacial reaction between Sn and Cu**

In most of the commonly used systems in electronics, IMC's are formed during soldering in three consecutive stages: dissolution, chemical reaction, and solidification. Dissolution is a stage where the contacted metal starts to dissolve in the molten solder, then chemical reaction takes place between M (conductor materials) and Sn in the liquid, and lastly the solidification of the remaining supersaturated melt occurs. The relative importance of each stage varies between systems depending on the solubility of conductor metal in Sn. (Laurila et al., 2005). Copper is the most common conducting metal that is used in contact with solder, thus the knowledge of the Sn/Cu metal interface reaction and phase evolution is important for the reliability of solder interconnection and for the optimization of the soldering process.

### **2.4.1 Liquid state reaction**

At the typical soldering temperature, i.e. 260 °C,  $\text{Cu}_6\text{Sn}_5$  forms immediately at the interface when Cu in contact with molten Sn-based solder. The primary stage of the interfacial reaction involved the dissolution of Cu in the molten Sn, until the liquid solder/Cu interface is saturated with Cu (Bader, 1969). This Cu dissolution is a non-equilibrium process, thus liquid Sn/Cu interface can be saturated with extremely high Cu

concentration. Heterogeneous nucleation promotes rapid formation and growth of  $\text{Cu}_6\text{Sn}_5$  crystallite at the liquid Sn/Cu interface. This instant formation of the  $\text{Cu}_6\text{Sn}_5$  has been observed experimentally (Gagliano, 2002). The concentration profile plays a very significant role in the typical reflow soldering. For the concentration of Cu which is rather uniform, scallop-type  $\text{Cu}_6\text{Sn}_5$  (uniphase) layers are formed, and the  $\text{Cu}_6\text{Sn}_5 + \text{Sn}$  (two phase layer) which are mostly enhanced by the local constitutional supercooling of liquid can form next to the uniphase layer. However, the dissolution rate can vary along the interface and thus the Cu concentrations along the interface are not as uniform as well. There are some Cu atoms not consumed for the formation of  $\text{Cu}_6\text{Sn}_5$  at the interface and thus reaction with molten Sn in the solder matrix and form long  $\text{Cu}_6\text{Sn}_5$  rod/tubes and bunches of fibers in the eutectic ( $\text{Cu}_6\text{Sn}_5 + \text{Sn}$ ) structure (Mattila et al., 2004). Laurila et al. (2005) stated that there are 2 factors in determining the thickness and morphology of this  $\text{Cu}_6\text{Sn}_5$  IMC layer. It is primarily determine by the dissolution rate of Cu atoms in molten Sn and the chemical reaction between Sn and Cu. The second factor is determined by the diffusion of Cu in Sn liquid. In short, the morphology and thickness of  $\text{Cu}_6\text{Sn}_5$  is determined by the metasolubility of Cu in liquid solder, while the morphology of the 2 phase zone is determined by the diffusion rate of Cu in liquid Solder (Laurila et al., 2005).

Under normal reflowing process, thermodynamically,  $\text{Cu}_3\text{Sn}$  ( $\epsilon$ ) layer should formed in between Cu and  $\text{Cu}_6\text{Sn}_5$ . However, the thickness is too small and can only be seen under very high magnification. If the contact between Cu and molten Sn is sufficient,  $\text{Cu}_3\text{Sn}(\epsilon)$ -phase will be formed between the  $\eta$ -phase and Cu. Unlike the formation of the  $\eta$ -phase which mainly dictated by dissolution and reaction controlled formation, the formation of the  $\epsilon$ -phase is diffusion and reaction type growth.

#### 2.4.2 Solid state reaction

Solid state reaction between solid Sn and Cu takes place at the temperatures below the melting temperature of both metals. Owing to the fact that the IMC layer in the interface has a great impact on the reliability of the solder joint, the interfacial reactions between solid Cu and Sn have been investigated extensively at different temperature ranges that below the reflow temperature. However, the results are not in entire agreement with each other. Some are even contradictory to each other, especially with respect to which one is the main diffusing species in  $\text{Cu}_3\text{Sn}$  ( $\epsilon$ ) and  $\text{Cu}_6\text{Sn}_5$  ( $\eta$ ).

Tu et al. (1973) stated that even after one year at room temperature, the only compound formed is still  $\text{Cu}_6\text{Sn}_5$ . The reaction is controlled by the release of Cu atoms from Cu lattice and the main diffusing species at room temperature is Cu. As the annealing temperature increases to above 50-60 °C,  $\text{Cu}_3\text{Sn}$  ( $\epsilon$ ) will form and grow at the expense of  $\text{Cu}_6\text{Sn}_5$  (Tu, 1973; Tu & Thompson, 1982).

Oh et al. (1994) has studied the factors that influence the growth of  $\text{Cu}_3\text{Sn}$ ( $\epsilon$ ) and  $\text{Cu}_6\text{Sn}_5$  ( $\eta$ ) at temperature around 200 °C. They found that the diffusion flux of Sn in  $\eta$  phase is the first factor, the second one being the decomposition rate of  $\eta$  as  $\epsilon$  grows and the third factor is the change in the relative magnitudes of Sn and Cu fluxes in the  $\eta$  -phase. It shows that at higher temperature around 200 °C, the first factor dominates and the  $\text{Cu}_6\text{Sn}_5$  ( $\eta$ ) grow faster. But, as the temperature decreases, the other two factors start to influence the growth of IMCs.

Laurila et al. (2005) have investigated on the solid state reaction of Cu and Sn as well. Based on the results of investigations done by others and their own, Laurila et al. have come to agreement with the studies done by Tu et al.(1996) and Oh et al.(1994). In addition, Laurila et al (2005) stated that at the temperature range of 60-200 °C,  $\text{Cu}_3\text{Sn}$  ( $\epsilon$ ) continues to grow at the expense of  $\text{Cu}_6\text{Sn}_5$  ( $\eta$ ). Both Cu and Sn are mobile during  $\text{Cu}_3\text{Sn}$  ( $\epsilon$ ) growth.

It is consistent with the  $\text{Cu}_3\text{Au}$  rule and Cu is the more mobile species in the  $\epsilon$ -phase. The fraction of the  $\text{Cu}_3\text{Sn}$  ( $\epsilon$ ) phase out of the total intermetallic layers is larger at temperatures 160–200 °C than at 220 °C, as the inter-diffusion in the  $\text{Cu}_6\text{Sn}_5$  ( $\eta$ ) phase at temperatures 160–200 °C requires higher activation energy (Laurila et al., 2005).

Based on Cu-Sn binary phase diagram,  $\text{Cu}_6\text{Sn}_5$  has at least two structural forms, the transformation of high temperature metastable hexagonal phase  $\eta$  to room temperature phase,  $\eta'$  occurs at  $\sim 186$  °C (Massalski, 1996). During reflow and subsequent cooling, the transformation into the low temperature stable form is not sufficient, thus the high temperature hexagonal  $\text{Cu}_6\text{Sn}_5$  ( $\eta$ ) remain in the metastable phase. This metastable  $\text{Cu}_6\text{Sn}_5$  ( $\eta$ ) will not transform into the stable form  $\eta'$  at room temperature within a reasonable time, due to kinetic restraint. However, the transformation would take place under a relatively high temperature, around 150 °C, and the time required for the transformation is significantly shortened. This high temperature can be reached during the use of electronic devices due to the strong local heating of power component. This hexagonal/monoclinic transformation will cause a volume expansion of the  $\text{Cu}_6\text{Sn}_5$  if this transformation is to happen at room temperature. The theoretical densities of  $\eta$  and  $\eta'$  at room temperature are 8.448 and 8.270  $\text{gcm}^{-3}$  respectively, the solid state phase transformation of hexagonal  $\eta$  to monoclinic  $\eta'$  would be accompanied by 2.15 % expansion in volume (Nogita, 2010). It should be noted that such volume change during service could introduce significant stress to the solder joint and possibly cause crack initiation and crack propagation.

## **2.5 Effect of fourth alloying element on lead-free solder**

Over the years, SAC solder with promising ductility and joint strength has become a preferred Pb-free solder for electronic assemblies. However, as mentioned previously, it

still has some drawbacks. Thus, many researches have been done on the addition of fourth minor alloying elements (0.05-0.1 wt. %) into SAC solder in the hope that it could outperform SAC solder. These elements include Ni, Ti, In, Zn, Fe, Co, Mn, Zn, Al, Ce, In and etc. (Ahmad, 2013; Kim et al. 2003; Anderson et al. 2009; Shi et al. 2008; Fallahi et al. 2012; Szurdan, 2019; Kang et al. 2005; Chuang et al., 2012; Zhao et al. 2007). However, the amount of alloying elements added need to be carefully tailored so that no additional brittle intermetallic compound IMC /layers are formed which in turn reduce mechanical reliability.

The effects of the fourth minor alloying element on the microstructure and mechanical properties have been investigated. It was found that the addition of these elements influences the wetting behaviour, bulk microstructure, interfacial reactions between solder and substrate, and also the mechanical properties (Gao et al., 2011). Improvement in wettability, mechanical properties, Sn grain refinement and IMC suppressions have been reported (Shi et al., 2008; Ahmad, 2011; Sun & Zhang, 2015; Kang et al., 2004)

It was reported that fourth alloying elements imparted their influence in mechanical properties by modifying the microstructure of the solder. In general, there were three ways of modifying the microstructure of the solders, (i) microstructure refinement in solder matrix, (ii) suppressed brittle intermetallic compound (IMC) formation at the solder matrix or/ and at the interface and lastly, (iii) changed the morphology of the IMC at the solder/ substrate interface (Laurila et al., 2010).

Addition of minor alloying element can influence the bulk microstructure in several ways. It is highly dependent on the type and also the amount of minor alloying element added. Some minor alloying elements react with Sn, Ag or Cu to form new IMC in the bulk microstructure (Anderson et al., 2009; Kotadia et al. 2010; Seo et al. 2011) Some elements

that do not react with Sn, Ag or Cu to form new IMC, but has marked solubility in Sn, Cu, Ag, or Cu-Sn IMC, and thus suppress/ enhance the growth of IMC in the bulk microstructure (Nogita, 2010; Anderson et al., 2006; Amagai, 2003). Some additions of minor alloying element also act as heterogenous nucleation site during solidification and thus refine the bulk microstructure, eg. Sn grains refinement or IMCs refinement (Kang et al., 2004).

Minor alloying elements that influence the IMC, can be roughly categorized into two major: (i) elements that show prominent solubility in the intermetallic compound (IMC), soluble in one or both Cu-Sn IMC and (ii) elements that are insoluble in Cu-Sn IMC. Elements in category (i) generally take part in the interfacial reaction; they impart their influencing by increase/decrease the reaction or growth rate of IMC and changing the morphology of IMC. Elements in category (ii) affect the growth of IMC by changing the activities of metal atoms taking part in the interfacial reaction and do not participate themselves (Laurila et al., 2010).

Anderson et al. (2006) have used analysis of electronegativity and atomic radius, to predict and used it as a guideline which elements would dissolve in solid solution to around 5 at. % in a solvent element (Figure 2.8). In Figure 2.8, the solvent element Cu, is placed at the center of the ellipse, and all the elements (Ni, Si, Ge, Mn, Zn, Ti, Cr and Ge,) they studied lie within the ellipse except Ti. However, it is known from the Cu-Ti phase diagram that Ti will dissolve in Cu up to 8 at. %, so they concluded it in the list of potential alloying elements.

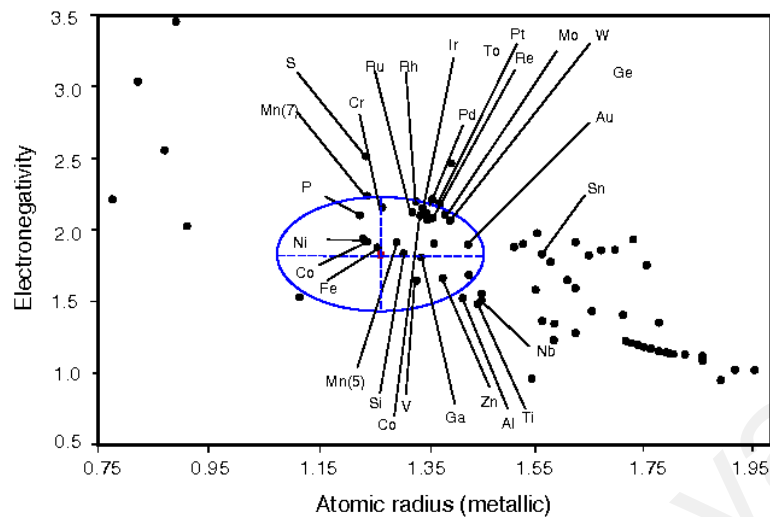


**Figure 2.8** A Darken–Gurry ellipse plot with Cu as the central atom, and electronegativity elements were plotted against the element atomic radius. The elements within the ellipse are likely to have high solubility in Cu (up to 5 at.%) (Anderson et al., 2006).

### Nickel (Ni)

With the addition of Ni to SAC-Ni system, it was revealed that varying the Ni content would affect bulk microstructure significantly and thus has to be carefully engineered. It was reported that with the addition of Ni  $\leq 0.2$  %, the undercooling of SAC did not change significantly (Moon et al., 2009; Tay et al., 2013). However, for those studies with Ni addition  $\geq 0.4$  %, it was found that it would reduce the undercooling of SAC solder significantly (Moon et al., 2009; A.E Ahmad, 2008). Moon et al. (2009) found that with the addition of 0.2 % Ni, there is no significant changes in the bulk microstructure and  $(\text{Cu,Ni})_6\text{Sn}_5$  is formed. However, as Ni was added up to 0.4%, a new needle like IMC was seen, and it was identified as  $\text{Ni}_3\text{Sn}_4$ . They reported that the formation of  $\text{Ni}_3\text{Sn}_4$  was attributed to the large reduction in undercooling as it acts as a heterogenous nucleation site (Moon et al., 2003). On the other hand, the effect on addition of Ni (0.01-5 %) at the interface are similar for all added Ni content, where it enhanced the growth of  $(\text{Cu,Ni})_6\text{Sn}_5$

and suppressed that of  $\text{Cu}_3\text{Sn}$  (Tay et al, 2013, Nogita et al., 2013). It produced much thinner layers of  $\text{Cu}_3\text{Sn}$  at all Ni% addition even after 2000hr aging. Besides, it was reported that the addition of 0.05 % Ni improved the microhardness, yield strength and UTS of Sn-2.0Ag-0.5Cu solder, which was (El-Daly and El-Taher, 2013).

### Cobalt (Co)

The minor addition of cobalt to SAC solder system modifies both bulk and interfacial microstructure and mechanical properties (Cheng et al., 2008; ZL Ma et al. 2016). It was reported that micro-alloying Co (0.04 %) causes grain refinement in the bulk microstructures by reducing the nucleation undercooling for  $\beta\text{Sn}$  because of Co-Sn IMC particles form in the melt act as nucleation catalysts for  $\beta\text{Sn}$ . Anderson et al. (2006) have reported that with the addition of Co (0.05-0.25 %), flat thin  $(\text{Cu},\text{Co})_6\text{Sn}_5$  IMC was formed at the interface after reflow on Cu substrate. Similar to Ni addition, after thermal aging, it enhanced the growth of  $(\text{Co},\text{Cu})_6\text{Sn}_5$  and suppressed that of  $\text{Cu}_3\text{Sn}$  (Amagai, 2008; Anderson et al, 2006). However, addition of Co has showed no improvement in tensile strength and caused a significant reduction in strain (Anderson et al., 2006; Cheng et al., 2007). However, other study has found different results when Co nanoparticle was added into SAC by the flux with Co nanoparticle (2 %) (Bashir et al., 2016). Bashir et al. found that addition of Co nanoparticle in flux improve the electron migration of SAC, and it also improved the tensile strength of SAC before and after electron migration.

### Bismuth (Bi)

Studies on the addition of Bi (1-5 %) to SAC solder shows that Bi modifies the properties of SAC. The effect of Bi on suppressing undercooling increases as a function of Bi content. Bi suppresses the formation of IMCs ( $\text{Ag}_3\text{Sn}$  and  $\text{Cu}_6\text{Sn}_5$ ) phases, especially

$\text{Cu}_6\text{Sn}_5$ , and reduces the size of  $\beta$ -Sn grains in the solder matrix. Addition of 1 wt. % Bi into a SAC solder also suppressed the formation of IMC at solder/substrate interface during aging. Bismuth alters the thickness of  $\text{Cu}_6\text{Sn}_5$  interfacial IMCs in such a way that IMCs thickness shows a descending trend at first (1 %), then the thickness of IMC increase in an ascending trend as Bi was added up to 2 % to 5 %. However, in general, interfacial IMC formed by SAC+ Bi is lower than that of SAC solder (Ahmed et al., 2016, Sayyadi and Nafakh, 2019). In the case of Sn-2.5Ag-0.7Cu-1Bi joint, the interfacial IMC thickness shows a 14 % reduction in the thickness comparing to base solder. In terms of mechanical properties, addition of 1 % Bi has increased the impact toughness by 20 %, though further increase of Bi content does not further improve impact toughness. Besides, it was reported that the addition of Bi to SAC has doubled the hardness and shear strength of SAC solder (Bktiar Ali et al., 2016). It was reported that Bi increased the shear strength of the solder alloys by solid solution strengthening mechanism (Ahmed et al., 2016; Bktiar Ali et al., 2016).

### 2.5.1 Al

Several studies have been done on addition of aluminum (Al). Research on Al addition as nanoparticles or minor alloying element has been reported (Amagai, 2008; Boesenberg et al., 2012; Kotadia et al., 2012; Li et al., 2012; Kantarcioglu et al., 2014, Zhang et al. 2019). As addition in the form of nanoparticles, Amagai (2008) observed that the addition of 0.05 % Al nanoparticle did not show any changes on the interfacial IMC. While for Al addition as minor alloying element, it was reported that Al changed the thermal properties, the bulk and interfacial structure of the solder and improved mechanical properties (Anderson et. al., 2006).

In all studies that investigate the effect of Al on thermal properties of SAC, they have reported that the addition of Al as minor alloying (0.01-2 %) have minimized the undercooling of SAC solder and suppressed the formation of  $Ag_3Sn$  blade significantly blade (Shnawah et al., 2012; Boesenberg et al., 2012). There are several studies which reported the effects of Al on the solder matrix. Addition of Al into lead free solders that have been studied are listed in the table below:

**Table 2.3** Summary of lead free solders with addition of Al as minor alloying element that have been studied so far.

<b>Lead free solder</b>	<b>Al content(%)</b>	<b>Findings in bulk microstructure</b>	<b>Reference</b>
Sn-Cu	0.01 -0.05	* 0.03 & 0.05 % Al changed the microstructure by reducing $Cu_6Sn_5$ in the bulk microstructure.  * $\beta$ Sn grain refinement in all composition  * Found Cu-Al IMC in the solder matrix in all composition, it was proposed as $Cu_{33}Al_{17}$ based on TEM-EDX ratio and (SAED)	Khoo et al., 2015
Sn-Ag	0.50 -2.00	* $Ag_3Al$ , $Al_2Cu$ and undefined Al-Cu IMC formed in the solder matrix.	Kotadia et. al , 2012

**Table 2.3** continued

<b>Lead free solder</b>	<b>Al content(%)</b>	<b>Findings in bulk microstructure</b>	<b>Reference</b>
Sn-Ag-Cu	0.05– 0.50	<p>* With addition of 0.05 % Al, distribution of Sn-Al-Cu IMC was found in the bulk.</p> <p>* With addition of 0.05-0.15 Al % reduced formation of Ag<sub>3</sub>Sn, very few Ag<sub>3</sub>Sn blades were seen in the bulk.</p> <p>* With addition of 0.1 -0.5%, Al-Cu IMC, Ag<sub>3</sub>Sn , and Ag-Al IMC are found.</p> <p>* 0.1 % Al reduced UTS, yield strength and Young's modulus. Fracture surface shows dimples fracture, ductile fracture</p> <p>* 0.5Al % increase yield strength, UTS &amp; E, intergranular fracture.</p>	<p>Kantaciuglu et. al , 2014</p> <p>Shnawah et. al, 2012</p>
Sn-Ag-Cu	0.05 – 0.50	<p>*Cu<sub>33</sub>Al<sub>17</sub> particles formed in the bulk, faceted, hexagonal in shape, and some attached to the Cu<sub>6</sub>Sn<sub>5</sub> interface.</p> <p>*Hardness of Cu<sub>33</sub>Al<sub>17</sub> =31.4±5.8 GPa Young's modulus of Cu<sub>33</sub>Al<sub>17</sub> = 49.1±2.5 GPa.</p> <p>*0.05Al reduced shear strength of SAC by 10MPa, but maintained shear strength even after thermal aging 1000hr., intergranular fracture .</p> <p>* Cu<sub>33</sub>Al<sub>17</sub> particles formed in the bulk, faceted, hexagonal in shape, and some attached to the Cu<sub>6</sub>Sn<sub>5</sub> interface.</p> <p>*Hardness of Cu<sub>33</sub>Al<sub>17</sub> =31.4±5.8 GPa Young's modulus of Cu<sub>33</sub>Al<sub>17</sub> = 49.1±2.5 GPa.</p> <p>*0.05Al reduced shear strength of SAC by 10 MPa, but maintained shear strength even after thermal aging 1000hr.</p>	<p>Anderson et. al, 2006</p>

In summary, with the addition of Al into SA solder, even with the absence of Cu atom in the solder,  $\text{Al}_2\text{Cu}$  IMC and undefined Al-Cu IMC were found in the solder matrix of SA solder on Cu substrate. Whereas, only one type of Al-Cu IMC was found in the solder matrix of SAC and SC solder, and Anderson et al.(2006) reported and Khoo et al.(2012) reported it as  $\delta\text{-Cu}_{33}\text{Al}_{17}$ . Though the effects of Al on the solder matrix reported by other researchers seem consistent, there are contradictory reports on the effects of Al addition on the interfacial SA/Cu reaction. When 0.5 % Al was added into SA solder, Xia et al. (2008) observed a spalled layer of  $\text{Al}_2\text{Cu}$  compound layer near the interface (right above  $\text{Cu}_6\text{Sn}_5$  layer at the interface) and the suppression of  $\text{Cu}_6\text{Sn}_5$  layer at the solder/Cu interface. While with addition of Al up to 1 %, only  $\text{Al}_2\text{Cu}$  compound layer was found at the solder/Cu interface, and it completely replaced  $\text{Cu}_6\text{Sn}_5$  layer. On the other hand, when Kotadia et al. (2012) added 0.5 to 2.0 wt. % of Al into SA solder, they observed that spherical Al-Cu IMC spalled away from the solder matrix due to the depletion of Al in the solder. Besides, they have reported that there was no suppression of the growth of interfacial  $\text{Cu}_6\text{Sn}_5$  with the addition of Al from 0.5 to 2.0 wt. %.

For effect of Al on the interfacial reaction of SAC solder, it was reported that with the addition of 1 wt % Al into SAC387 solder, only AlCu ( $\eta_2$ ) layer was observed at the interface after 10 min reflow (Li et al. 2012). By using dipping method, Shnawah et al. (2012) have investigated the effect of 0.1 wt. % Al addition on the interfacial reaction. They reported that addition of 0.1% Al has reduced the thickness of  $\text{Cu}_6\text{Sn}_5$  layer (Shnawah et al, 2012). To date, no detailed study has been done for the effect of minor Al addition (< 1 wt. %) on interfacial reaction of SAC/Cu.

Al addition was also found to improve the mechanical properties of solder (Anderson et al., 2009). It was also reported that addition of Al reduced tensile strength and promoted

ductile failure (Shnawah et al., 2012). It has been reported to result reduced the shear strength of solder as compared to SAC, however it has great shear strength retention even after aging for up to 1000hr at 150°C (Anderson et al., 2006). Ability to retain its thermomechanical properties an interesting aspect of addition of Al, as deterioration in mechanical properties of SAC after thermal aging is one of the major drawbacks which caused researcher to seek for alternatives. However, there is no study reported on the shear fracture analysis on SAC+Al which is vital in the solder's reliability. Thus, in this study, effect of minor aluminium addition (less than 1 wt.%) on bulk microstructure, interfacial reaction and mechanical properties (hardness, modulus, shear) will be focused, and shear fracture analysis will be studied as well .

### **2.5.2 Zn**

Addition Zn has also attracted much attention as well. In fact, more detailed studies have been done on addition of Zn in recent years (Amagai, 2008, Sujan et al. 2017, Haseeb et al. 2014). Zn has been added as nanoparticle and as minor alloying element in solder. A few studies have been done on Zn added as nanoparticles. Amagai (2008) observed that the addition of 0.05-0.1 % Zn nanoparticle into SAC did not show any prominent effect on the interfacial IMC. On the other hand, it was reported by Chan et al. (2007) that addition of 0.3 % Zn nanoparticles in SAC suppressed the growth of interfacial  $\text{Cu}_6\text{Sn}_5$  and  $\text{Cu}_3\text{Sn}$  layers during reflow. When the zinc nanoparticle content was increased to 0.8 %, an additional  $\text{Cu}_5\text{Zn}_8$  layer was found to form between solder and  $\text{Cu}_6\text{Sn}_5$ . The addition of Zn (~0.1-0.3 %) nanoparticles into SA solder has suppressed the IMC growth at the interface significantly during reflow and after one month thermal aging (Haseeb et. al, 2014). It is suggested that Zn nanoparticles actually undergo dissolution during reflow and exert their influence through in-situ alloying effect.

Effects of minor alloying Zn on the thermal properties, microstructures and mechanical properties have been investigated (Chan et. al, 2007; Anderson et. al, 2009; Kotadia et. al, 2008; Kang et. al, 2007). Many studies have reported that Zn could lower the undercooling of lead free solder substantially (undercooling  $< 7$  °C). For the bulk microstructure, Chan et al. (2007) has investigated the effect of Zn on the grain size of the  $\text{Cu}_6\text{Sn}_5$  after reflow and did not notice any refinement. Amagai (2008) also obtained similar results regarding effect of 0.1 wt. % of Zn nanoparticle on the grain size after one and four reflows.

The most prominent effect of Zn would be its effect on the interfacial IMC, where many studies reported that very minimal amount of addition of Zn was found to suppress the formation of  $\text{Cu}_3\text{Sn}$  during solid state annealing. It was reported to hinder the growth of  $\text{Cu}_3\text{Sn}$  even at an addition of a low amount such as 0.2 wt. % (Laurila et al. 2010; Anderson et. al, 2009). Zn is soluble in both Cu-Sn IMC layers ( $\text{Cu}_6\text{Sn}_5$  and  $\text{Cu}_3\text{Sn}$ ). It was reported that Zn has solubility values of 6 at. % in  $\text{Cu}_6\text{Sn}_5$  and 9 at. % in  $\text{Cu}_3\text{Sn}$  (Chou et. al, 2006). Yu and Duh (2011) reported that solubility of Zn at 1 at. % in  $\text{Cu}_6\text{Sn}_5$  promotes phase stabilization of hexagonal  $\eta$ - $\text{Cu}_6\text{Sn}_5$  from transforming into monoclinic  $\eta'$ - $\text{Cu}_6\text{Sn}_5$  even after high temperature aging (Yu & Duh, 2011). The phase stabilization of hexagonal  $\eta$ - $\text{Cu}_6\text{Sn}_5$  could improve the reliability of the solder joints by preventing volume change of  $\text{Cu}_6\text{Sn}_5$ . Besides, Chen et al. (2015) reported that incorporation of Zn atoms in  $\text{Cu}_6\text{Sn}_5$  can increase the elastic modulus and hardness of  $\eta$ - $\text{Cu}_6\text{Sn}_5$  compound.

Zn as minor alloying element in lead free solder was also reported to reduce the voids at the IMC/Cu interface (Kang et al., 2012, Kotadia et al., 2012). Cho et al. (2006) has also reported that the reduction of  $\text{Cu}_3\text{Sn}$  IMC growth by addition of Zn was beneficial in suppressing Kirkendall voids at the IMC/Cu interface upon thermal aging. For effects of Zn on the mechanical properties of solder, Anderson et al. (2009) reported that 0.2 Zn reduced

the shear strength of SAC. Many studies have shown that Zn addition improve ultimate tensile strength (UTS) and drop impact of SAC. The improvement of drop impact test was reported to be due to voids reduction at the interface the suppressions of interfacial IMC. Besides that, SAC+Zn joints lost only 3 % of their as-soldered impact strength after thermal aging at 150 °C for 1000hr, which is an important aspect in improving the thermomechanical properties of SAC (Anderson et. al, 2009).

In brief, several studies have been done on the effect of minor alloying Zn on the SAC solder. Although the  $\text{Cu}_6\text{Sn}_5$  and  $\text{Cu}_3\text{Sn}$  IMC suppression, improvement in UTS and drop impact test appear to be consistent on all studies, there is a lack of knowledge regarding the Zn distribution in  $\text{Cu}_6(\text{Zn}, \text{Sn})_5$  and their relationship with the mechanical properties of SAC+Zn.

## **2.6 Mechanical Properties**

Mechanical properties of a solder joints are important consideration for ascertaining the reliability of solder. Information of mechanical properties of solder joint is important as it lays a fundamental to the design of reliable microelectronic devices. When the mechanical properties of a solder joint is mentioned, there are two points that should be considered. Firstly, solder joints are usually found in electronic devices that will be subjected to device working temperature and cool down to room temperature/ environment temperature while not in use. Therefore, such thermally activated process and thermal cycling process must be taken into consideration. Secondly, a solder joint has bulk microstructure as well as the interface. The mechanical test performed on the dog boned shape bulk solder alloys without interface could be very different from those solders joints with interfaces. In some mechanical tests, brittle failure tends to occur near the interfaces due to the brittle nature IMC as compared to the solders, especially under high strain rate or impact condition.

### 2.6.1 Effect of fourth alloying element on mechanical properties of SAC/Cu solder joints

Many minor fourth alloying elements have been added to SAC solder to improve in the mechanical properties. SAC solders are ductile by nature, however due to the interfacial reaction of Cu- Sn and polarity effect of electromigration on the interface, a ductile solder can transform into a brittle solder joint. Thus, fourth minor alloying elements were added into SAC to improve its mechanical properties by refining its microstructure and suppressing the brittle IMC formation at the interface. Some of these mechanical properties that have been studied include, shear, tensile, thermal cyclic, hardness, bend test, etc. The effect of different minor alloying elements (<5 %) on the mechanical properties of SAC are summarized in Table 2.4. Table 2.4 summarized the improvement in mechanical properties on the SAC solder joint/ solder matrix by adding various types of fourth alloying elements.

**Table 2.4** Effects of minor alloying element on the mechanical properties of SAC solder matrix.

<b>Element</b>	<b>Mechanical Properties on the solder joint/ solder matrix</b>	<b>Reference</b>
Ni	Improve UTS and yield strength.	El-Daly et al.,2013
	Improve ductility & proof stress. Improve creep.	A.E Hammad, 2013
	Similar or slightly reduced in hardness.	Liu et al, 2018
		Li et al, 2018
	Improved drop impact resistance.	Syed et al. ,2007
	Improved shear strength.	Sujan et al., 2014
Sb	Improved UTS at room temperature and after aging.	Li, 2006

**Table 2.4** continued.

<b>Element</b>	<b>Mechanical Properties on the solder joint/ solder matrix</b>	<b>Reference</b>
Co	Do not have effect on UTS, but reduced strain. Marginal increase in shear strength.	Fangjie et al.,2008 Anderson e al., 2004 Sujan et al., 2017
Mn	Increased hardness due to presence of MnSn <sub>2</sub> . Improved impact.	Lin, et al., 2008 ; Liu et al.,2007
In	Improved tensile strength and strain. Improved hardness. Improved impact.	Lin, et al., 2008 Kanyalasiri et al.,2009 Amagai et al., 2004
Zn	Improved UTS. Reduced shear strength, exhibit ductile shear. Improved hardness. Improved impact strength at room temperature and after aging.	El-Daly et al., 2013; Anderson et al., 2009
Bi	Improved UTS significantly. Improved hardness. Improved shear strength.	Huang & Wang, 2005 Bktiar Ali et al., 2016
Fe	Improve shear strength.	Fallahi et al., 2012
Al	Reduced in shear strength, but able to retain shear strength even after 1000hr aging. Improve tensile strength when 0.1 % Al was added, and Reduced in tensile strength whn 0.5 %Al was added.	Anderson et al., 2009 Shnawah et al., 2012
Rare earth element (Ce, La)	Improved tensile strength Similar creep properties	Zhang et al., 2009 Chen et al., 2003 Dudek & Chawla, 2010
Ga	Improved shear strength	Zhang et al. 2015 Luo et al., 2014
Ti (up to 1 %)	Improve impact	Chuang et al.2012

### 2.6.2 Nanomechanical properties

Nanoindentation as a mechanical testing method has attracted enormous attentions from many fields of research due to its ability in measuring properties of sample in extremely small scales size such as coatings and thin films in nanometer range (Huang et al. 2006; Bull, 2005). Nowadays, solder joints can have size ranged from micrometers to nanometers. Thus, conventional mechanical characterization test such as tensile, hardness or creep test obtained from bulk solder rod may not be appropriate and representative to the mechanical properties of small scale size solder joints. As the electronic devices are under going through miniaturization, this technique is suitable to investigate the mechanical properties of solder joints and intermetallic compound which have dimension as small as few micrometers or nano-meters. Thus, nanoindentation has been utilised extensively and has become essential modern mechanical testing equipment in characterizing properties of solder joints. Its ability to measure accurately at nanoscales has made it a powerful tool in characterizing of the hardness, elastic modulus, and creep behaviour of the various microphases in solder joints. Information on improving the mechanical properties of  $\text{Cu}_6\text{Sn}_5$  is especially important in the mechanical reliability of new lead-free solder interconnects as  $\text{Cu}_6\text{Sn}_5$  is a commonly formed IMC between Sn based solder and Cu substrate, and its brittle nature has cause much trouble in the reliability issues of solder joints.

Numerous works on the nanomechanical properties of solder matrix and Cu-Sn IMC has been done (Marques et.al, 2013; Mu et.al, 2012; Tsukamoto et.al, 2012; Jiang et al., 2010). The naomechanical properties of solder joints have been studied extensively, where there is systematic study on the relationship between the multiple reflow, aging hour, crystal orientation and location (relative to IMC boundaries) with respect to the nanomechanical properties of  $\text{Cu}_6\text{Sn}_5$  (Marques et.al, 2013; Mu et.al, 2013; Tsukamoto et.al, 2009; Jiang et

al., 2010). Table 2.5 shows the elastic modulus and hardness of all the phases that is found in the SAC/Cu and SA/Cu joints.

It was reported that at room temperature, the hardness of  $\text{Cu}_6\text{Sn}_5$  is ~6-7 GPa, while the Young's modulus have been reported in a wider range of 110-140 GPa (Marques et.al, 2013; Mu et.al, 2013; Deng et al., 2004; Song et al., 2012). The hardness of  $\text{Cu}_3\text{Sn}$  is slightly lower to that of  $\text{Cu}_6\text{Sn}_5$ , ~6 GPa, Young's modulus of  $\text{Cu}_3\text{Sn}$  is higher than that of  $\text{Cu}_6\text{Sn}_5$  by ~10 GPa in every reported literature (Marques et.al, 2013; Chawla et al., 2004; Song et al., 2012). Nogita et al., 2013 have found that multiple reflow have little influence on the elastic modulus and hardness of  $\text{Cu}_6\text{Sn}_5$ . On the other hand, increase of aging time and operating temperature, could reduce the elastic modulus significantly (Marques et.al, 2013; Mu et.al, 2013). Besides that, it was also found that there is a closed relationship between crystal orientation of  $\text{Cu}_6\text{Sn}_5$  and the mechanical properties of  $\text{Cu}_6\text{Sn}_5$ . A strong anisotropy in elastic modulus and hardness of  $\text{Cu}_6\text{Sn}_5$  found suggesting different deformation behaviours of (001) and (110) crystal planes (Mu et al., 2012).

**Table 2.5** Elastic modulus and hardness of Sn, eutectic, Cu,  $\text{Cu}_6\text{Sn}_5$ , and  $\text{Cu}_3\text{Sn}$  phase in SAC/ Cu or SA/Cu.

Phase	25°C		175°C		Ref
	H( GPa)	E( GPa)	H( GPa)	E( GPa)	
Sn	0.15 ± 0.04	49 ± 6	0.05 ± 0.01	24 ± 6	Marques et al, 2013
	0.22 ± 0.03	46.9 ± 2.7	-	-	Deng et al. 2004
Eutectic (SAC/Cu)	0.21 ± 0.03	62 ± 8	0.07 ± 0.01	32 ± 6	Marques et al, 2013

**Table 2.5** continued

Phase	25°C	175°C	Ref	Phase	25°C
Eutectic (SA/Cu)	0.21 ± 0.03	62 ± 8			Deng et al. 2014
Cu	1.97 ± 0.21	129 ± 5	1.45 ± 0.21	105 ± 16	Marques et al, 2013
	1.65 ± 0.17	116.5 ± 4.7	-	-	Deng et al. 2004
Cu <sub>3</sub> Sn	6.18 ± 0.39	140 ± 13	6.08 ± 0.63	139 ± 15	Marques et al, 2013
	6.70 ± 0.2	126.6 ± 3.0	-	-	Song et al, 2013
Cu <sub>6</sub> Sn <sub>5</sub>	6.67 ± 0.43	130 ± 9	5.58 ± 0.70	160 ± 30	Marques et al, 2013
	6.70 ± 0.08	117.3 ± 1.4	-	-	Song et al, 2013
	6.70 ± 0.7	124.6 ± 7.9	-	-	Mu et al, 2013
	6.38 ± 0.2	112.3 ± 5.0	-	-	Deng et al. 2004

### 2.6.3 Effect of additional element on the nanomechanical properties of Cu-Sn intermettalic.

As mentioned previously, there are a few fourth alloying elements that are soluble in Cu-Sn intermetallic compound. The solubility of these elements in Cu-Sn IMC was expected to have some impact on the mechanical properties of Cu-Sn. Only a few types of elements have been studied for their effects on the nanomechanical properties of Cu-Sn IMC. Table 2.6 shows the effect of Ni, Mn and Zn on the hardness and reduced modulus of Cu-Sn IMC. Nogita and co-workers has done numerous work on the effect of nickel atoms substitution in the (Cu,Ni)<sub>6</sub>Sn<sub>5</sub> IMC (Nogita et al., 2010; Mu et al., 2012; Mu et al., 2013). They have also investigated the effect of Ni on the nanomechanical properties of (Cu,Ni)<sub>6</sub>Sn<sub>5</sub>. Ni with solid solubility up to 4 at. % has increased both the elastic modulus and hardness of Cu<sub>6</sub>Sn<sub>5</sub>

significantly where elastic modulus has increased from 124.3 – 139.5 GPa while hardness has increased from 6.75 GPa – 8.6 GPa (Mu et al. 2013). The effect of Ni on Cu-Sn is even obvious after the sample has undergone thermal aging at 125 °C for 49 days, where solubility of Ni in Cu-Sn has increased the hardness and modulus significantly. After thermal aging,  $\text{Cu}_6\text{Sn}_5$  has hardness and modulus of 4.63 GPa and 54.67 GPa, while  $(\text{Cu},\text{Ni})_6\text{Sn}_5$  has hardness and modulus of 7.0 GPa and 139 GPa (Mu et al. 2013). Besides that, presence of Ni in Cu-Sn has also increased both Young's modulus and hardness of (110) and (001) planes (Mu et al. 2012). While the anisotropy in the elastic modulus of hexagonal  $\text{Cu}_6\text{Sn}_5$  was not significantly affected by Ni addition, the anisotropy in hardness was largely reduced. Song et al. (2012) have studied the effect of Mn in  $(\text{Cu},\text{Mn})_6\text{Sn}_5$  and  $(\text{Cu},\text{Mn})_3\text{Sn}$ . They reported that with solubility of Mn up to 1 % in  $(\text{Cu},\text{Mn})_6\text{Sn}_5$ , the hardness of the IMC has increased from 6.7- 7.1 GPa and while the effect on elastic modulus is not significant. On the other hand, there are no significant differences in the hardness and elastic modulus of  $\text{Cu}_3\text{Sn}$  and  $(\text{Cu},\text{Mn})_3\text{Sn}$ . They suggested that  $(\text{Cu},\text{Mn})_6\text{Sn}_5$  becomes harder due to the solid solution strengthening effect and it has a relatively lower plastic deformation due to the high E/H ratio (Song et al. 2012). Chen et al. (2015) has studied the effect of Zn additions on nanomechanical properties of  $\text{Cu}_6\text{Sn}_5$  at room temperature. They reported with solubility of Zn atom up to 0.5 at. % in  $\text{Cu}_6\text{Sn}_5$ , the hardness and Young's modulus of the IMC has slightly increased from 6.35 to 6.44 GPa and 120 to 128 GPa respectively, which does not seem very significant (Chen et al. 2015).

Table 2.7 summarizes the effect of solubility of Ni, Mn and Zn on the mechanical properties of Cu-Sn IMC. It could be seen that till date, detailed studies have been done only on the effect of Ni on the mechanical properties of Cu-Sn. Solubility of 0.5 % Zn in Cu-Sn shows slight increment on the hardness and reduced modulus, thus detailed studies

with various solubility of Zn % should be done to further verify the effect of Zn on Cu-Sn IMC.

**Table 2.6** Average values of elastic modulus and hardness of Cu-Sn IMC with and without addition of the fourth alloying element under various condition solder/Cu (after reflow, after aging, (001) and (100) crystal plane)

Element soluble in Cu-Sn IMC	Phase	As reflow		Thermal Aging (Ni – aging 125 °C, 49 days Mn- aging 150°C, 800 hr)		Reference
		H( GPa)	E( GPa)	H( GPa)	E( GPa)	
Ni	Cu <sub>6</sub> Sn <sub>5</sub>	6.7 ± 0.7	124.3±7.9	4.63 ± 0.56	54.27 ± 4.54	Mu et. al, 2013
	(Cu,Ni) <sub>6</sub> Sn <sub>5</sub> ~4 at. % Ni	8.6 ± 0.9	139.5 ± 4.9	7.0 ± 0.42	139.5 ± 4.9	Mu et. al, 2013
	Cu <sub>6</sub> Sn <sub>5</sub> (001)	6.0 ± 0.2	121.0 ± 2.5	-	-	Mu et. al, 2012
	Cu <sub>6</sub> Sn <sub>5</sub> (110)	5.7 ± 0.1	105.0 ± 1.8	-	-	Mu et. al, 2012
	(Cu,Ni) <sub>6</sub> Sn (001)	7.08± 1.8	128.39± 3.2	-	-	Mu et. al, 2012
	(Cu,Ni) <sub>6</sub> Sn (110)	7.04± 0.8	114.08± 2.4	-	-	Mu et. al, 2012
Mn	Cu <sub>6</sub> Sn <sub>5</sub>	6.749 ±0.147	125.845 ±3.054	6.628 ± 0.482	114.752 ± 7.814	Song et al, 2013
	(Cu,Mn) <sub>6</sub> Sn <sub>5</sub> ~1 at. % Mn	7.128 ±0.317	129.367 ±3.732	7.135 ±0.168	111.520 ±3.865	Song et al, 2013
	Cu <sub>6</sub> Sn <sub>5</sub>	6.25 ± 0.18	119.7± 3	-	-	Chen et al, 2015
Zn	Cu <sub>6</sub> (Sn,Zn) <sub>5</sub> ~0.5 at. % Zn	6.44 ± 0.14	127.8 ± 5	-	-	Chen et al, 2015

**Table 2.7** Summary of effect of fourth alloying element on Cu-Sn IMC

Element from Solubility to Cu-Sn Category (i)	IMC	Effect of minor alloying element on nanomechanical properties of Cu-Sn IMC
Ni	(Cu,Ni) <sub>6</sub> Sn <sub>5</sub>	(Cu,Ni) <sub>6</sub> Sn <sub>5</sub> becomes harder and more brittle at room temperature and high temperature compare to Cu <sub>6</sub> Sn <sub>5</sub> . Ni reduced creep of $\eta$ at room temperature and improve creep at 125 °C and 150 °C Ni also suppressed the $\eta$ to $\eta'$ transformation.
Mn	(Cu,Mn) <sub>6</sub> Sn <sub>5</sub> and (Cu,Mn) <sub>3</sub> Sn	$\eta$ becomes harder and more brittle. $\epsilon$ was not influence by Mn
Zn	Cu <sub>6</sub> (Sn,Zn) <sub>5</sub> and Cu <sub>3</sub> (Sn,Zn)	$\eta$ become slightly harder. Zn suppressed the $\eta$ to $\eta'$ transformation

## 2.7 Summary

In order to improve mechanical properties and reliability of solder joints, many studies on addition of minor fourth alloying element have been done. Many mechanical testing on the solder joints have been carried out and all these studies showed that some of the elements carry great potential in improving the reliability solder joints. However, as the solder joints are going through miniaturization, and the ratio of IMC to bulk solder are getting higher, it was at most important to investigate the effect of minor alloying element on the nanomechanical properties of the bulk solder joints and each IMC phases presence in the solder joint. Al and Zn are chosen as they have shown potential in improving the

interfacial reaction and mechanical properties of solder based on previous study. Till date, there are limited studies on effect of Al and Zn on the mechanical properties of SAC solder at the bulk microstructure and interfacial IMC, thus there is still a wide gap in investigating and understanding the mechanical properties, such as hardness, elastic modulus and creep properties of the bulk solder joints and IMC after reflow and after thermal aging on SAC with addition of Al and Zn. In this study, effect of (0.1-0.5 %)Al and Zn addition on the microstructure and mechanical properties the bulk SAC solder joints and IMC after reflow and after thermal aging will be investigated. Study on interrelation between solubility and distribution of Zinc in Cu-Sn IMC with the mechanical properties of Cu-Sn which is one of the research gap will be studied as well. Besides that, shear properties of SAC+ X will also be tested, and interrelationship between the microstructure and mechanical properties of bulk solder and IMC with the fracture mode will be study.

## CHAPTER 3: RESEARCH METHODOLOGY

### 3.1 Introduction

This chapter provides an outline of research methods used in the study. This chapter will give detailed procedure for solder joints sample preparation. Instruments used for characterization will be described and detailed parameters for each test will be provided. This chapter will also discuss the methods used to analyze the data. Figure 3.1 shows the flow chart of the experimental work in this study.

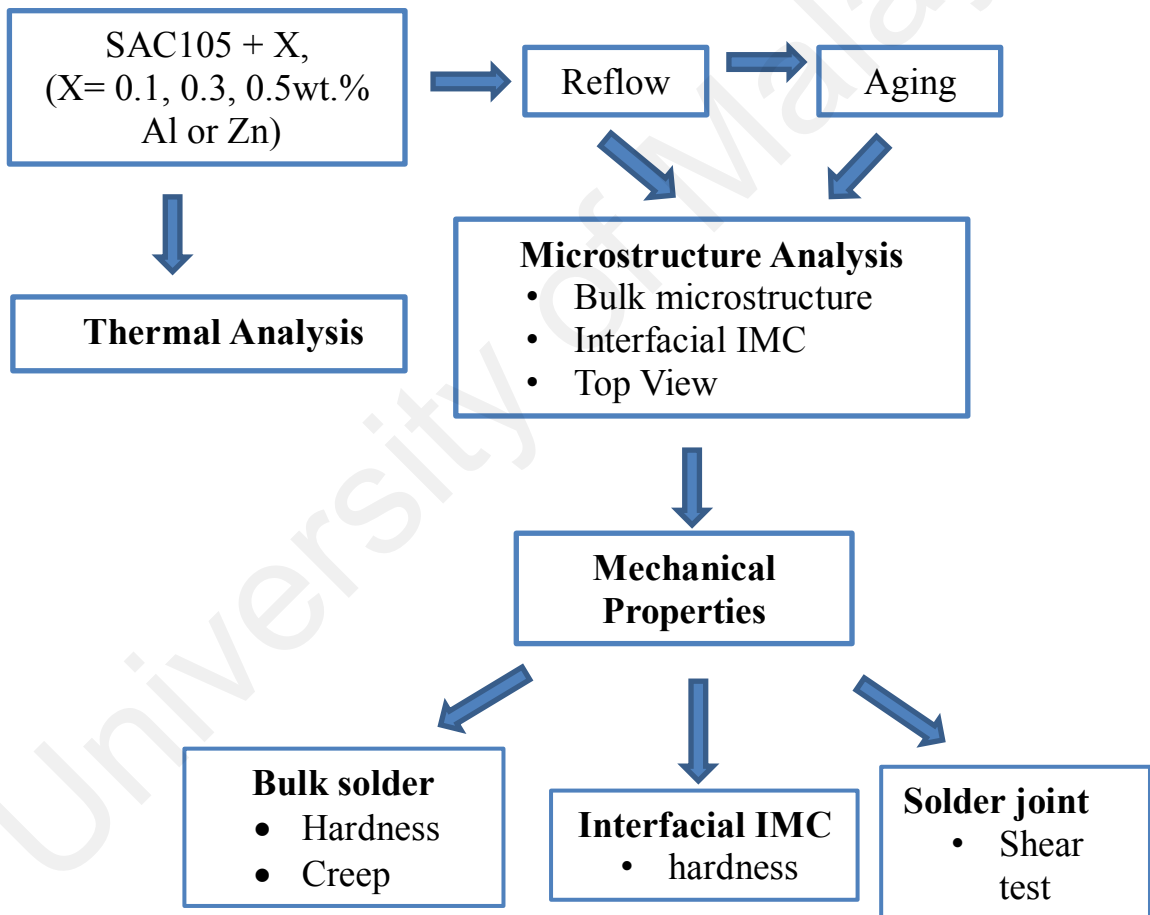


Figure 3.1 Flow chart of experimental work.

### **3.2 Solder joint sample preparation**

The solder alloys, SAC105+xAl and SAC+xZn solders (where  $x=0, 0.1, 0.3, 0.5$  wt. %), were supplied by Beijing Compo Advanced Technology Co Ltd (Beijing, China). The solder alloys were prepared by melting Sn and master alloys (such as SnAg, SnCu, SnZn, SnAl) in a medium frequency induction furnace at 300°C for 10 minutes. The molten was stirred for every 3 minutes for mixing. Then, the molten solder alloys were cast in a rod form with a diameter of 2 cm and a length of 15 cm. The solder alloys were then analyzed by inductively coupled plasma-optical emission spectrometry (ICP-OES) to determine the actual amount of Sn, Ag, Cu, Al or Zn composition in the solder. The ICP-OES test was conducted by Beijing Compo Advanced Technology Co Ltd and the results are shown in the table 3.1 below:

**Table 3.1** Alloy Compositions.

Alloy	Alloy composition (wt. %)												
	Sn	Ag	Cu	Al	Zn	Hg	As	Ni	Pb	Sb	Cd	Bi	Fe
SAC 105	98.372	1.023	0.540	<0.001	<0.001	<0.001	<0.005	<0.002	0.018	0.019	<0.005	0.014	0.014
SAC+0.1Al	98.270	1.036	0.526	0.110	<0.001	<0.001	<0.005	<0.002	0.012	0.019	<0.005	0.013	0.014
SAC+0.3Al	98.021	0.986	0.630	0.301	<0.001	<0.001	<0.005	<0.002	0.009	0.018	<0.005	0.014	0.012
SAC+0.5Al	97.911	0.997	0.538	0.496	<0.001	<0.001	<0.005	<0.002	0.014	0.018	<0.005	0.013	0.013
SAC+0.1Zn	98.288	1.004	0.553	0.002	0.101	<0.001	<0.005	<0.002	0.009	0.019	<0.005	0.012	0.012
SAC+0.3Zn	98.120	0.999	0.522	<0.001	0.312	<0.001	<0.005	<0.002	0.008	0.019	<0.005	0.014	0.014
SAC+0.5Zn	97.923	0.986	0.540	0.002	0.496	<0.001	<0.005	<0.002	0.011	0.018	<0.005	0.012	0.012

As-received alloy samples were cut into thin disk with a diameter of 6.5 mm and thickness of 1.4 mm by using wire-cut electric discharge machining (EDM). The disc-shaped solder alloys were ground with 3000 grit paper to smoothen the rough surface and remove surfaces oxides. Solder samples are soft alloys, thus they need to be prepared meticulously to avoid any scratches.

Polycrystalline copper plates were used for fabricating the solder joints. Copper plates with two different dimensions are prepared by using EDM machine. For the top copper plate of the joint, a disc shaped copper with a diameter of 7 mm and a thickness of 2 mm was used. While for the bottom plate, square-shaped copper substrates with dimension of 15 mm x 15 mm were cut into thickness of 3 mm. The copper substrates were ground with 3000 grit paper to smoothen the rough surface. They were then washed with detergent to remove the grease and oil stains. After that, Cu plates were soaked into 10 %  $H_2SO_4$  solution for 15-30 minutes to remove the oxides, and wiped it with acetone, to ensure that there was no contamination on the surface of the Cu substrates. Water soluble flux (Sparkle Flux WF-6317) supplied by Senju Material Industry Co., Ltd. was used. Flux was used to prepare the metal surface for soldering by removing any oxides and impurities during reflow. Water soluble flux is chosen in this study as it is a commonly used type of fluxes in the industry due to its ease of cleaning (flux residue can easily be removed by washing with water). A thin layer of water soluble flux was evenly spread on the top Cu substrate and the centre of bottom Cu substrate.

A SAC+ X solder disc was then placed between the top disc and bottom copper plates as shown in Figure 3.2. Samples were then subjected to reflow in a reflow oven in ambient air under a compression pressure of 5 MPa. Figure 3.3 shows the reflow profile used. The solder joints were preheated up to 220 °C, and soaked for 2 min for the activation of water

soluble flux. The solder joints were then heated up to 270 °C, reflowed for 2 min and cooled down to room temperature.

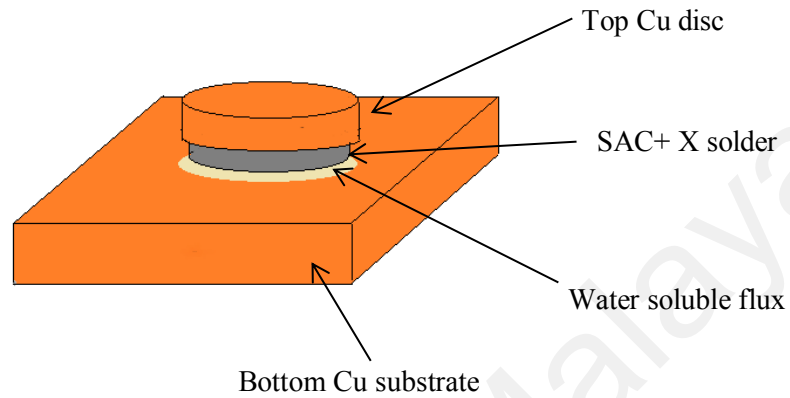


**Figure 3.2** Schematic diagram of SAC+X solder joint before it was subjected to reflow.

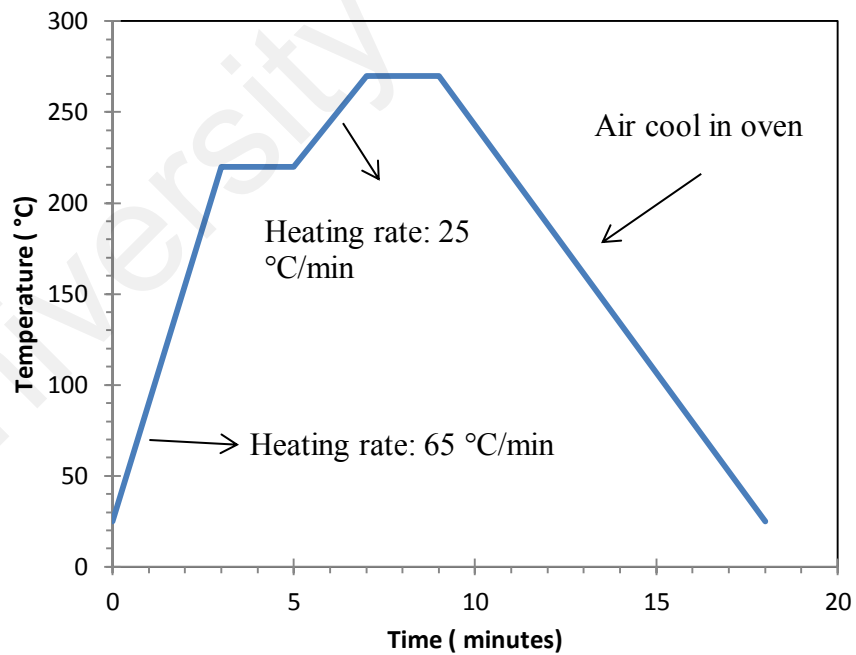


**Figure 3.3** Reflow soldering profile.

After reflow, some of the solder joints were subjected to thermal aging for 168 hr (1 week) and 1008 hr (1 month) in a Memmert universal oven (Mettler UN 260) at  $150 \pm 2$  °C. Thermal aging was used to accelerate the solid-state growth of the reaction layer (intermetallic compound) between the solder and the Cu substrate.

### **3.3 Sample characterization**

Thermal characterization, microstructure characterization and mechanical testing were conducted on SAC+ X samples. As received SAC+ X solders were subjected to X-ray diffraction (XRD), differential scanning calorimeter (DSC) test, and microstructure investigation. Microstructure investigation and mechanical testing (indentation test and shear test) were performed on SAC+ X solder joint samples.

#### **3.3.1 Differential scanning calorimeter (DSC)**

DSC (TA Instrument, Q20) was used to determine the effect of the addition of microalloying element (Al, Zn) on the melting characteristics of the SAC105 solder. The as-received solder was cut into small pieces (approximately  $10 \pm 0.5$  mg) to place into the Al pan. The aluminum pan was covered with a lid and was heated up to 300 °C and then cooled down to room temperature. Heating and cooling of test were controlled at a rate of 10 °C/min in air atmosphere. For each solder composition, DSC test was repeated for 3 times to ensure the reproducibility of the DSC results.

In general, there are 2 methods in determining the onset of melting, (i) first detectable deviation method and (ii) linear extrapolation method. Despite of the prevalent used of the method (ii), Boettinger et al. showed that there is actually smaller heating rate dependence and also lesser deviation from the actual melting point by using method (i) (Boettinger et al., 2006). Figure 3.3 shows the examples of errors that happened when the onset of melting of

non-eutectic alloy was determined by using extrapolation method. As seen in figure 3.4, pure metal has narrower trough, and the differential signal ( $\Delta T$ ) drops sharply right after the onset. Thus, there is not much difference in the onset temperature by using both methods. However, for non-eutectic composition metal alloy which have a wider trough and does not have a sharp drop in differential signal ( $\Delta T$ ) after the onset, there is no obvious linear portion to construct an extrapolated onset. Thus, in this case of non-eutectic composition metal alloy here is no theoretical basis in determining the onset by using extrapolation method (Boettinger et al., 2006). Since non-eutectic SAC105 solders were used in this study, thus first detectable deviation method was used in determining the onset of melting.

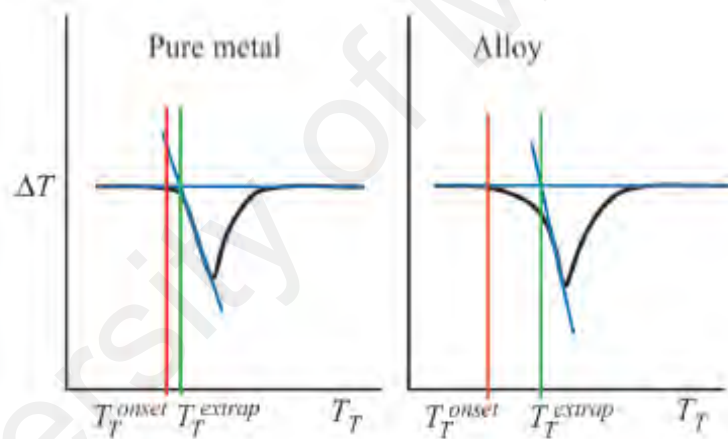


**Figure 3.4** Schematic DSC plots showing error induced by using extrapolation method for onset determination (Boettinger, 2006).

### 3.3.2 X-ray diffraction (XRD)

Phases present in the as-received solder (SAC105, SAC+ 0.5Zn, and SAC+ 0.5Al) were investigated by using XRD. Empyrean, PANalytical X-ray diffractometer using Cu K $\alpha$  ( $\lambda$  of 1.5418 Å) at 40 kV and 40 mA was used. The step size was set at 0.26 ° and the scan step time was 2.11s. Solder samples were scanned in Bragg angle ( $2\theta$ ) of 0 ° to 90 °. As-received samples alloy used were in the form of thin disk (diameter = 6.5 mm and thickness =1.4 mm). The disc-shaped solder alloys were ground with 3000 grit paper to smoothen the rough surface and remove surfaces oxides prior to the test. Peaks obtained from the XRD pattern were indexed by using the International Centre for Diffraction Data (ICDD) database. For each composition, XRD test was repeated for 3 times to ensure the reproducibility of the XRD results.

### 3.3.3 Field-emission Scanning Electron Microscopy (FESEM) equipped with Energy dispersive X-ray spectroscopy (EDS)

(a) Cross sectioned of as-received, reflowed solder and aged samples

Microstructure investigation of as-received, reflowed solder joints and aged solder joints samples were prepared by standard metallographic technique prior to the test. As received sample, reflowed and aged solder joints sample (cross-sectioned by diamond cutter) were mounted in epoxy and resin and dried in room temperature for 12 hours. The epoxy mounted samples were then ground by using 600, 800, 1000, 1500, 2000 and 3000 grit paper. It was then followed up with polishing by using diamond suspension of size 9  $\mu\text{m}$ , 3  $\mu\text{m}$  and 1  $\mu\text{m}$  and final polishing with colloidal silica (size 0.02  $\mu\text{m}$ ).

Zeiss Ultra-60 and FEI Quanta FEG 450 field emission scanning electron microscope were used to observe the cross sectional view of the solder. EDAX-Genesis Utilities and

Oxford instruments energy dispersive X-ray were used to determine the elemental composition of the phases presents in the solder by using spectroscopy spot analysis and elemental mapping. EDX analysis was carried out at 10-15 kV electron beam voltage and working distance of 8 mm-10 mm. By using image analysis software, IMC thickness was calculated from the FESEM micrographs. Mean thickness values were reported from measurement obtained from 5 micrographs.

#### (b) Top view of interfacial IMC

Prior to the top view microstructure investigation of the interfacial IMCs, solder joints were dipped in an etchant solution in order to remove the bulk microstructure and expose the interfacial IMC grain. Etchant solution was prepared by mixing 93 % Ethanol ( $\text{CH}_3\text{OH}$ ), 5 % Nitric Acid ( $\text{HNO}_3$ ) and 2 % Hydrochloric acid ( $\text{HCl}$ ).

The exposed IMC were observed under Zeiss Ultra-60 FESEM equipped with EDAX-Genesis Utilities EDS at various stages of experiments. EDX spectroscopy spot analysis and map scanning were carried out to determine the element distribution on the top of interfacial IMCs.

#### **3.3.4 Field emission electron probe for micro-analysis (FE-EPMA)**

JEOL-8500F field emission electron probe micro-analysis equipped with wavelength dispersive X-ray spectroscopy (WDS) was carried out at Joining and Welding Research Institutes, Osaka University, Japan. It was used to quantify the composition of IMC which could not be accurately quantified by EDX, for example composition of Zn in  $\text{Cu}_6\text{Sn}_5$  IMC. The EDX results might not be accurate as the result can be affected by the peak interference. A mutual interference of Cu and Zn can occur since the peaks between Cu  $K\alpha$  (8.04

keV)-Zn K $\alpha$  (8.637 keV), and Cu L $\alpha$  (0.93 keV)-Zn L $\alpha$  (1.012 keV) lie only in the energy range of 0.65 keV and 0.17 keV respectively (Goldstein, 2003; Internet Reference, 18/4/2011). In EDX qualitative analysis, it is very difficult to detect the minor element when it is interfered by the major element peak (Goldstein, 2003). Thus, solubility of Zn in Cu<sub>6</sub>Sn<sub>5</sub> (reported max solubility = 6 at. %) could only be quantified by EPMA. WDS analysis was carried out at 20 kV electron beam voltage and working distance of 11 mm. Spot analysis, line scanning and map scanning were carried out to determine the compositions Zn in the interfacial IMC.

### **3.4 Nanoindentation**

Nanoindenter machine (Brand: Hysitron, Model: Ubi-750) was used to perform nanoindentation testing. Prior to the test, an isotropic standard silica sample was used to calibrate the system. Nanoindentation performed on the small IMC phases were precisely positioned by using In-Situ Scanning Probe Microscopy (SPM). Berkovich diamond tip with radius of 100 nm was used to carry out the nanoindentation testing.

Reflowed and aged solder joints samples were prepared by standard metallographic technique (Section 3.3.3(a)) prior to the test. Nanoindentation test was conducted immediately after the final polishing to prevent oxidation of the samples.

#### **3.4.1 Hardness and Modulus**

There are two nanoindentation mode used in this study: Load- control Quasi Static and Continuous dynamic measurement (CMX). For nanoindentation performed on the bulk microstructure, quasi static mode was used (loading rate and unloading rate = 16.67 N/s, maximum load = 0.1 N, hold time at the peak = 2 s.). For each sample, arrays of 100

indentations with spacing of 10 $\mu$ m apart were positioned at the region of interest (center of the solder matrix). The large spaced out between indents was necessary so that the impression from one indent does not affect the readings taken for the next indent. For nanoindentation performed on the small IMC in the solder matrix and interfacial IMC, continuous dynamic measurement mode was used (loading rate and unloading rate = 16.67  $\mu$ N/s, maximum load = 1000  $\mu$ N, hold time at the peak = 2 s).

Oliver and Pharr's method is a popular method used to obtain hardness (H) and elastic modulus (E) in nanoindentation. This method assumed that the unloading behavior was completely elastic. Thus, by plotting load vs displacement curve, contact stiffness can be obtained from the slope of the unloading curve. This information enabled the computation of reduced elastic modulus.

The reduced elastic modulus can be computed by,

$$E_r = \frac{S}{2\beta} \sqrt{\frac{\pi}{A_c}} \quad (3.1)$$

Where S is the stiffness at the onset of the unloading curve,  $A_c$  is the projected contact area between the probe and material and  $\beta$  is the correction factor for the shape of indenter constant (usually taken as 1.034 for Berkovich tip).

By assuming elastic displacement occur in both indenter and sample, the elastic modulus of the sample  $E_s$  can be calculated from the reduced modulus  $E_r$  using the following equation:

$$\frac{1}{E_r} = \frac{(1 - \nu_i^2)}{E_i} + \frac{(1 - \nu_s^2)}{E_s} \quad (3.2)$$

where  $\nu_i$  is the poisson ratio of indenter,  $E_i$  is the elastic modulus of indenter,  $\nu_s$  is the poisson ratio of sample. For a diamond indenter tip,  $E_i = 1140$  GPa and  $\nu_i = 0.07$  while  $\nu_s$  was assumed to be 0.309 for  $\text{Cu}_6\text{Sn}_5$  (Oliver & Pharr, 2004).

Hardness is defined the ability of a material to resist deformation when it was subjected to load. Thus, hardness is measured by, the maximum indentation load ( $P_{\max}$ ) divided by the projected contact area ( $A_c$ ).

$$H = \frac{P_{\max}}{A_c} \quad (3.3)$$

#### 3.4.2. Creep

Nanoindentation creep tests were performed on the bulk specimens at a loading rate of 1 mN/s up until maximum load of 10 mN and were hold for time of 900 s. The test was conducted using Hysitron nanoDMA® III reference creep mode. 20 indentations were made for each sample to obtain the mean values. All results with drift rates exceed 0.5 nm/s was eliminated to ensure accountability of the creep test.

### 3.5 Shear test

For shear test, solder joints samples were placed in a customized shear jig and were sheared by using a universal testing machine (Instron 3369). Figure 3.5 shows the image and schematic setup of the shear test. The bottom Cu substrate of the solder joints was clamped to a customized jig. The bottom customized jig remained stationary throughout the test while a customized shearing top fixture moved downwards and shear pushed the top Cu substrate with a shear strain rate of 0.1 mm/s. The strength of the on each SAC+ X solder

joints were obtained by the average of three trials. After shearing, the fracture surfaces were observed by FESEM equipped with EDS for failure analysis.

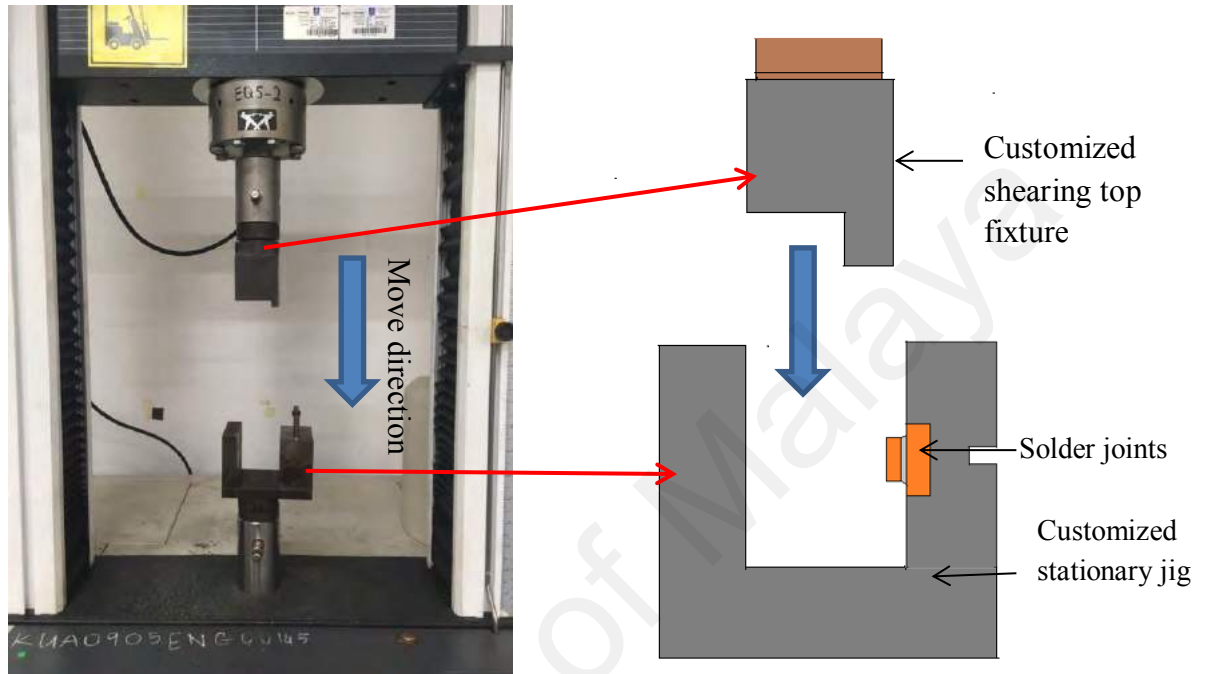


**Figure 3.5** Image and schematic diagram of the shear test set up.

## CHAPTER 4: RESULTS AND DISCUSSIONS

This chapter contains two major parts: (1) Thermal and microstructural analysis of SAC + X (X= Al, Zn) alloy and (2) Mechanical properties of SAC +X solder joints. In the first section, thermal analysis and the microstructural properties of SAC+ X samples are decided. Mechanical properties of SAC + X solder joints characterized by nanoindentation and shear test are presented in the second section.

### 4.1 Thermal Analysis

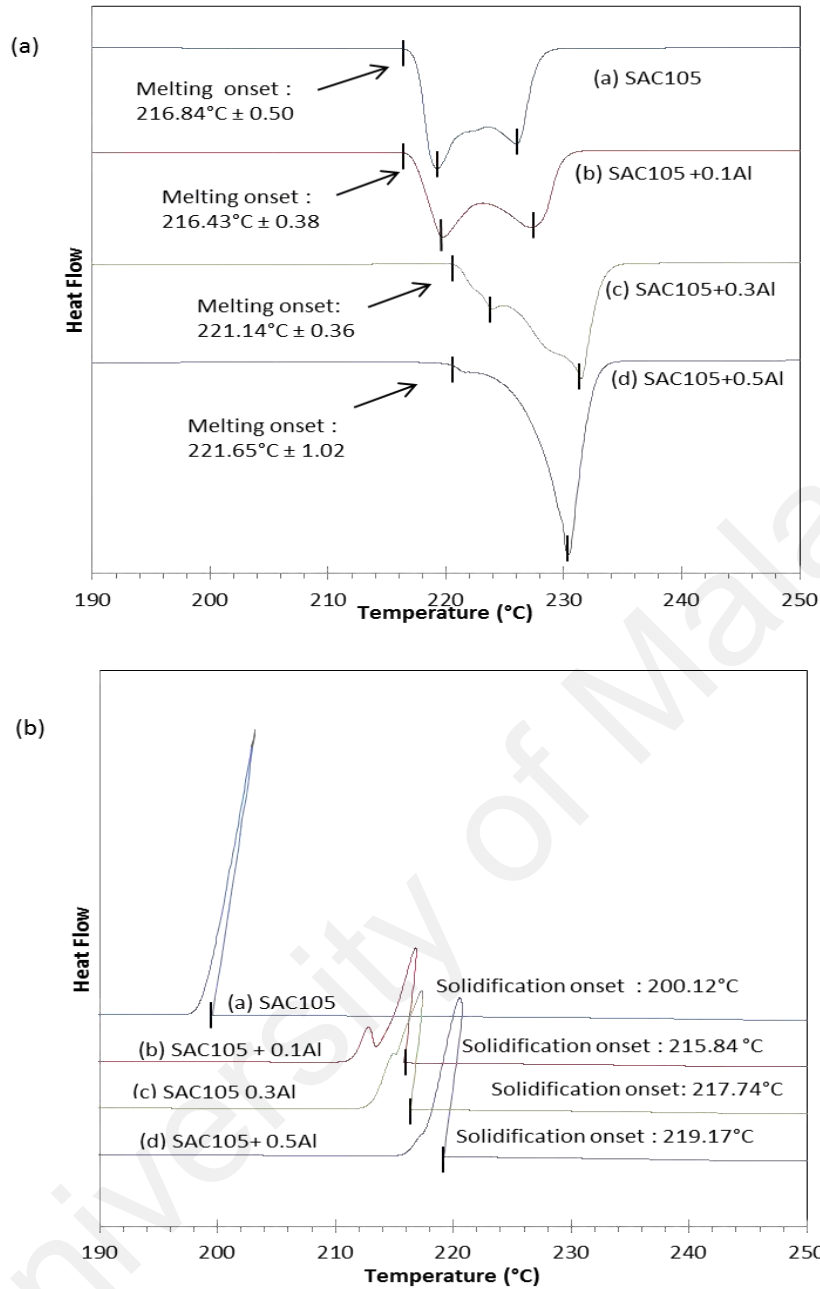
The first approach of this investigation is to characterize the effect of Al and Zn on of SAC 105. Thermal analysis of SAC + X (X =0, 0.1, 0.3, 0.5 % Al or Zn) solders were carried out by DSC. Studying the endothermic and exothermic curves of SAC + X will reveal the effect of minor alloying element Al and Zn on the phase transformation of SAC105. The melting and solidification of the solders play an important role in the microstructure properties of solder joints.

#### 4.1.1 Melting and Solidification Behaviour of SAC +X

Figure 4.1 shows the DSC curves for SAC + X (X = 0, 0.1, 0.3, 0.5 % Al). The onset melting temperature ( $T_m$ ) of SAC 105 is  $216.84\text{ }^\circ\text{C} \pm 0.50$  while that for SAC+0.1Al is  $216.43\text{ }^\circ\text{C} \pm 0.38$ . Based on the Sn-Ag-Cu phase diagram, the onset melting temperature for both SAC105 and SAC+0.1Al corresponds to the ternary eutectic reaction  $L \rightarrow \text{Ag}_3\text{Sn} + \text{Cu}_6\text{Sn}_5 + \text{Sn}$  at  $217\text{ }^\circ\text{C}$  (Kattner, 2000). From Figure 4.1a and 4.1b, it was observed that there were 2 prominent peaks at temperature of  $\sim 221\text{ }^\circ\text{C}$  and  $\sim 228\text{ }^\circ\text{C}$  for SAC105 and SAC+0.1Al solders. Referring to phase diagram (Fig. 2.3 and Fig. 2.5), the 2

peaks are associated with the eutectic temperature for Sn-Ag ( $L \rightarrow Ag_3Sn + Sn$ ) and Sn-Cu ( $L \rightarrow Cu_6Sn_5 + Sn$ ) respectively (Hayes et al., 1985; Oh et al., 1996). As Al is added up to 0.3 % and 0.5 %, the shape of the DSC curve changes (Fig 4.1a). For SAC+0.3Al, the onset temperature shifted to a higher temperature of  $221.14 \pm 0.36$  °C while for SAC+0.5Al, it shifted to  $221.65 \pm 1.02$  °C. These temperatures corresponds to Sn-Ag eutectic temperature ( $T_m=221$ °C). For SAC105+0.3Al, a first smaller peak of heat absorption appears immediately thereafter at 224 °C, a second larger peak of heat absorption then appears at  $\sim 231$  °C (Fig. 4.1a). Whereas for SAC105+0.5Al, only one large peak of heat absorption appears at  $\sim 231$  °C. The peak at  $\sim 231$  °C corresponds to the melting temperature of Sn ( $T_m=231$  °C).

The onset solidification of the exothermic peak during cooling can determine the nucleation temperature (Fig.4.1 b) (Gunther et al., 2011; Kashchiev et al., 2000). SAC105 has onset solidification at  $200.12$  °C  $\pm 0.64$ . Addition of aluminium to SAC105 have shifted the exothermic peak to the right, where the onset solidification temperature is  $215.84 \pm 1.39$  °C,  $217.74 \pm 0.83$  °C and  $219.17 \pm 0.21$  °C for SAC+0.1Al, SAC+0.3Al and SAC+0.5Al respectively. The degree of undercooling,  $\Delta T$ , was calculated by the difference of onset of melting and onset of solidification ( $T_s$ ),  $\Delta T = T_m - T_s$ . From Table 4.1, it is seen that SAC105 has the largest undercooling of  $\sim 17$  °C. The addition of Al up to 0.5 % into SAC105 solder has reduced the degree of undercooling significantly. Besides that, it could be seen SAC+0.1Al has two exothermic peaks. The two peaks at  $\sim 217$  °C and  $\sim 213$  °C correspond to the solidification of  $\beta$  Sn and eutectic reaction respectively (Luo et al., 2010).



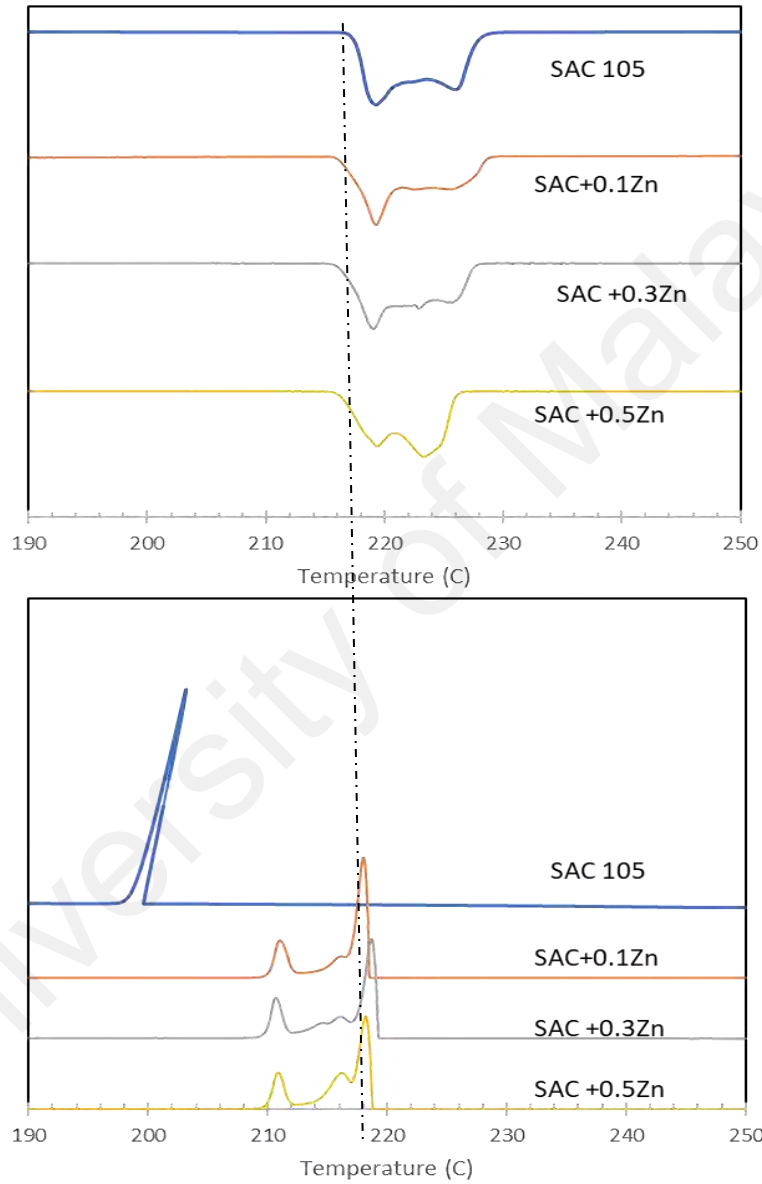
**Figure 4.1** shows the (a) endothermic and (b) exothermic DSC curves of SAC 105, SAC +0.1Al, SAC +0.3Al and SAC +0.5 Al.

Figure 4.2 shows the DSC curves for SAC + X (X = 0, 0.1, 0.3, 0.5 % Zn). From Figure 4.2, it could be seen that the addition of minor alloying Zn does not alter the melting profile

of SAC105. All the SAC 105 and SAC +Zn samples show the ternary eutectic  $T_m$  of ~216-217 °C. From the exothermic curve of SAC + Zn, it is seen that the addition of Zn has shifted the onset of solidification and reduced the undercooling greatly. It could be seen that the onset of melting and onset of solidification is very close in all SAC + Zn samples, and the undercooling does not seem to vary much with the Zn content ranges from 0.1-0.5 % in SAC. However, from table 4.1, it could be seen that onset of solidification is higher than the onset of melting, this leads to a negative value of undercooling. Some DSC studies in the literature have reported such phenomenal. It was surmised that these variations could come from several sources such as heating, cooling rate (recrystallisation events are influenced by the scan rate where onset of solidification shifted to higher temperatures as a function of increasing scan rate) or specimen size effects (large sample size could induce thermal lag on the sample causing shifting of higher temperature) (Gibbs et al., 2016; Gabbot, 2007)

The sample size we used in the DSC test was 10 mg (maximum acceptable sample size weight for the equipment DSC Q20, TA instrument). Since the minimum sample size we could prepare for the DSC sample is 10mg, thus, the only variation we could made is by changing the heating and cooling rate. Another set of DSC test was carried out at heating rate and cooling rate of 1 °C/min, 10 times slower than the previous test. Yet, another set of DSC test was carried out at 1 °C/min under heat-cool-heat-cool cycle to reduce the test error. However, all the results are still the same where SAC+Zn samples exhibited exothermic curve which has a slightly higher onset of solidification (~2-4 °C) than the onset of melting. Kang et al. (2007) also reported a slightly higher onset of solidification (undercooling ~ -2 °C) when they added 1 % Zn into Sn-1.0Ag-0.9Cu and that Zn is effective in reducing the amount of the undercooling. When they added Zn up to 0.6% into Sn-3.0Ag-0.5Cu, the undercooling of SAC was reduced significantly with a positive value

(undercooling  $\sim +2$  °C). Although it was unsure what causes the slight negative value of undercooling, but both studies (Kang et al. and our studies) shows that minimal addition of Zn would reduced the undercooling of SAC close to zero.



**Figure 4.2** shows the (a) endothermic and (b) exothermic DSC curve of SAC 105, SAC +0.1Zn, SAC +0.3Zn and SAC +0.5Zn

**Table 4.1** shows the onset of melting, onset of solidification and undercooling of SAC 105, and SAC +X( X= 0.1, 0.3, 0.5 % Al or Zn).

<b>Sample</b>	<b>Onset of melting ( °C)</b>	<b>Onset of solidification ( °C)</b>	<b>Undercooling ( °C)</b>
SAC105	216.84 ± 0.5	200.12 ± 0.64	17
SAC+0.1Al	216.43 ± 0.38	215.84 ± 1.39	0.6
SAC+0.3Al	221.14 ± 0.36	217.74 ± 0.83	3.4
SAC+0.5Al	221.65 ± 1.02	219.17 ± 0.21	2.48
SAC+0.1Zn	216.8± 0.30	219.5± 0.50	-2.7
SAC+0.3Zn	216.5± 0.12	220.5± 0.48	-4.0
SAC+0.5Zn	216.48± 0.03	219.2 ± 0.36	-2.8

## 4.2 Microstructure Analysis

The few microstructure of the solder alloys were examined to study the effect of minor alloying Al or Zn on the bulk as well as interfacial microstructure after reflow and after 1 month aging. EDS elemental analysis was also carried out to identify type of IMC that formed in the solder joints.

#### **4.2.1 Microstructure Characterization of As-received Solder**

Figure 4.3 (a-d) shows the optical images of cross sections of as received solder. The as received solders are produced by melting master alloys in a medium frequency induction furnace at 300 °C, the molten alloys are then cast into a cylindrical rod. Cross sectional images of SAC105 before reflow shows primary Sn phase having a lighter contrast while  $\text{Cu}_6\text{Sn}_5$  phase having a darker contrast. With the addition of 0.1 % Al,  $\text{Cu}_6\text{Sn}_5$  and another new small and even darker phase are seen distributed rather evenly in the Sn phase. At 0.3 % Al, the new small and darker IMC phase (this particle is actually  $\text{Cu}_3\text{Al}$ , it will be discussed further in section 4.2.2) is seen to have agglomerated and segregated into ‘islands’ in the Sn matrix. For SAC+0.5Al solder, the segregation of the darker IMC phase is even more obvious as seen in Figure 4.3(e). Besides that, the grain size of Sn in the as-received solder decreased as a function of Al content. With the addition of Zn, finer  $\text{Cu}_6\text{Sn}_5$  phase network are seen distributed in the Sn phase. Sn grain size in the as-received solder decreased as a function of Zn content. No Cu-Zn IMC compound was found and detected in all the as received Zn added solder.

#### **4.2.2 Microstructure of Bulk Solder After Reflow and Thermal Aging for 1 Month**

The bulk microstructure of SAC +X solder joints was characterized by field emission scanning electron microscope (FESEM) equipped with energy dispersive X-ray (EDX) spectroscope, X-ray diffraction (XRD) and transmit electron microscope (TEM). In the following sections the details of the characterization of SAC +X will be presented.

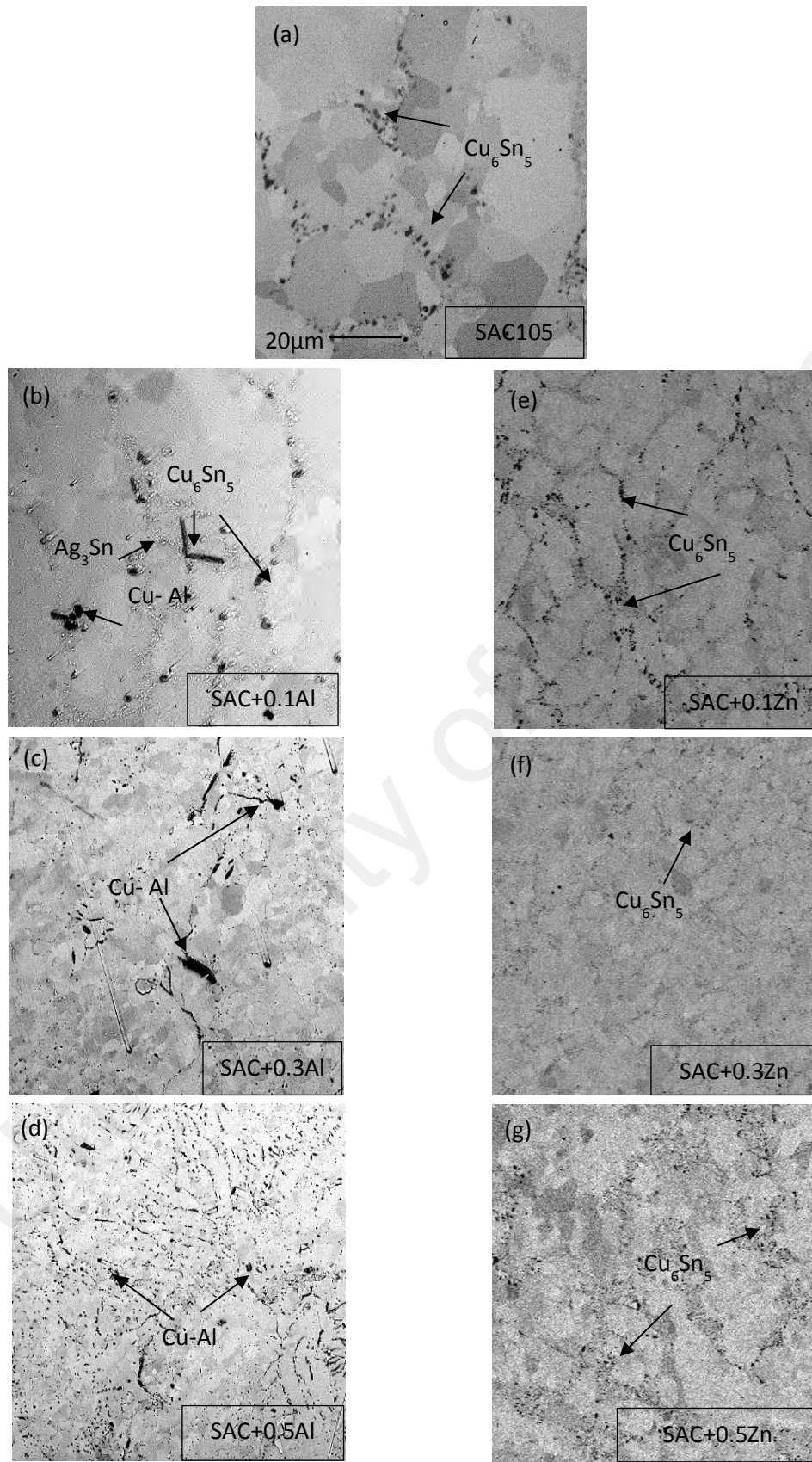
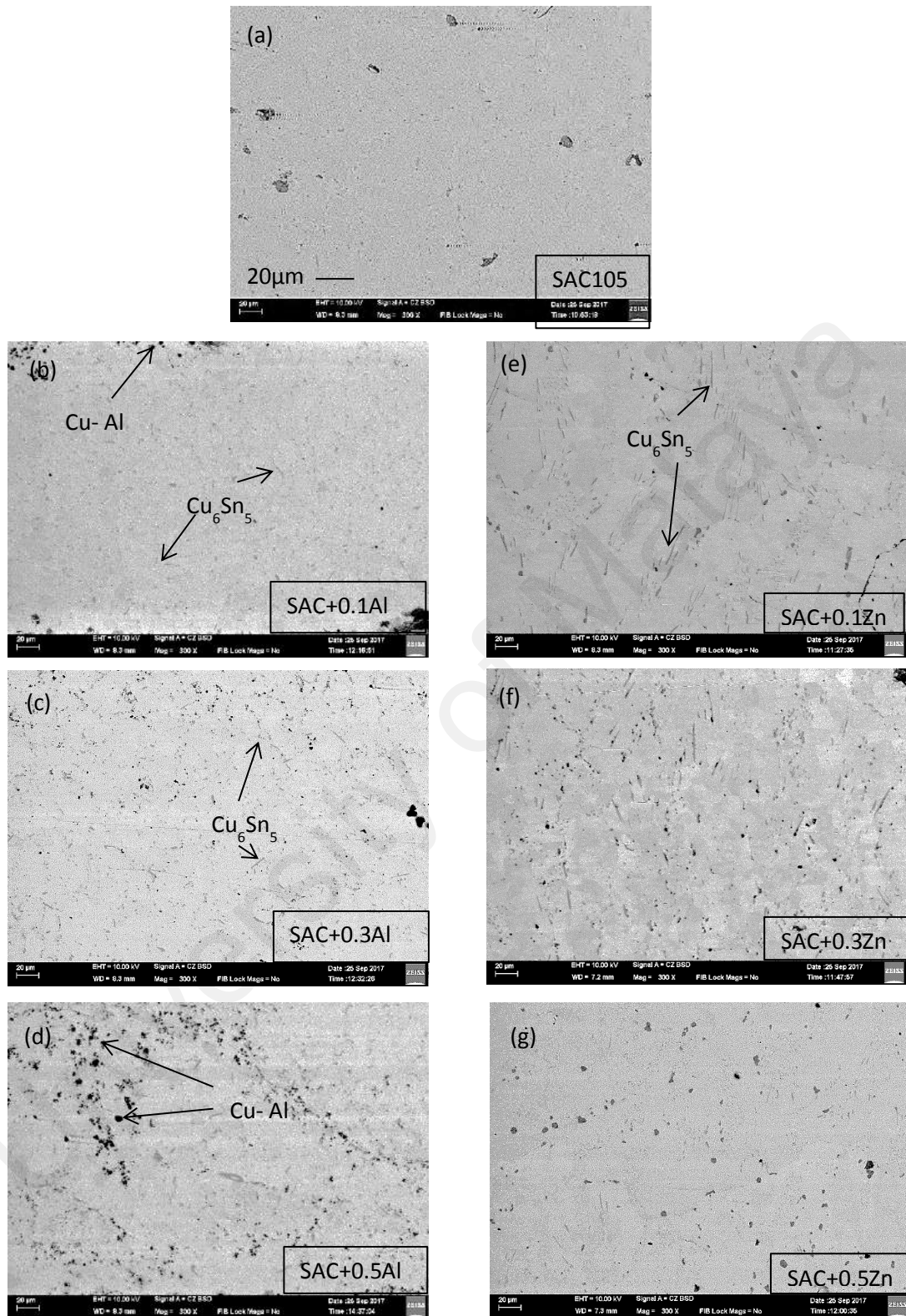


**Figure 4.3** Cross sectioned SEM micrographs of as-received SAC +X.

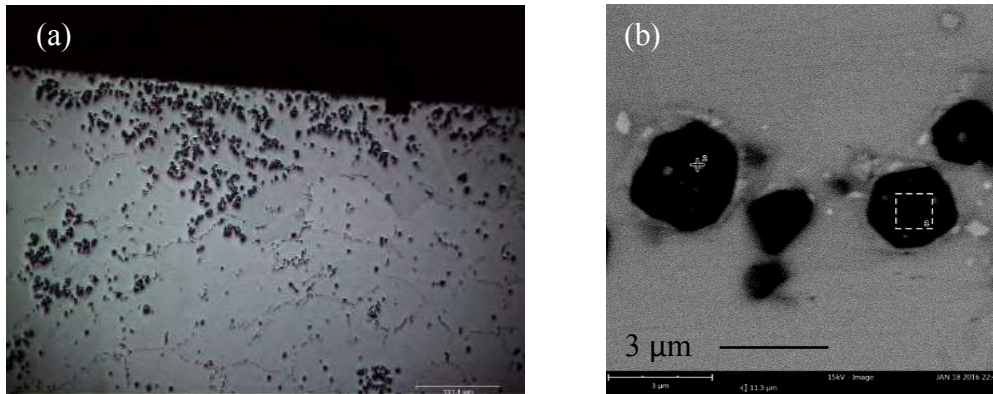
**(a) Field Emission Scanning Electron Microscope (FESEM)- Energy dispersive X-ray (EDX) spectroscopy**

Figure 4.4 shows the FESEM images of cross section of SAC +X after reflow sandwiched between two Cu substrates. For minor Al addition, the bulk microstructure of the SAC+Al/Cu is similar to the microstructure of as-received solder after reflow. Agglomeration and segregation of small and darker IMC phase is found as Al is added up to 0.3 %. From FESEM observation,  $\text{Ag}_3\text{Sn}$  is found in SAC105 and  $\text{Cu}_6\text{Sn}_5$  phase has long small, thin needle-like morphology (Fig 4.4b). Under high magnification (Fig 4.5), the new darker IMC phase shows a rather equiaxed but faceted morphology, with sizes ranged from 1 to  $5\mu\text{m}$ . Besides, when the solder was reflow on a copper substrate without sandwiched between 2 copper substrates, it can be observed that the new darker phase equiaxed IMC was mostly found near the top surface of the solder joint (Fig 4.5). While in a solder joints with solder sandwiched between 2 copper substrates, the new darker IMC phase was seen agglomerated randomly in the solder joints with most of them in the middle region between 2 copper substrates.

On the other hand, with addition of Zn, more rounded shaped  $\text{Cu}_6\text{Sn}_5$  IMCs was found in the solder matrix SAC+0.3Zn and SAC+0.5Zn, in contrast with the elongated rod-shaped  $\text{Cu}_6\text{Sn}_5$  that was found in SAC105 and SAC 105+0.1Zn.



Figures 4.4 Cross-sectioned FESEM image of SAC +X after 1 x reflow.



**Figure 4.5** (a) Optical microscope cross sectional images SAC105+0.5Al near top surface of the solder after 1 × reflow and (b) FESEM images of equiaxed but faceted IMCs found at cross-sectioned of SAC105+0.5Al.

Figure 4.6 shows the bulk microstructure of SAC + X after 1 month aging. From Figure 4.5 and 4.6, it is observed that the  $\text{Cu}_6\text{Sn}_5$  IMC in the bulk microstructure of aged sample is larger as compared to those in 1x reflow. For all SAC +X samples, not much difference was seen as compared to after reflow besides the IMCs enlargement, except for SAC +0.5 Al. It can be seen in Figure 4.7 that besides the darker new IMC phase found after 1x reflow, some of the dark new IMC seems to grow horizontally along the Sn grain boundary and forms an irregular line.

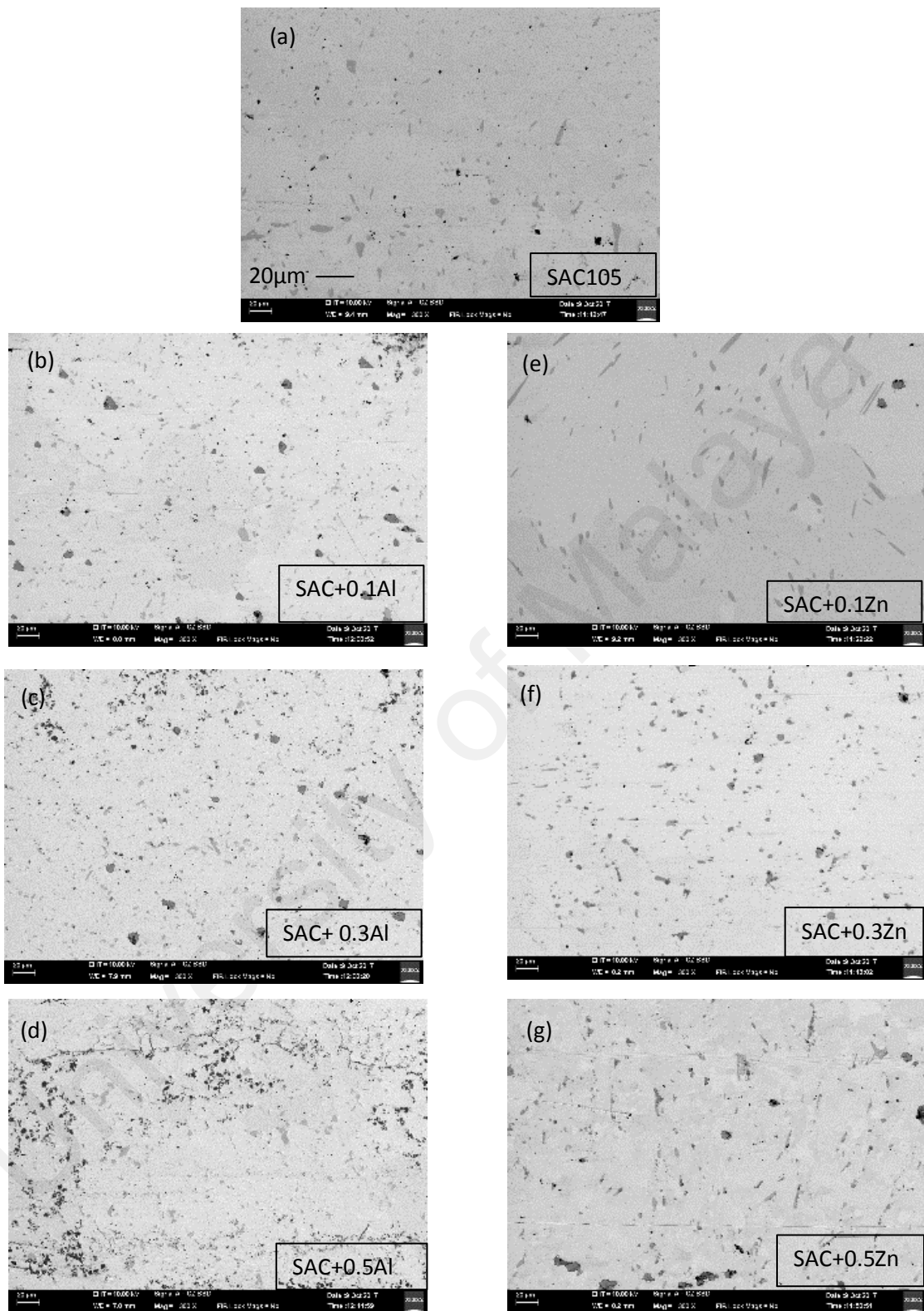


**Figure 4.6** Cross-sectioned FESEM image of SAC +X after 1 month aging.

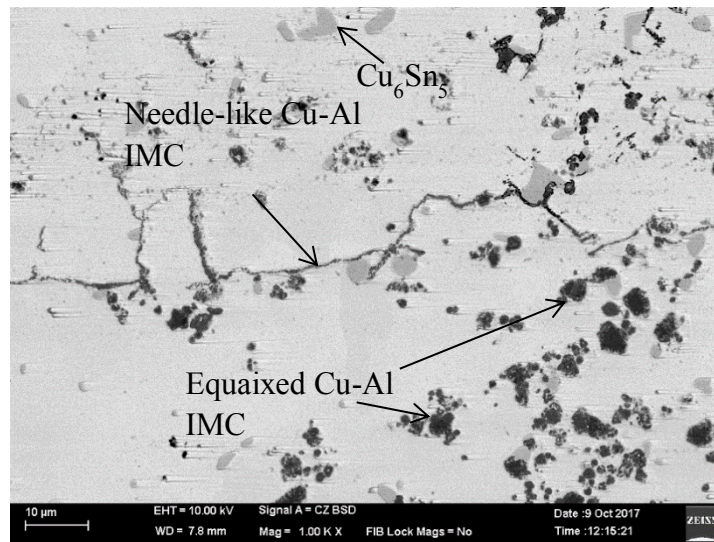


**Figure 4.7** The ‘needle-like’ IMC found in solder matrix of SAC+0.5 Al (after 1 month aging) under high magnification.

EDS analysis was conducted on the new darker equiaxed IMC phase found in SAC+ Al samples (after reflow and after aging) and the irregular line IMC that was found in SAC+0.5Al after thermal aging for 1 month. Compositional analysis conducted by EDS showed that the composition of both new phases consists of only Cu and Al (Figure 4.8), where it consists of 60–65 at. % Cu and 35–40 at. % Al. To further investigate these IMCs, EDS line scan and elemental mapping analysis were conducted on the new equiaxed IMC phase (Figures 4.9 and 4.10) while elemental mapping analysis were conducted on the irregular line IMC (Figure 4.11). Both analysis confirmed that this dark equiaxed IMC and irregular line phase consists of only Al and Cu. Based on the ratio of Al and Cu content, possible identification of this darker IMC phase is  $\text{Cu}_3\text{Al}_2$  ( $\delta$ ) or  $\text{Cu}_9\text{Al}_4$  ( $\gamma_1$ ), both of which could exist in the temperature range below 300 °C. However, the chemical composition taken from EDS cannot be used to quantify the exact composition of a phase under

investigation, thus further XRD analysis would be conducted to identify the new Al-Cu phase found in SAC+ Al samples.

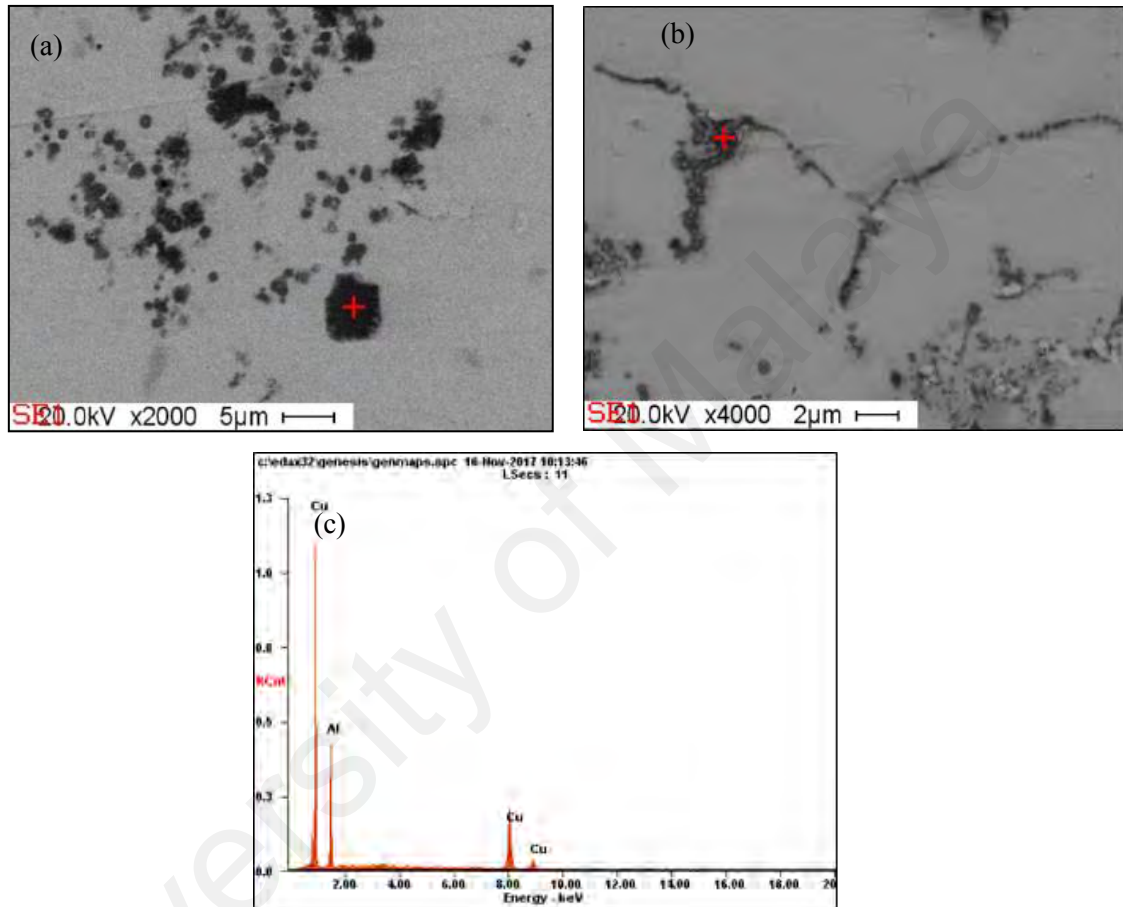


**Figure 4.8** Crossed sectional FESEM images of (a) equiaxed IMC and (b) needle-like IMC found in SAC+0.5Al after 1 month aging. (c) EDX spectrum of equiaxed and needle-like IMC.

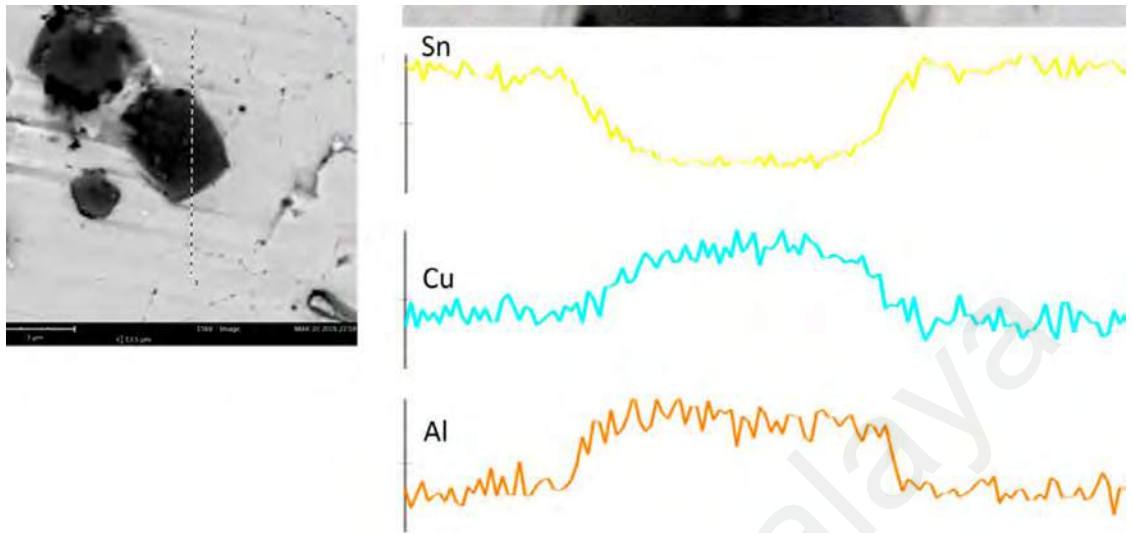


**Figure 4.9** EDS line scan across equiaxed IMCs in SAC+0.5Al after reflow.

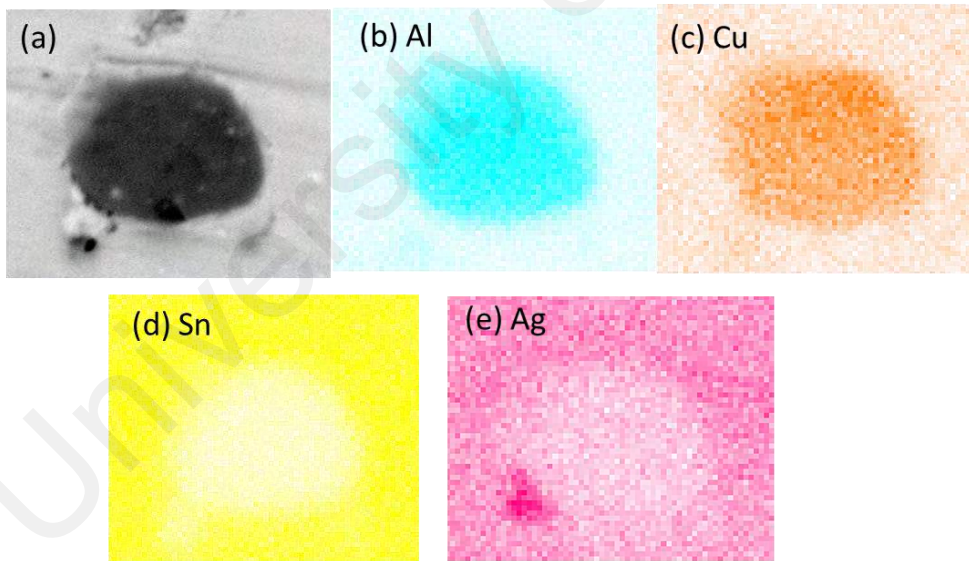


**Figure 4.10** (a) Cross-sectioned image of SAC+0.5Al after reflow. Elemental maps for the constituent elements: (b) Al; (c) Cu; (d) Sn; and (e) Ag.

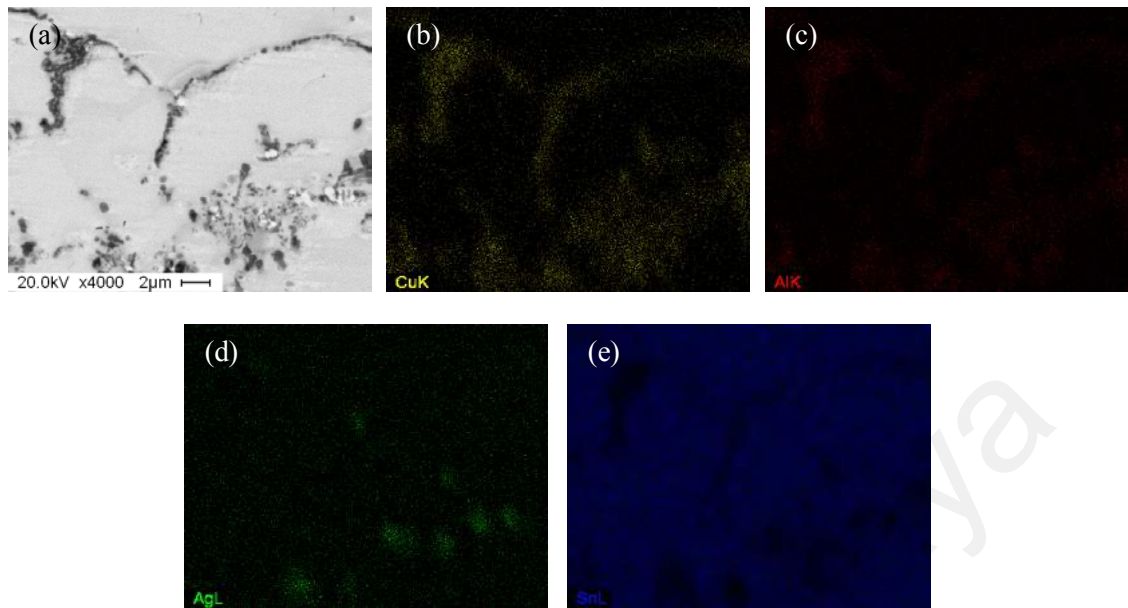


**Figure 4.11** (a) Cross-sectioned FESEM image of SAC+0.5Al after 1 month thermal aging. Elemental maps for the constituent elements: (b) Cu; (c) Al; (d) Ag; and (e) Sn.

**(b) XRD (X- Ray Diffraction)**

XRD analysis was tested on SAC105 and SAC+ 0.5Al samples. Figure 4.12 shows the X-ray diffractogram of both samples. There are many similar peaks in both diagrams which corresponded to the Sn, Cu,  $Ag_3Sn$ ,  $Cu_6Sn_5$  peak. According to the phase diagram of the Al-Cu system (Figure 4.13), there are six IMC phases that may form at temperatures below 363 °C, which are  $\theta$ - $CuAl_2$ ,  $\eta_2$ - $CuAl$ ,  $\gamma_1$ - $Cu_9Al_4$ ,  $\zeta_2$ - $Cu_4Al_3$ ,  $\delta$ - $Cu_3Al_2$ , and  $\alpha_2$ - $Cu_3Al$ . After indexing all the XRD peaks with all the possible elements, it is very likely the new Cu-Al phase found in SAC+ Al sample is  $\alpha_2$ - $Cu_3Al$ , although the EDS analysis for the Al and Cu content tell otherwise. The evidence that the new phase is  $\alpha_2$ - $Cu_3Al$  in the presence of the 42.85 ° (111) and 74.85 ° (110) superlattice peaks (dashed circle in diagram 4.12). The 2 $\theta$

peaks at  $42.85^\circ$  and  $74.85^\circ$  that exist in SAC + Al samples are the only characteristic superlattice peaks that are expected from an ordered  $\alpha_2$ -Cu<sub>3</sub>Al and at the same time these could not be indexes to other phase (Sn, Cu, Ag<sub>3</sub>Sn, Cu<sub>6</sub>Sn<sub>5</sub>,  $\theta$ -CuAl<sub>2</sub>,  $\eta_2$ -CuAl,  $\gamma_1$ -Cu<sub>9</sub>Al<sub>4</sub>,  $\zeta_2$ -Cu<sub>4</sub>Al<sub>3</sub> and  $\delta$ -Cu<sub>3</sub>Al<sub>2</sub>).

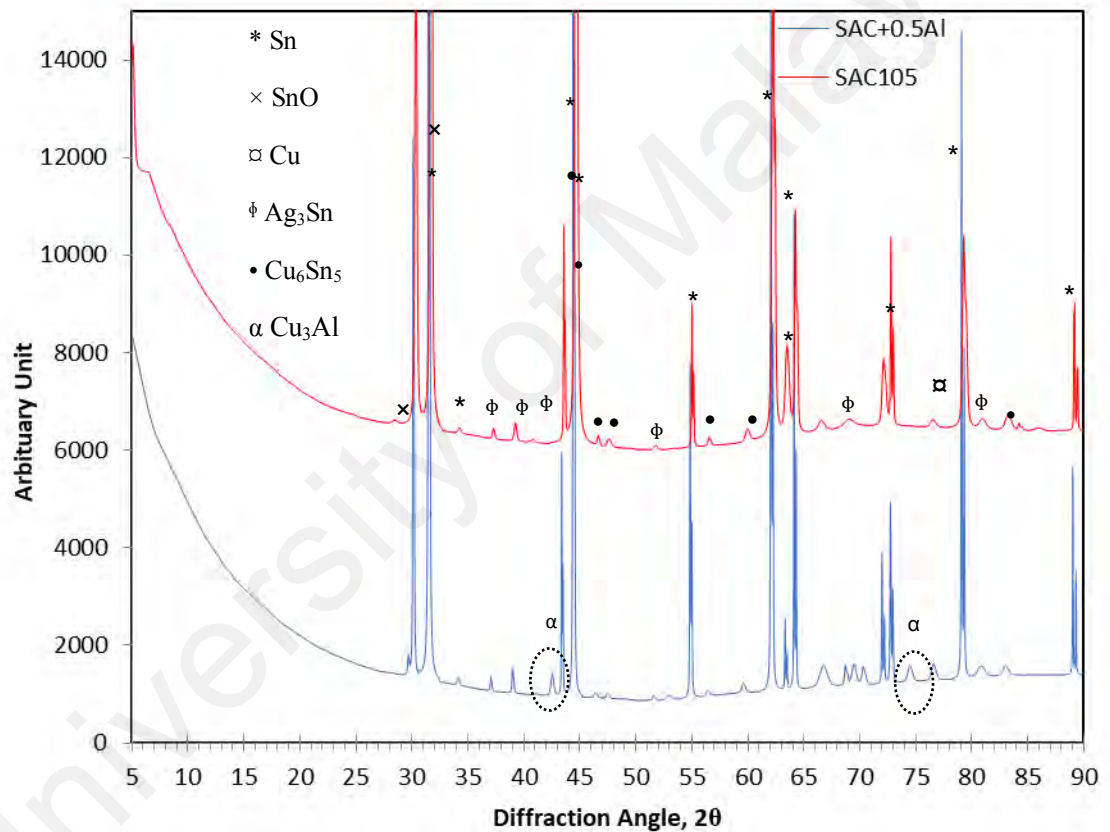


**Figure 4.12** XRD diffractogram of SAC and SAC+0.5Al.

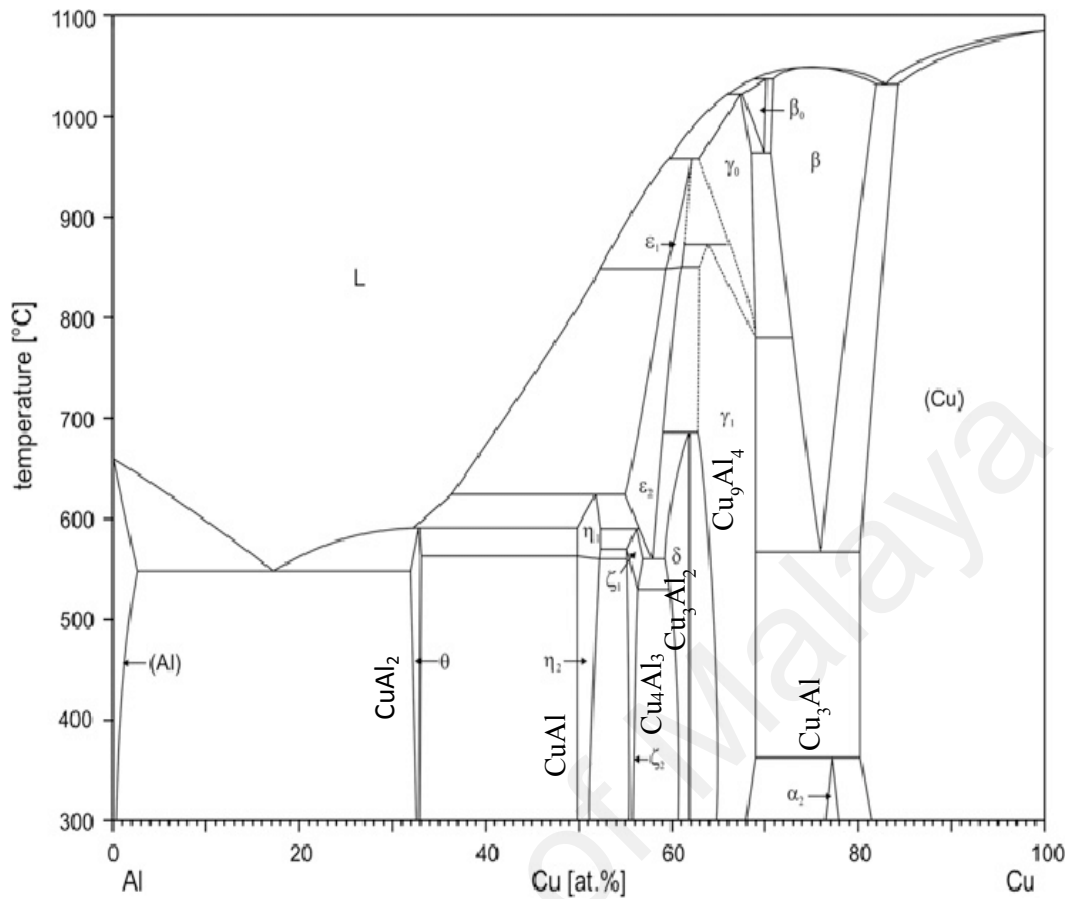


Figure 4.13 Cu-Al phase diagram (Murray, 1985).

(c) TEM-EDS

TEM EDS analysis is conducted on SAC+Al sample to further identify the Cu-Al phase, since it provides a better spatial resolution than FESEM EDS. Prior to TEM EDS, FIB (Focused Ion Beam) technique was used to mill out a thin slice of Cu-Al IMC from the crossed section of SAC + Al joint. Figure 4.14 shows the elemental map of the Cu-Al phase. From the TEM-EDS elemental map, it further confirmed that this new IMC consist only Cu and Al. EDS analysis at the new IMC phase indicated it consists of 72-79 at. % Cu and 21-

28 at. % Al. This result provides evidence supplementary to result obtained by XRD analysis and suggests formation of  $\alpha_2$ -Cu<sub>3</sub>Al.

### 4.2.3 Microstructure of Interfacial IMC (After Reflow and After Thermal Aging)

#### (a) FESEM

Figure 4.15 shows cross-sectional micrographs of SAC+X samples at the solder/Cu interface after reflow. Scallop type Cu<sub>6</sub>Sn<sub>5</sub> layer forms at the SAC105/Cu interface. Upon the minor addition of aluminium or zinc, the scallop morphology is still seen, but the IMC becomes flatter as Al is added up to 0.5 wt. % (Fig. 4.15(d)). The IMC thickness is reduced with the addition of Al or Zn. The average thickness of the total IMC layer is plotted as a function of Al and Zn content in Figure 4.16. The influence of Al and Zn addition on the interfacial IMC thickness is obvious, where there is a definite reduction of Cu<sub>6</sub>Sn<sub>5</sub> with addition of Al and Zn. However, with error bar taken into consideration, the thickness of the interfacial IMC does not seem to vary much with the Al or Zn content of the solder in the range 0.1–0.5 wt. %. This may indicate that the addition of Al or Zn beyond a certain percentage does not bring additional benefit in terms of suppression of IMC growth. Figure 4.17 shows FESEM image and EDX spectrum of the interfacial Cu<sub>6</sub>Sn<sub>5</sub> of SAC+Al and SAC+Zn samples. Cu<sub>6</sub>Sn<sub>5</sub> was the only IMC found at the interface, and no trace of Al in Cu<sub>6</sub>Sn<sub>5</sub> and Al-Cu compound could be detected at the interface of all aluminum-added solder (Figure 4.17a). As for Zn added sample, no Cu-Zn compound was found at the interface, however trace of Zn was detected in the Cu<sub>6</sub>Sn<sub>5</sub> IMC (Figure 4.17b). Thus, wavelength-dispersive spectroscopy (WDS) analysis was carried out to further quantify the amount of Zn presence in Cu<sub>6</sub>Sn<sub>5</sub>.

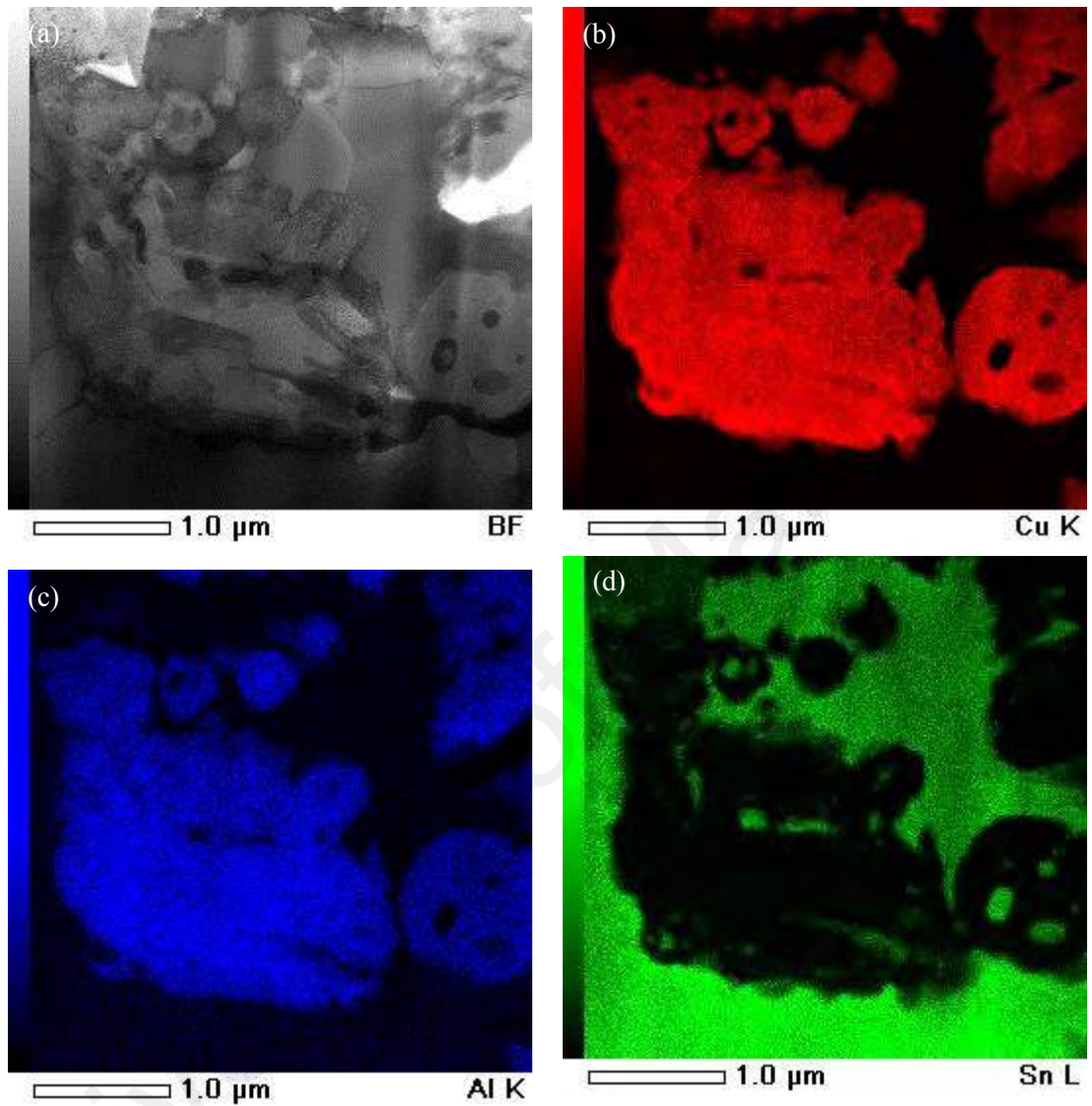


**Figure 4.14** (a) TEM image of FIB sliced Cu-Al IMC. Elemental maps for the constituent elements: (b) Cu, (c) Al, (d)Sn.

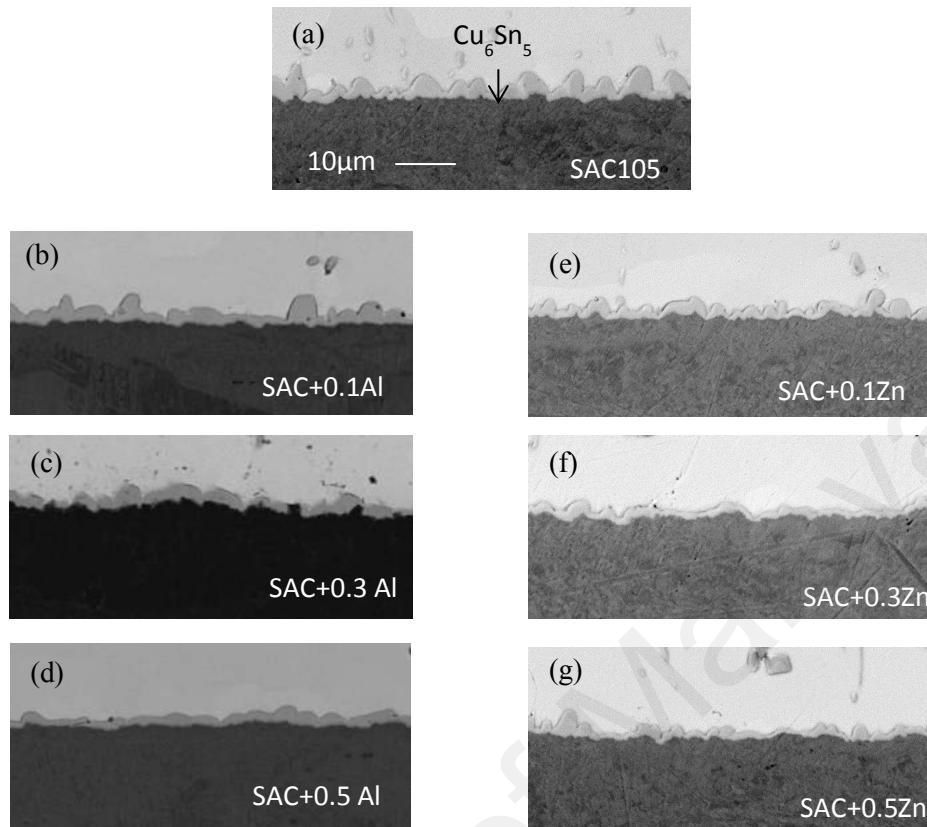


**Figure 4.15** Cross-sectioned image at interfacial of SAC+X/Cu after 1 x reflow

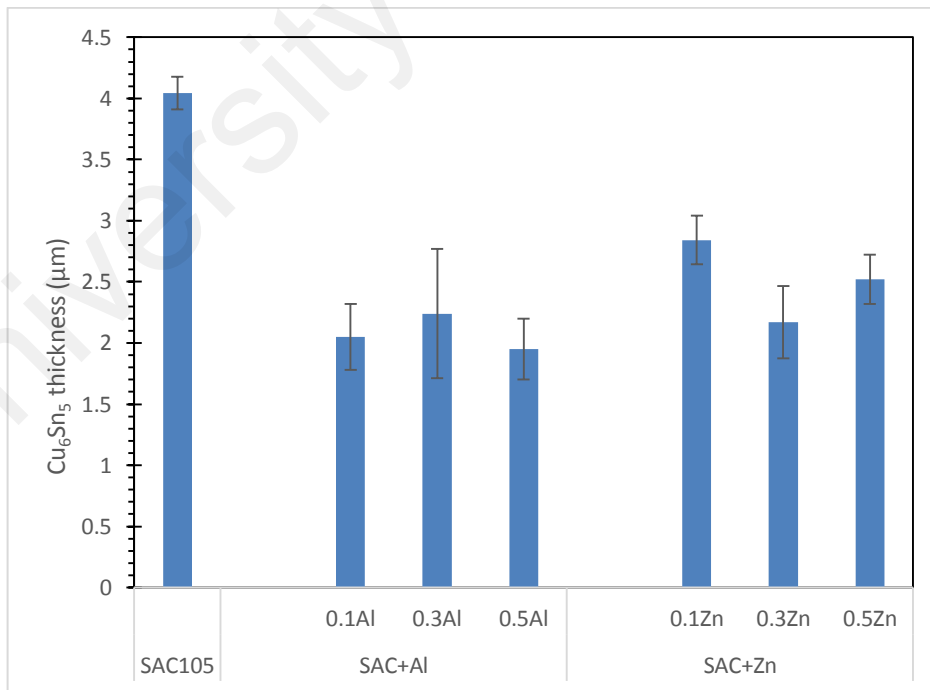


**Figure 4.16** Variation of  $\text{Cu}_6\text{Sn}_5$  thickness with SAC + X samples after reflow.

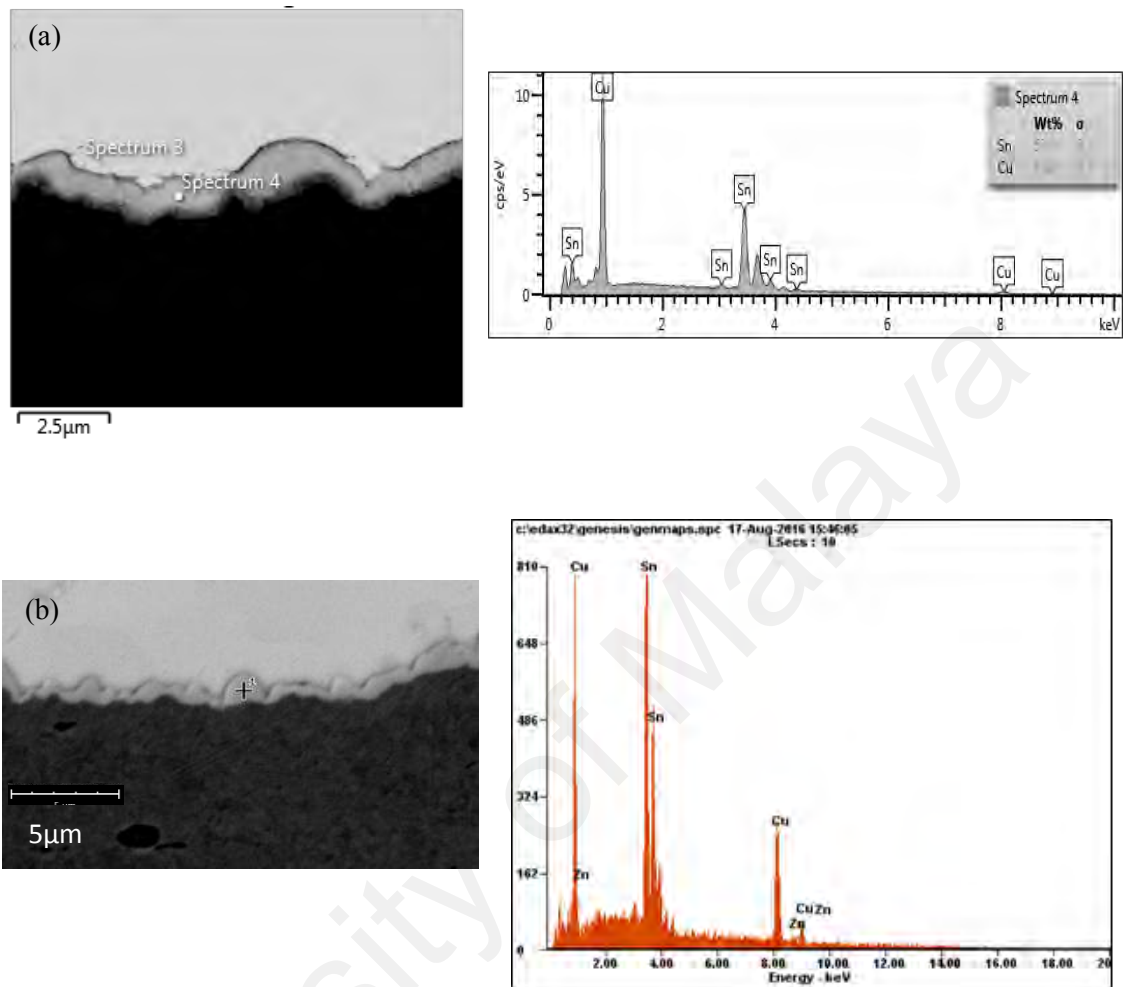


**Figure 4.17** FESEM and EDX spectrum of interfacial  $\text{Cu}_6\text{Sn}_5$  of (a) SAC+Al and (b) SAC+Zn samples.

After reflow, some of the solder joints samples were also subjected to isothermal aging at 150 °C for up to 1 month to study the effects of minor Al and Zn addition on the solid state reaction between SAC+ X and copper substrate. Figure 4.18 shows the cross sectional FESEM images of isothermally aged SAC+X at the interface. After thermal aging for 1 month, it was observed that a continuous intermetallic compound with a darker contrast

formed in between the first intermetallic layer (lighter contrast) and Cu substrate in both SAC105 and SAC+Al solder. With the use of elemental ratio, EDS analysis was used to confirm the intermetallic layers. It was confirmed that the lighter outer layer is  $\text{Cu}_6\text{Sn}_5$  and the darker inner layer is  $\text{Cu}_3\text{Sn}$ . Similar to SAC+Al after reflow, within the resolution of EDS, there was no trace of Al detected in both  $\text{Cu}_6\text{Sn}_5$  and  $\text{Cu}_3\text{Sn}$  after thermal aging. It is seen that the addition of Al up to 0.5 wt. % has slowed down the growth of the total interfacial IMCs. On the other hand, it was observed that submicron  $\text{Cu}_3\text{Sn}$  is discontinuous at the interface and could only be seen under high magnification in all SAC+Zn samples. Similar to SAC +Zn after reflow, only trace of Zn is found in  $\text{Cu}_6\text{Sn}_5$  and no Cu-Zn compound was found in the interface of all SAC+Zn solders.

Figure 4.19 shows the thickness of  $\text{Cu}_6\text{Sn}_5$  and  $\text{Cu}_3\text{Sn}$  plotted as a function of Al and Zn content. It could be seen that the thickness of  $\text{Cu}_6\text{Sn}_5$  is decreased as Al is added up to 0.5 wt. %. However, the thickness of  $\text{Cu}_3\text{Sn}$  is almost the same for SAC and all SAC+Al samples. The effect of Zn addition on the interfacial IMC thickness is obvious after thermal aging, where  $\text{Cu}_3\text{Sn}$  IMC is almost completely suppressed and thus the total IMC is significantly reduced with addition of Zn. Since the presence of  $\text{Cu}_3\text{Sn}$  is almost negligible, thus only thickness of  $\text{Cu}_6\text{Sn}_5$  was plotted for SAC+ Zn samples. From figure 4.19, it could be seen that the total IMC is reduced as a function of Zn content in the solder.

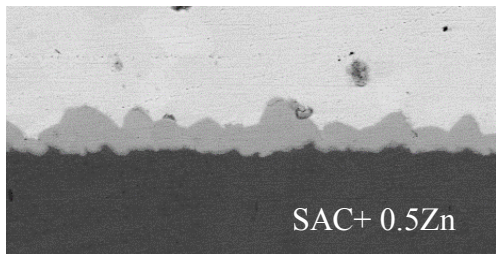
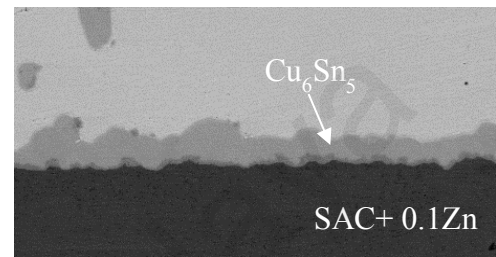
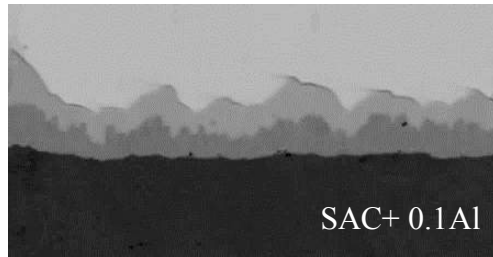
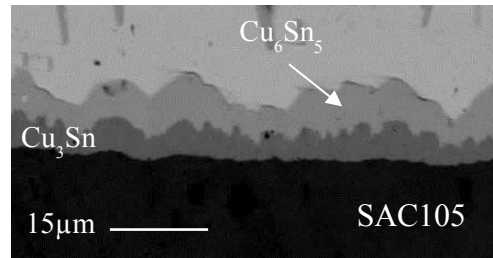


**Figure 4.18** Cross-sectioned FESEM image at interfacial of SAC+X/Cu after 1 month aging.

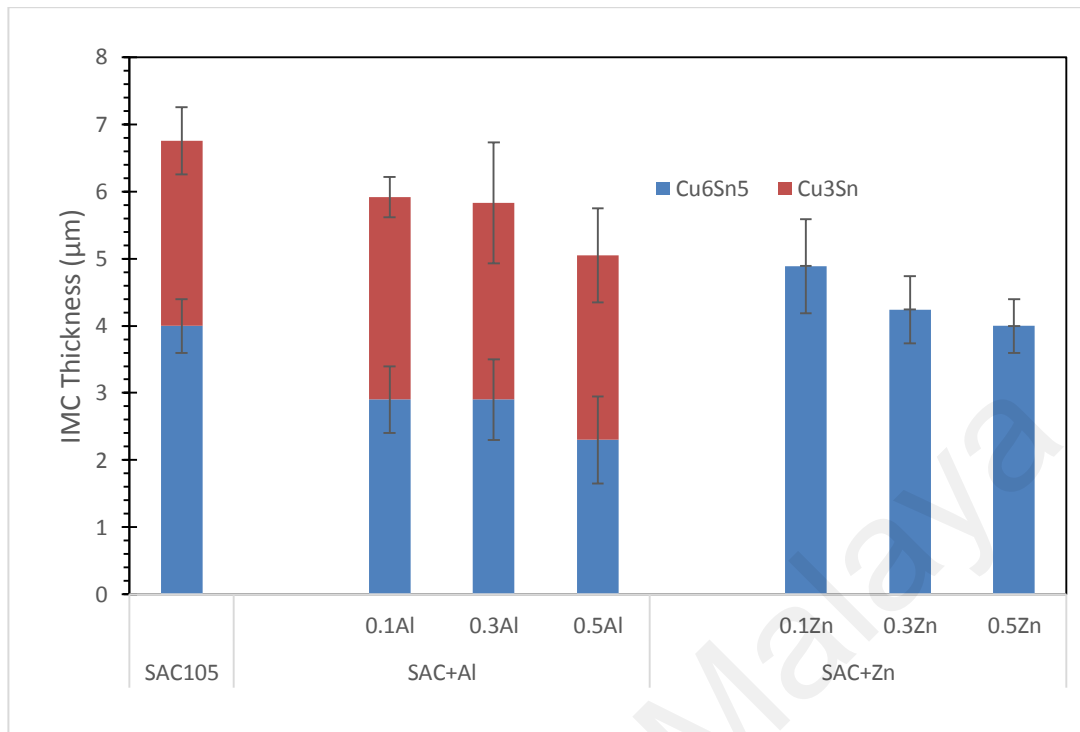


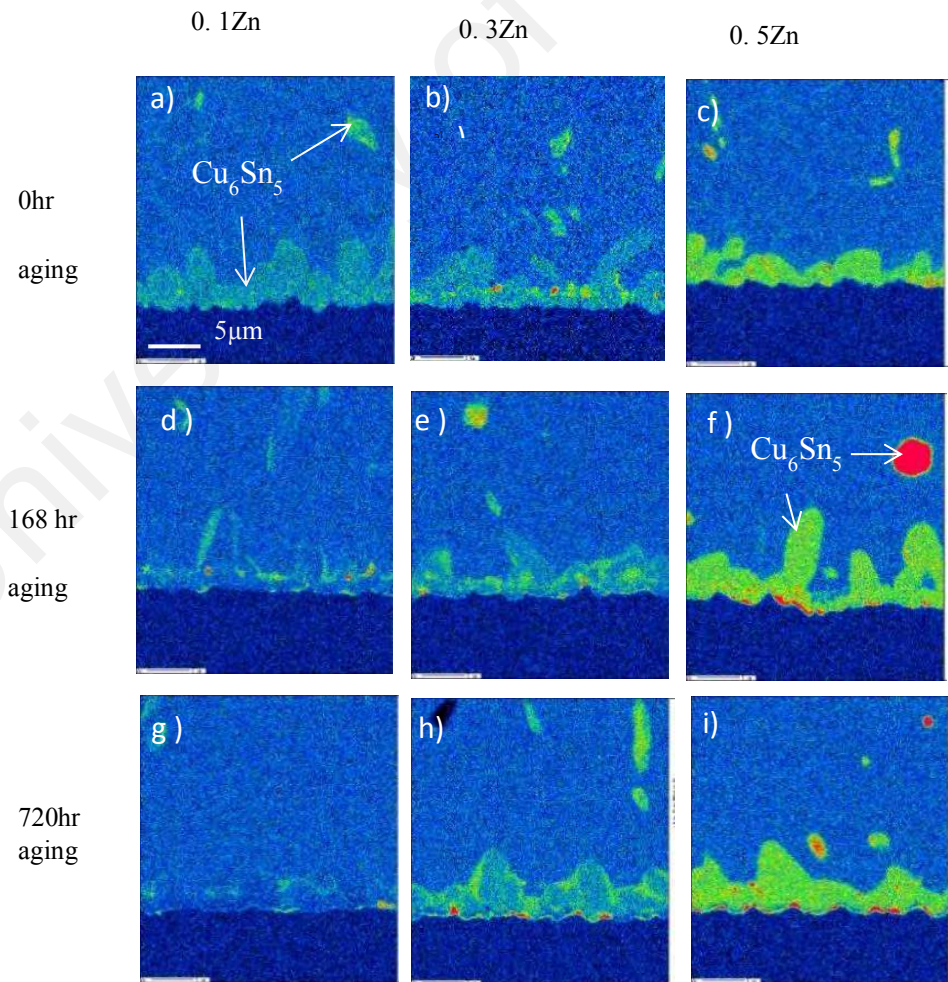
**Figure 4.19** Variation of Cu<sub>6</sub>Sn<sub>5</sub> and Cu<sub>3</sub>Sn thickness with SAC + X samples after 1 month aging.

**(b) Wavelength-Dispersive X-Ray Spectroscopy (WDS)**

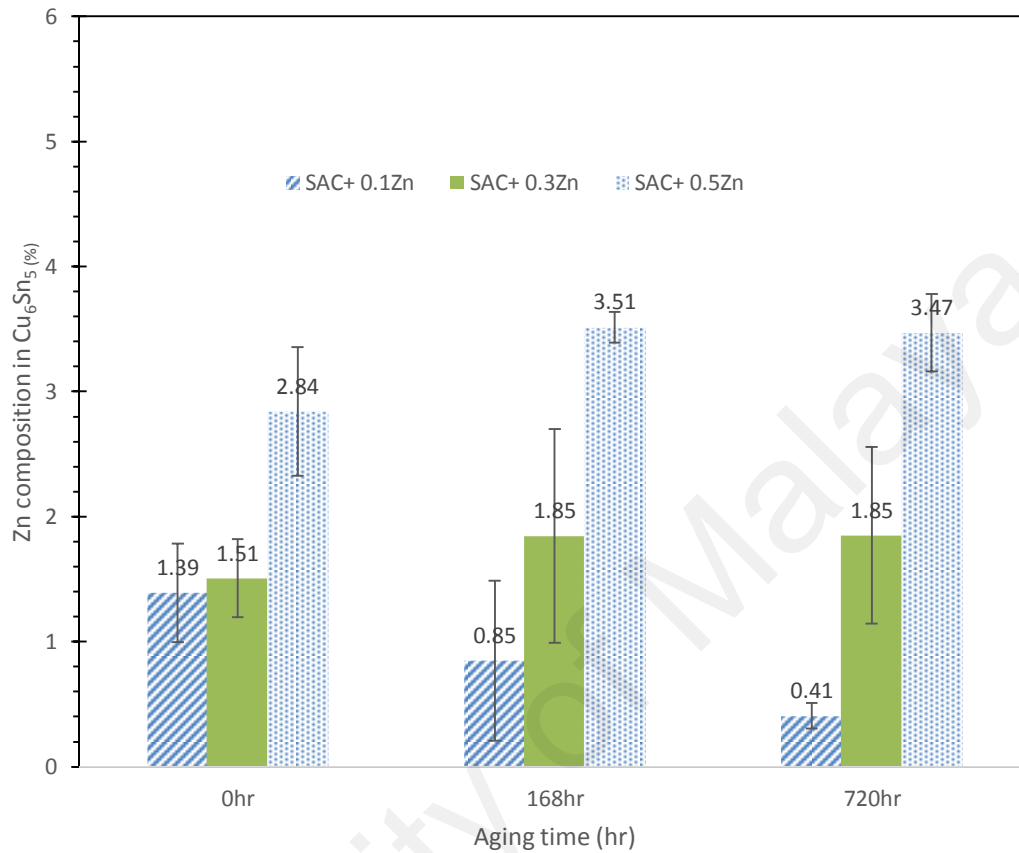
EPMA equipped with WDS is used to characterize interfacial IMC of SAC +Zn solder joints. WDS is used to quantify the amount of Zn atom in the interfacial IMC as WDS has a much finer spectral resolution than EDS (Newbury & Ritchie, 2015).

Figure 4.20 shows the Zn elemental distribution in Cu<sub>6</sub>(Sn,Zn)<sub>5</sub> using EPMA. From Figure 4.20, it is seen that the Zn concentration in Cu<sub>6</sub>(Sn,Zn)<sub>5</sub> increases with the increase of Zn % in SAC105. For SAC+0.1Zn, SAC+0.3Zn and SAC+0.5Zn, the Zn distribution in Cu<sub>6</sub>(Sn,Zn)<sub>5</sub> was rather uniform after reflow. However, after aging up to 168 and 720 hr, Zn tends to concentrate at the solder/Cu<sub>6</sub>Sn<sub>5</sub> interface and Cu<sub>6</sub>Sn<sub>5</sub>/Cu interface. It was apparent that the concentration of Zn at the centre of Cu<sub>6</sub>Sn<sub>5</sub> is low in SAC+0.1Zn and SAC+0.3Zn after aging (Figure 4.20 (d,e,g,h)). From Figure 4.20(c,f,i), it can be seen that

the Zn concentration in  $\text{Cu}_6(\text{Sn,Zn})_5$  is high in SAC+0.5Zn compared with SAC+0.1Zn and SAC+0.3Zn. As the aging time increases, more Zn was seen distributed at the IMC/ Cu interface. Figure 4.21 shows the Zn atomic % in  $\text{Cu}_6(\text{Sn,Zn})_5$  in SAC+0.1Zn, SAC+0.3Zn and SAC+0.5Zn investigated by EPMA after aging up to 720 hr. In general, the Zn at % in  $\text{Cu}_6(\text{Sn,Zn})_5$  increases with increase of Zn addition in SAC105. After aging up to 720 hr, it can be seen that the Zn at. % in  $\text{Cu}_6(\text{Sn,Zn})_5$  in SAC+0.1Zn decreases as a function of aging time, while the Zn at. % in  $\text{Cu}_6(\text{Sn,Zn})_5$  in SAC+0.3Zn and SAC +0.5Zn remain the same even after aging. It is suggested that during aging, Zn tends to diffuse out of the interfacial region. Thus, when the addition of Zn is low (at 0.1 %), the Zn concentration in  $\text{Cu}_6\text{Sn}_5$  reduced.



**Figure 4.20** Zn distribution elemental maps at the solder/ Cu interface in SAC +0.1Zn, SAC+0.3Zn and SAC+0.5Zn after aging 0hr, 168hr and 720 hr.



**Figure 4.21** Variation of Zn composition in  $\text{Cu}_6(\text{Zn}, \text{Sn})_5$  in SAC +0.1Zn, SAC+0.3Zn and SAC+0.5Zn after aging at 0hr, 168hr and 720 hr.

#### 4.2.4 Top View of Interfacial IMC

Solder joints were subjected to deep etched in an etchant to strip off the solder matrix and therefore expose the interfacial IMC of the Cu substrate. Figure 4.22 shows the exposed interfacial IMC grains of SAC 105 and SAC105+0.5Al after reflow. The IMC grains found on the interface of were identified as  $\text{Cu}_6\text{Sn}_5$  for both SAC105 and SAC+0.5Al. From the images,  $\text{Cu}_6\text{Sn}_5$  grains found in SAC105+0.5Al were somewhat faceted. The number of IMC grains of SAC105 and SAC+0.5Al are similar where both have around

40 grains / 10,000  $\mu\text{m}^2$ . This shows that addition of minor Al does not have much effect on the number or size of interfacial IMC grains. High Al concentration region was found on some of the exposed IMC in SAC +0.5Al samples. Figure 4.23 shows the top view of interfacial IMC with high Al region and its EDS elemental maps. Elemental maps detected Cu, Al, and Ag on the surface of the exposed IMC. By zooming in onto the high Al concentration region, small and agglomerated particles are seen (encircled in yellow dotted line Fig. 4.23a). In Figure 4.23 (b) the presence of Al is indicated in green. The region of high concentration of Al is encircled in yellow. It can be seen that the region with high Al concentration corresponds to that of Cu (compare Figure 4.23 b,c). The agglomerated particles are identical to the Cu-Al IMC that was found in the bulk microstructure. The elongated and plate-like particles (right corner of Figure 4.23d) on the  $\text{Cu}_6\text{Sn}_5$  IMC grains are identified as  $\text{Ag}_3\text{Sn}$ .

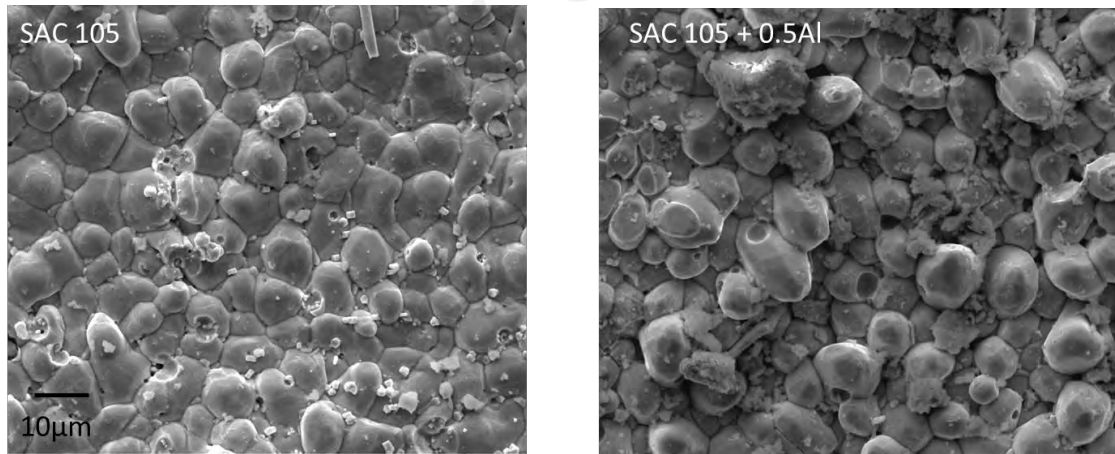


**Figure 4.22** Top view FESEM image of exposed interfacial IMC grains in SAC and SAC105+0.5Al after reflow.

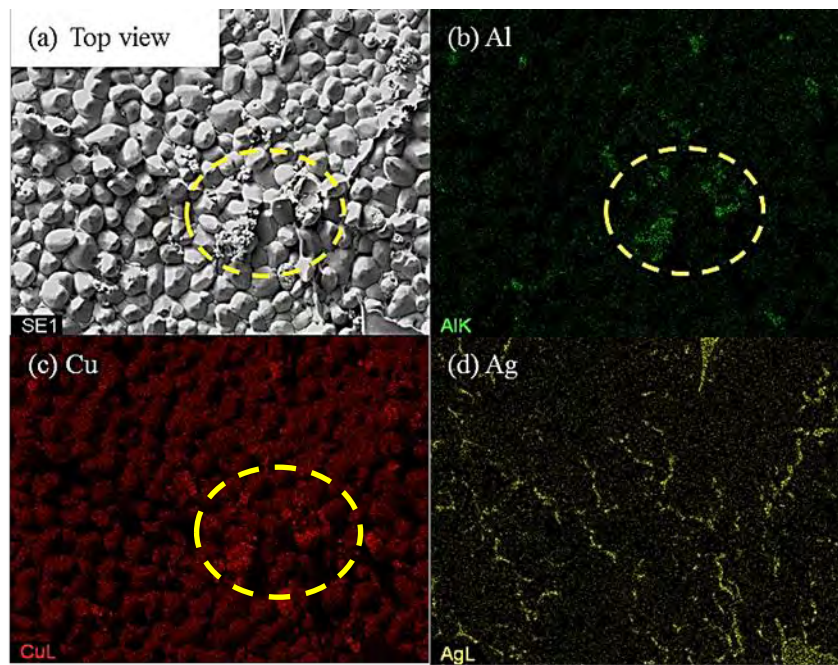


**Figure 4.23** (a) Top view image of deeply etched SAC105+0.5Al after 1x reflow.

Elemental maps for the constituent elements: (b) Al, (c) Cu and (d) Ag.

On the other hand, from Figure 4.24, the top view IMC image of SAC and SAC+Zn, Zn seems to have a more substantial effect on the grain size of interfacial IMC. By using EDX analysis, all the exposed IMC grains on SAC and SAC+Zn samples were identified as  $\text{Cu}_6\text{Sn}_5$ . It is obvious that Zn has significantly reduced the interfacial  $\text{Cu}_6\text{Sn}_5$  grain size. Typical scallop morphology of interfacial  $\text{Cu}_6\text{Sn}_5$  was seen in all SAC and SAC+Zn samples. It is seen that the  $\text{Cu}_6\text{Sn}_5$  grains in SAC+Zn solders has a few edges and flat faces (Figure 4.24 b-d). Thus, the  $\text{Cu}_6\text{Sn}_5$  grains in SAC+Zn solders were slightly more faceted than that of SAC105 solders. Figure 4.25 shows that the number of  $\text{Cu}_6\text{Sn}_5$  in a  $10,000\mu\text{m}^2$  area at the interface in SAC+Zn solder is almost 3-4 times more compared to SAC solder.

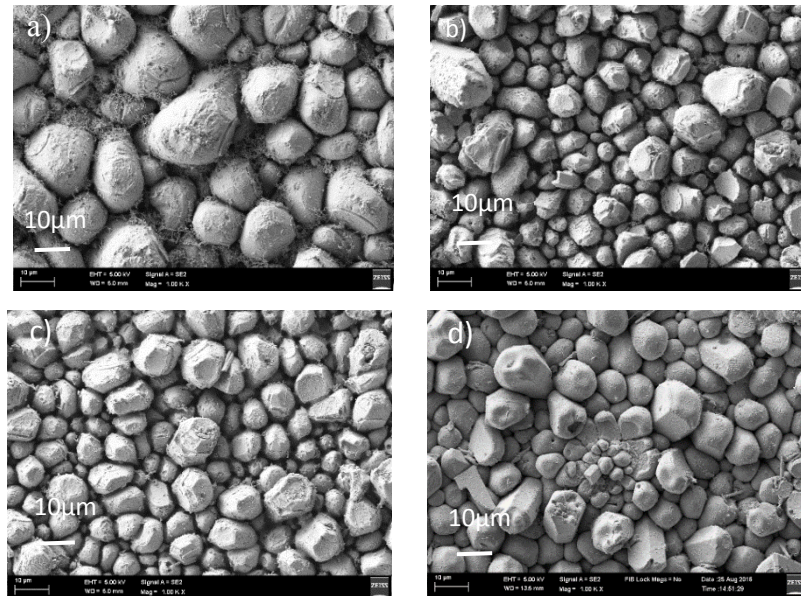


**Figure 4.24** FESEM top view image of IMC a) SAC105, b) SAC +0.1Zn, c) SAC+0.3 Zn and d) SAC+0.5Zn after reflow.

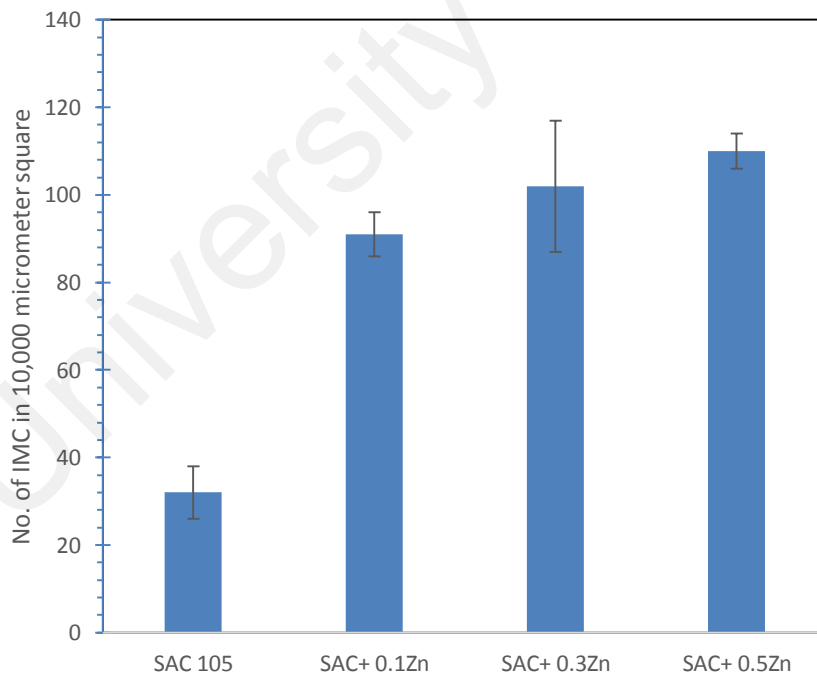


**Figure 4.25** Number of top  $\text{Cu}_6\text{Sn}_5$  grains in  $10,000 \mu\text{m}^2$  in SAC105, SAC +0.1Zn, SAC+0.3Zn and SAC+0.5Zn

## 4.2.5 Discussions of Thermal and Microstructure Properties of SAC + X

### (a) Thermal Properties

When 0.1 wt. % of Al was added to SAC105, it did not change the melting characteristics of SAC. Its endothermic curve is similar to that of SAC105 (Figure 4.1). Both have the same onset of melting ( $\sim 217$  °C) and exhibit twin peaks endothermic. The twin peaks endothermic are associated with the eutectic temperature for Sn-Ag ( $L \rightarrow Ag_3Sn + Sn$ ) and Sn-Cu ( $L \rightarrow Cu_6Sn_5 + Sn$ ) respectively. We started to see some changes as Al was added up to 0.3%. It is seen that SAC+0.3Al and SAC+0.5Al shifts the onset of melting to  $\sim 221$  °C (Sn-Ag eutectic temperature) (Karakaya & Thompson, 1987). The endothermic curves of SAC+0.3Al and SAC+0.5Al are very similar to the endothermic curve of non-eutectic SnAg solder (Kato et al., 2003). This shows that free Cu atoms are not available in SAC + 0.3Al and SAC + 0.5Al solders as Sn-Ag-Cu solder alloy always shows the onset melting at  $\sim 217$  °C (Kumar & Kubaschewski, 2007). One possible explanation for this is the formation of  $\alpha_2$ -Cu<sub>3</sub>Al found in the solder matrix, which has reduced the available Cu to react with Sn and Ag. The Cu<sub>3</sub>Al compound already formed in the as-received samples, which were supplied in the as-cast condition as seen in Figure 4.3 b–d. Cu<sub>3</sub>Al has a higher peritectoid decomposition temperature of 363 °C,  $\gamma_1 + Cu \leftrightarrow \alpha_2$  (Murray, 1985). Thus, during the melting of solders for up to 300 °C, the stable Cu<sub>3</sub>Al IMC did not react and this lowers the activity of Cu in solder melts. The lack of free Cu atom in the solder is further indicated by the shift of a prominent peak in the DSC curves of SAC105 and SAC+ 0.1Al (Figure 4.1). The  $\sim 228$  °C (Sn-Cu eutectic temperature) peak in SAC105 and SAC+0.1Al has shifted to  $\sim 231$  °C ( $T_m$  of Sn = 232 °C) in SAC+0.3Al and SAC+0.5Al. This shift indicates that the deficiency of Cu atom in SAC+0.3Al and SAC+0.5Al has reduced the eutectic reaction of Sn-Cu,  $L \rightarrow Cu_6Sn_5 + Sn$ . With Al addition, the peak indicating Sn

melting is seen, as fractions of un-melted Sn remaining in the solder melted when temperature increased to 232 °C (Karakaya et al., 1987).

Result shows that SAC105 has the largest undercooling of ~17 °C (Table 4.1). This is well within range of undercooling values, 10–30 °C reported for Sn-Ag-Cu solder (Kang et al., 2004). This is because  $\beta$ -Sn requires large undercooling to induce nucleation and solidification (Kang et al., 2004). The presence of Al in SAC105 has reduced the undercooling significantly. It is seen that with addition of Al up to 0.5 %, undercooling has reduced to 1–5 °C. Kotadia et al. (2010) and Anderson et al. (2012) have observed the effect of Al in reducing undercooling of Sn-3.5Ag and Sn-3.5Ag-0.95Cu solder to 7 °C and 4 °C respectively. The addition of minor alloying element into solder has been one of the effective ways of reducing undercooling by promoting nucleation of  $\beta$ -Sn. Minor alloying atoms which have a much higher melting temperature can exist in molten Sn and provide heterogeneous site for  $\beta$ -Sn nucleation. In the case of Al as minor alloying,  $\text{Cu}_3\text{Al}$  compound is formed even when the addition of Al is as low as 0.1%. During exothermic reaction in DSC, the existing Al-Cu intermetallic compounds act as a preferential site to promote heterogeneous nucleation of  $\beta$ -Sn, and thus lowering the undercooling of SAC105.

Although, the undercooling of SAC+Zn could not be determined in this study, many studies reported that the addition of Zn can reduce undercooling of SAC significantly, where it could lower the undercooling ranging from 1-8 °C (Kang et al., 2004; Kotadia et al., 2010; Anderson et al., 2009). Many studies on the effect of Zn on the melting characteristic of SAC has suggested that even with a minimal Zn addition (as low as 0.1 wt. %) could reduce the undercooling of  $\beta$ -Sn significantly (Subramanian, 2012). Besides, it is believed that Zn which is easily oxidised formed small solid zinc oxide, ZnO particles within molten solder during heating, this act as heterogeneous nucleants for  $\beta$ -Sn which

results in minimizing undercooling and provide more refined microstructures (Swenson, 2007).

**(b) Bulk microstructure**

Segregated  $\text{Cu}_3\text{Al}$  IMC was found near the top surface of the solder sample after reflow (Figure 4.2a). With addition of higher Al content (0.5-2.0 wt. %) into Sn-3.5Ag solders, Kotadia et al. have also reported the segregation of  $\text{CuAl}_2$  in SA solder. They suggested that the segregation of Al rich phase and Al-Cu compound is caused by Stokes and Marangoni motion, which is due to large stable liquid miscibility gap in binary Sn-Al and ternary Sn-Al-Cu (Kotadia et al., 2012).

From Figure 4.3, the addition of Al and Zn as minor alloying element has refined the bulk microstructure of SAC solder significantly. SAC solder has been reported to have large undercooling (ranged 17-30 °C) due to the delayed nucleation of  $\beta$ -Sn during solidification. This permitted extended formation of primary intermetallic compounds (IMCs) far from thermodynamic equilibrium. Thus, results in large  $\beta$ -Sn dendrites, large grains, reduced amounts of eutectic, and undesired morphologies of the intermetallic compounds (e.g., large  $\text{Ag}_3\text{Sn}$  plates or long  $\text{Cu}_6\text{Sn}_5$  needles) (Kang et al., 2004; Lalonde et al., 2004). Hence, large undercooling of  $\beta$ -Sn was responsible for the coarsening of SAC microstructure which reduced the reliability of solder joints. It has been reported that adding minor alloying element into solder could reduce the undercooling of solder. Addition of minor alloying element reduced undercooling by promoting nucleation of  $\beta$ -Sn. Minor alloying atoms can exist as solutes or compounds (formed by reacting with element in solders eg. Sn, Cu, Ag) in molten Sn where it acts as a heterogeneous site for  $\beta$ -Sn to nucleate (Shang et al., 2017). In this study, addition of Al forms  $\text{Cu}_3\text{Al}$  compound which

act heterogenous nucleation site for  $\beta$ -Sn to nucleate, reducing the undercooling and thus refine the SAC-Al microstructure.

**(c) Interfacial reaction**

In general, minor alloying elements which could affect the growth of Cu-Sn compound are divided into two categories: (i) elements that show marked solubility in either one or both of the Cu-Sn IMCs; and (ii) elements that do not significantly dissolve in either of the Cu-Sn IMCs (Laurila, 2010). The effect of elements in category 1 on IMC growth could be explained by using thermodynamic argument. These elements stabilize  $\text{Cu}_6\text{Sn}_5$  and decrease the growth of  $\text{Cu}_3\text{Sn}$ . The elements in category 2 do not have a prominent effect on IMC as they only affect the growth of IMC layers indirectly. In this study, both addition of Al and Zn have imparted significant effects on the interfacial IMC formed between solder and Cu substrate. Both minor addition of Al and Zn reduced the  $\text{Cu}_6\text{Sn}_5$  IMC thickness similarly after reflow, but they have different effects on the IMCs after thermal aging of 1 month. Since both elements are of different categories where Al belongs to category 2 (does not shows any solubility in Cu-Sn IMCs), and Zn falls under categories 1, thus the mechanism on minor Al and Zn addition on the effects of IMCs formation will be different approach.

There is very limited amount of information available on the influence of Al on the Cu-Sn reaction. Li et al. (2012) have reported the suppression of  $\text{Cu}_6\text{Sn}_5$  IMC growth with addition of 1 % Al. They suggested that the suppression is due to the formation of an Al-Cu IMC layer at the interface, which acts as a barrier for Cu and Sn diffusion. However, Al-Cu IMC layer is not found at the interface in this study as the amount of Al added is less (0.5 %). The  $\text{Cu}_3\text{Al}$  IMC found at the  $\text{Cu}_6\text{Sn}_5/\text{Sn}$  interface (Figure 4.23) could account for the suppression of  $\text{Cu}_6\text{Sn}_5$ . The segregation of Al atoms at the IMC/Sn interface may have effect on the growth of IMC, by hindering the flow of Cu or Sn atom. With minor Al

addition, most of the Al reacts with Cu in the bulk solder to form Cu<sub>3</sub>Al. Hence, Al does not form a layer of compound at the interface. Reduction of free Cu atom in the bulk solder could also be attributed to the retardation of Cu<sub>6</sub>Sn<sub>5</sub> growth. By their presence at the interface, Cu<sub>3</sub>Al IMC hinders the flow of Cu or Sn atom to the solder thereby retarding IMC growth during reflow. During isothermal aging, the Cu<sub>6</sub>Sn<sub>5</sub> IMC layer grows by interdiffusion of Cu and Sn and reaction with each other, while the Cu<sub>3</sub>Sn IMC forms and grows by reactions between the Cu substrate and Cu<sub>6</sub>Sn<sub>5</sub> IMC layer, as given in the equation below (Laurila, 2010):



The presence of Cu<sub>3</sub>Al IMC at the Cu<sub>6</sub>Sn<sub>5</sub>/Sn interface hinders the flow of Cu or Sn atom to the solder, however it does not affect the reaction in Equation (4.1). Cu<sub>3</sub>Sn grows by consuming Cu<sub>6</sub>Sn<sub>5</sub> that is formed during reflow. Thus, the thickness of Cu<sub>3</sub>Sn was not significantly affected by the addition of Al in solder. On the other hand, with slower interdiffusion of Cu and Sn at the interface (due to presence of Cu<sub>3</sub>Al) and Cu<sub>3</sub>Sn formation by consumption of Cu<sub>6</sub>Sn<sub>5</sub>, the thickness of Cu<sub>6</sub>Sn<sub>5</sub> was reduced in SAC105 + Al solder.

Figure 4.15 & 4.16 shows that Zn addition has decreased the growth of Cu<sub>6</sub>Sn<sub>5</sub> during reflow and suppressed the formation of Cu<sub>3</sub>Sn during thermal aging. Many studies have been done on the effect of Zn on the Cu-Sn reaction, where Zn as alloying element was found to be effective in suppressing the growth of interfacial Cu<sub>6</sub>Sn<sub>5</sub> and Cu<sub>3</sub>Sn layers. As mentioned earlier, minor alloying elements that have influence on Cu-Sn IMC growth have been divided into two categories. Zn obviously fall under category 1 (element that is soluble in Cu-Sn IMC) as can be seen from Figure 4.20 where it shows marked solubility in Cu<sub>6</sub>Sn<sub>5</sub>. Although the solubility of Zn in Cu<sub>3</sub>Sn was not able to be quantified in this study due to the submicron size of the Cu<sub>3</sub>Sn layer which is due to suppression of Zn, it has been

reported that Zn is soluble in both  $\text{Cu}_6\text{Sn}_5$  and  $\text{Cu}_3\text{Sn}$  and that Zn goes to Sn sublattice in both compounds [ $\text{Cu}_6(\text{Sn,Zn})_5$  and  $\text{Cu}_3(\text{Sn,Zn})$ ] (Chou et al., 2010). Reported solubility values are (at 250°C) 6 at. % of Zn to  $\text{Cu}_6\text{Sn}_5$  and 9 at. % to  $\text{Cu}_3\text{Sn}$ , respectively (Chou et al., 2010). A few studies have tried to explain the mechanism through which Zn alloying affects the growth of interfacial IMC between the solder and Cu substrate. So far there are 2 main approaches or theories on how Zn could suppress the growth of IMC. During aging,  $\text{Cu}_6\text{Sn}_5$  IMC layer grows by interdiffusion of Cu and Sn, and the reaction with between Cu and Sn. On the other hand, it was suggested that  $\text{Cu}_3\text{Sn}$  IMC grows by reaction between the Cu substrate and  $\text{Cu}_6\text{Sn}_5$  IMC, following the Equation 4.1 shown above.

For the first approach, Kang et al. (2007) suggested that Zn atoms have a tendency to accumulate at the  $\text{Cu}_6\text{Sn}_5/\text{Cu}$  interface. Under high resolution STEM, Kang et al. (2007) noticed Zn atoms exist in a Cu–Zn solid solution between IMC and Cu substrate. By their presence at the interface, Zn atoms hinder the flow of copper atom to react with  $\text{Cu}_6\text{Sn}_5$  and thereby retarding IMC growth. The second approach is through thermodynamic explanation for cases with the absence of  $\text{Cu}_3\text{Sn}$  in Ni, Co, Pt and Au as minor alloying element. It is suggested that Zn dissolves into  $\text{Cu}_6\text{Sn}_5$  to form  $\text{Cu}_6(\text{Sn,Zn})_5$  during reflow and then stabilizes it against the growth of  $\text{Cu}_3\text{Sn}$  during thermal aging (Laurila, 2010). However, different from the addition of Ni, Co, Pt and Au, Zn was found to reduce the growth of  $\text{Cu}_6\text{Sn}_5$  as well during thermal aging, while addition of Ni, Co, Pt and Au has increased the growth of  $\text{Cu}_6\text{Sn}_5$  due to the more stabilized  $\eta\text{-Cu}_6\text{Sn}_5$  phase (Laurila 2010). One possible reason for why stabilization of  $\text{Cu}_6(\text{Sn,Zn})_5$  does not increase the growth of  $\text{Cu}_6\text{Sn}_5$  but suppress  $\text{Cu}_3\text{Sn}$  during aging could be explained by the synergy effect from both theories suggested above. During reflow, Zn dissolves into  $\text{Cu}_6\text{Sn}_5$  to form a stabilized  $\text{Cu}_6(\text{Sn,Zn})_5$ , and Zn tends to accumulate at the edge of solder/ IMC and especially at the IMC/ Cu

interface (Figure 4.20). During isothermal aging, stabilized  $\text{Cu}_6(\text{Sn,Zn})_5$  is against the growth of  $\text{Cu}_3\text{Sn}$ . On the other hand, presence of Zn at IMC/ Cu interface also hindered the flow of Cu atom from Cu substrate to form  $\text{Cu}_3\text{Sn}$ . Thus, it seems impossible for the growth of  $\text{Cu}_3\text{Sn}$ . Besides, the presence of Zn at solder/ IMC could have hindered Sn atom for the formation of  $\text{Cu}_6\text{Sn}_5$ . Presence of Zn at both interface has slow down the interdiffusion of Cu atom and Sn atom, thus unlike addition of Ni, Co, Pt and Au, the thickness of  $\text{Cu}_6\text{Sn}_5$  does not increased in SAC105 + Zn solder.

For the reflowed SAC+Zn solder joints, distribution of Zn atom was relatively homogenous in  $\text{Cu}_6(\text{Sn,Zn})_5$ . However, after subsequent annealing for 168 hr and 720 hr, it is observed that Zn tends to segregate at the Sn/IMC and IMC/Cu interface in SAC +0.1Zn and SAC+0.3Zn, leaving the centre of the IMC scarce with Zn distribution. It should be noted that only Zn was found segregated in  $\text{Cu}_6(\text{Sn,Zn})_5$  while we do not see segregation/compositional gradient of other elements such as Sn, Cu, Ag in  $\text{Cu}_6(\text{Sn,Zn})_5$  interface. Segregation of Zn has also been observed at the IMC/solder interface in Sn-Bi alloys recently (Zhou et al., 2018). Zhou et al. (2018) has suggested that the segregation of Zn in Sn-Bi was due to two reasons, (i) non-coherent Sn-Bi grain boundaries, which provides an energy difference between the lattice inside the phase and the phase boundaries, and (ii) Zn atoms as a supersaturated solid solution in Sn-Bi phases may tend to diffuse out of the individual supersaturated phase and predictably toward the phase boundaries to minimize the overall free energy in the matrix. Ni was also found to segregate at the interface after reflow as well as after aging (Tay et al., 2013; Zeng et al.,2014).

From Figure 4.24, SAC+ Zn solder has reduced the grain size of interfacial  $\text{Cu}_6\text{Sn}_5$  IMC significantly. Experimental and theoretical works show that the nucleation rate and growth of IMC grains can be controlled by the IMC/liquid interface energy (Park et al., 2010;

2012). From thermodynamic considerations, higher surface energy at solder and  $\text{Cu}_6\text{Sn}_5$  ( $\gamma_{\text{Solder}/\text{Cu}_6\text{Sn}_5}$ ) would promote the formation of semi-spherical IMC grains while the low  $\gamma_{\text{Solder}/\text{Cu}_6\text{Sn}_5}$  would promote the growth of an irregular or facet morphology in the IMC compound grains. Kotadia et al. (2017) suggested the influence of Zn on the  $\text{Cu}_6\text{Sn}_5$  can be caused by absorption of Zn atoms from the bulk solder into the  $\text{Cu}_6\text{Sn}_5$  forming the stable  $\text{Cu}_6(\text{Sn}, \text{Zn})_5$  and thus changes the interfacial energy between the molten solder and IMC grains,  $\gamma_{\text{Solder}/\text{Cu}_6\text{Sn}_5}$  (Handwerker et al., 2007). Phase-field modelling studies show that presence of Zn at the  $\text{Cu}_6\text{Sn}_5$  would lower the interface liquid/ $\text{Cu}_6\text{Sn}_5$  interface energy and thus induces a more rapid nucleation of  $\text{Cu}_6\text{Sn}_5$  grains (Kotadia et al., 2017).

#### 4.2.6 Summary of Thermal Properties and Microstructure of SAC+X

In summary, addition of minor Al and Zn (0.1-0.5 %) into SAC105 has reduced the undercooling significantly by promoting heterogenous nucleation. This reduction in undercooling has leads to the bulk microstructure refinement of SAC +X solder, where Sn grain and  $\text{Cu}_6\text{Sn}_5$  IMC was refined. With addition of Al as low as 0.1 %, new IMC ( $\text{Cu}_3\text{Al}$ ) was found at the bulk microstructure, while no new IMC phase was found with Zn addition up to 0.5 %. No new IMC phase was found at the interface during reflow or aging for both Al and Zn addition. However, Zn atom shows marked solubility in  $\text{Cu}_6\text{Sn}_5$ , where it's solubility in  $\text{Cu}_6\text{Sn}_5$  increase as a function of Zn addition during reflow. Zn atom tends to segregate at the solder/ $\text{Cu}_6\text{Sn}_5$  and  $\text{Cu}_6\text{Sn}_5$ /Cu interface after thermal aging.

Al and Zn minor addition has great influence on the interfacial IMC after reflow and thermal aging. Addition of Al suppressed the growth of  $\text{Cu}_6\text{Sn}_5$  during reflow and thermal aging. However, it does not have much effect on the  $\text{Cu}_3\text{Sn}$  during thermal aging.  $\text{Cu}_6\text{Sn}_5$

suppression was accounted by the lack of free Cu atom in bulk microstructure (Cu react with Al to form  $\text{Cu}_3\text{Al}$  compound) and the presence of  $\text{Cu}_3\text{Al}$  on the  $\text{Cu}_6\text{Sn}_5/\text{Sn}$  interface which hindered the flow of Cu or Sn atom during reflow and thermal aging.

On the other hand, addition of Zn has suppressed the growth of  $\text{Cu}_6\text{Sn}_5$  during reflow and  $\text{Cu}_3\text{Sn}$  effectively after thermal aging. Zn impart its influence on the interfacial reaction by stabilizing  $\text{Cu}_6(\text{Sn,Zn})_5$  and hindering the flow of reacting species at the interface during reflow and thermal aging.

### **4.3. Mechanical Properties**

As solder joints are subjected to stress and mechanical loading during service, hardness and shear strength are crucial properties to be considered. Vickers hardness and shear strength of the SAC+ X solder joints were investigated. Nanoindentation was performed on the bulk microstructure and interfacial IMC as well. It has become a major concern to understand the behaviour of IMCs. Understanding the mechanical properties of interfacial IMCs is essential in the understanding of deformation behaviour and failure mechanisms in lead-free solder joints.

#### **4.3.1 Vickers Hardness Test**

Figure 4.26 shows the variation of Vickers hardness of as received SAC+ X solder. From Figure 4.26, it could be seen that the hardness (HV) of solder increased as a function of Al % in SAC 105. SAC105 with ~10 HV has increased to 14 HV as the addition of Al was up to 0.5 %. On the other hand, with addition of Zn up to 0.5%, it seems to have only slight increase in Vickers hardness of SAC+ Zn as compared to SAC 105.

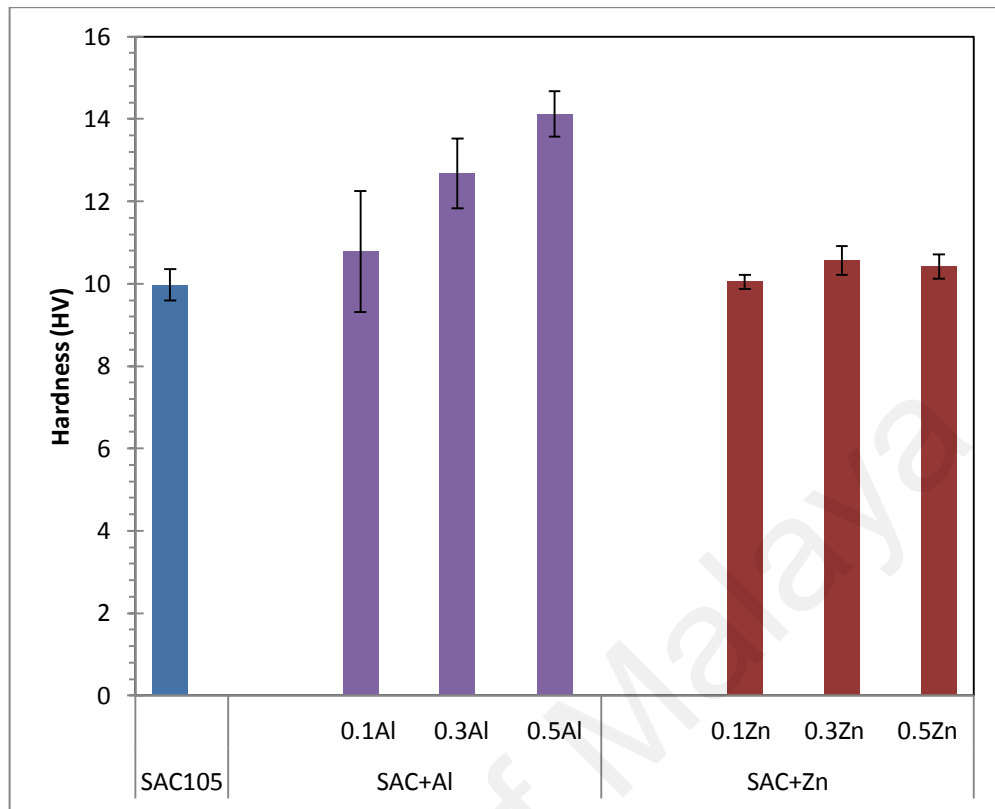
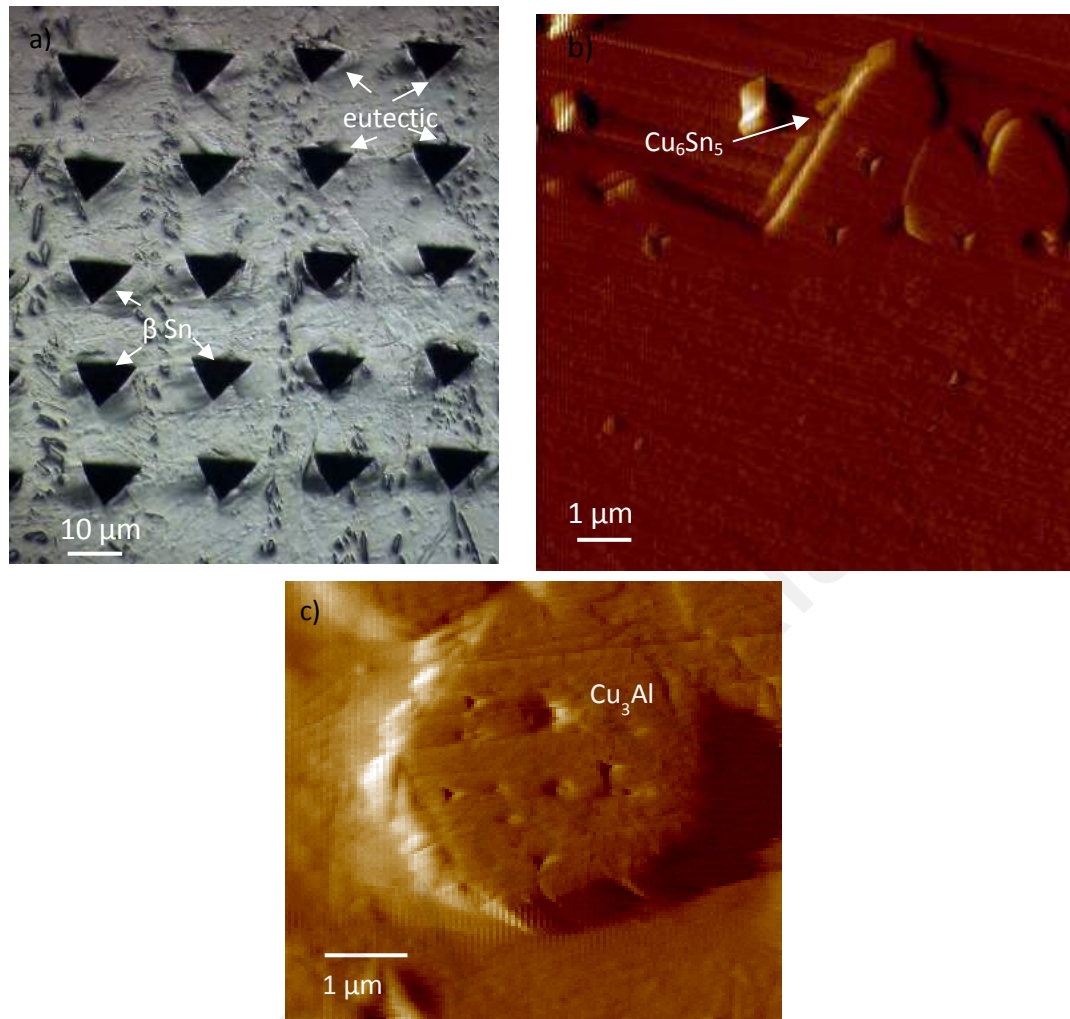


**Figure 4.26** Variation of Vickers hardness in as received SAC+ X solders.

#### 4.3.2 Nanoindentation on Bulk solder and IMC

Nanoindentation testing was carried out to investigate the mechanical properties, namely hardness and Young's modulus of the bulk microstructure (both Sn and eutectic phase) and constituent IMC phases found in SAC 105+ X such as  $\text{Cu}_6\text{Sn}_5$  and  $\text{Cu}_3\text{Al}$  (found in SAC+Al). Nanoindentation testing on the bulk microstructure was done by using an array of 100 indents. The indentation was performed at middle region of solder joints, at least  $100\mu\text{m}$  apart from the top and bottom Cu substrate. By using microscope, the indents were examined to determine if the indents fall on the Sn or eutectic region. The mechanical property of  $\text{Ag}_3\text{Sn}$  was not carried out in this study as the fine  $\text{Ag}_3\text{Sn}$  are too small for indentation.

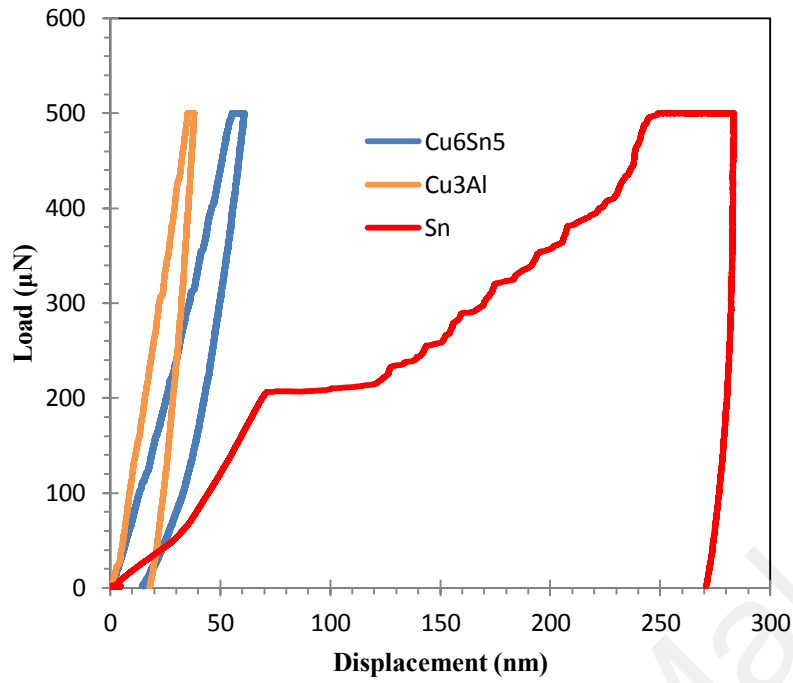
Figure 4.27 shows the array indentation in the bulk solder (FESEM), in-situ SPM image of indentation on  $\text{Cu}_6\text{Sn}_5$  at the solder/ Cu and  $\text{Cu}_3\text{Al}$  found in SAC +Al sample. Both bulk solder sample and  $\text{Cu}_6\text{Sn}_5$  was tested after reflow and after aging for 720 hr. Although Laurila et al. (2010) categorized Al as element which does not have marked solubility on Cu-Sn IMCs, they mentioned owing to the lack of solubility data of different elements in Cu-Sn IMCs, some elements exhibit solubility in Cu-Sn IMCs in the future. Therefore, we should not eliminate the effect of Al on the mechanical properties of  $\text{Cu}_6\text{Sn}_5$ , even though no aluminum detected in both  $\text{Cu}_6\text{Sn}_5$  and  $\text{Cu}_3\text{Sn}$  (from subchapter 4.2.3). Thus, for SAC +Al solder joints, nanoindentation on  $\text{Cu}_6\text{Sn}_5$  will only be carried out on SAC +0.5Al (highest amount of Al % added).



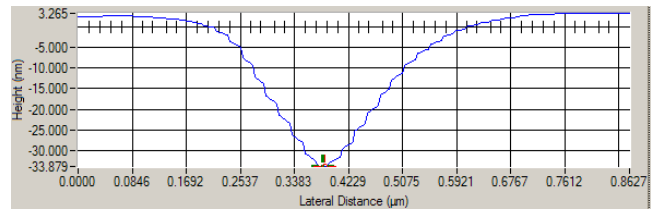
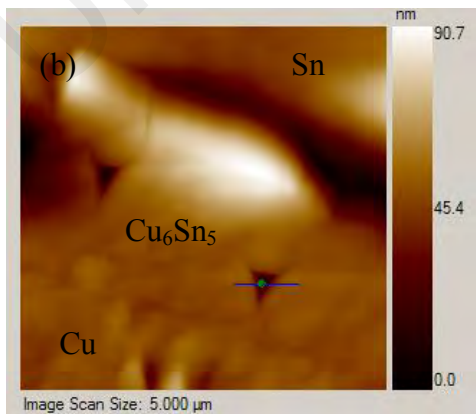
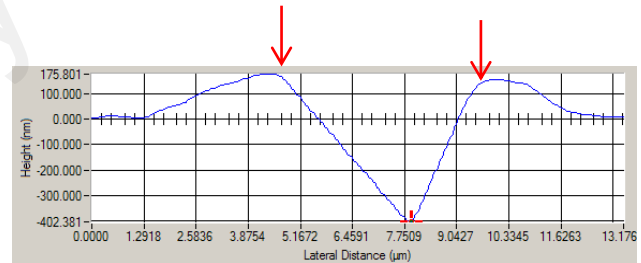
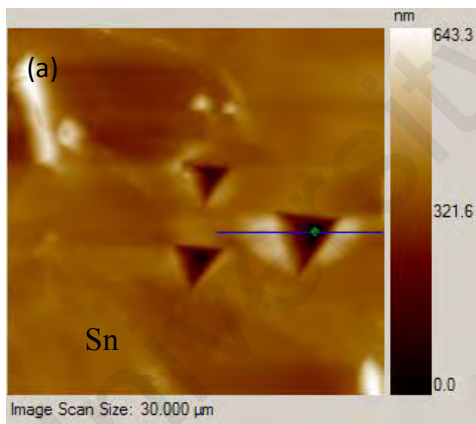
**Figure 4.27** (a) Optical micrograph of the indentation arrays on the Sn and eutectic region of bulk solder; (b) Scanning probe microscopy image of  $\text{Cu}_6\text{Sn}_5$  at the solder/Cu interface after indentation; (c) Scanning probe microscopy image of  $\text{Cu}_3\text{Al}$  in the bulk solder after indentation.

Figure 4.28 shows typical load displacement data obtained through indentations performed on Sn,  $\text{Cu}_6\text{Sn}_5$  and  $\text{Cu}_3\text{Al}$  of a maximum load of 500  $\mu\text{N}$ . For a test of the same maximum load, the maximum penetration of the indenter for Sn-Ag-Cu solder is approximately 4.5 times of that measured for  $\text{Cu}_6\text{Sn}_5$  and  $\text{Cu}_3\text{Al}$ . The solder matrix, as expected, is very soft, the matrix exhibited significant plasticity. Upon unloading, the solder

recovers only approximately 10 nm of the 230 nm that the indenter penetrated. In contrast to the solder, both intermetallics are significantly harder:  $\text{Cu}_6\text{Sn}_5$  (~6.2 GPa) and  $\text{Cu}_3\text{Al}$  (~10.50 GPa). The intermetallics typically recover around 40% of the maximum penetration of the indenter upon unloading. Scanning probe microscopy (SPM) was used to accurately perform indentation on specific IMC phases. It was also used to observe the residual indents, as shown in Figure 4.27(b, c). As expected from the nanoindentation data, the residual indents in the solder (much lower hardness than  $\text{Cu}_6\text{Sn}_5$  and  $\text{Cu}_3\text{Al}$ ) were much larger than in intermetallic. All of the residual indents observed for the intermetallics exhibited a smooth profile with no detected pile-up or sink-in of material, while softer materials like Sn exhibit a pile-up behavior. This can be seen in Figure 4.29, where the SPM (Scanning probe microscopy) images of a residual indent in Sn and  $\text{Cu}_6\text{Sn}_5$  is shown along with a height profile. Sn solder exhibited pile-up behavior, as seen in Figure 4.29a where there is a significant height difference at the edge of the indent (red arrow). On the other hand, a smooth profile with no detectable pile-up was observed for indents performed in  $\text{Cu}_6\text{Sn}_5$  (Figure 4.26b).



**Figure 4.28** Load vs displacement plot for indentations performed on bulk solder, Cu<sub>6</sub>Sn<sub>5</sub> and Cu<sub>3</sub>Al in SAC +X.



**Figure 4.29** SPM images of residual indents and the measured height profiles for (a) Sn and (b) Cu<sub>6</sub>Sn<sub>5</sub>.

**Table 4.2** Hardness and modulus of bulk solder and Cu<sub>6</sub>Sn<sub>5</sub> IMC in SAC105, SAC +0.1Zn, SAC+0.3Zn and SAC+0.5Zn after 1x reflow.

Sample	% of Al and Zn	Bulk solder		Cu <sub>6</sub> Sn <sub>5</sub>			
		As reflow		As reflow		1 month Aging	
		Hardness (GPa)	Reduced Modulus (GPa)	Hardness (GPa)	Reduced Modulus (GPa)	Hardness (GPa)	Reduced Modulus (GPa)
SAC 105		0.153	71.44	6.43	107.11	6.28	103.15
		±0.014	±5.45	±0.45	±8.5	±0.18	±8.5
SAC+Al	0.1Al	0.161	77.87	-	-	-	-
		±0.014	±3.54				
	0.3Al	0.180	79.60	-	-	-	-
		±0.018	±4.89				
	0.5Al	0.178	71.63	6.54±0.5	100.99±	6.26±1.07	100.99±
		±0.020	±5.06	9	10.09		10.09
SAC+Zn	0.1Zn	0.155	83.46	6.78 ±0.8	103.48	6.21	105.28
		±0.011	±6.61		±10.08	±0.23	±10.09
	0.3Zn	0.169	77.86	6.93 ±0.3	120.36	6.55	102.76
		±0.013	±6.43		±6.61	±0.33	±7.62
	0.5Zn	0.184	77.16	7.09	117.63	6.65	119.01
		±0.016	±5.54	±0.37	±8.43	±0.38	±13.27

### 4.3.3 Nanoindentation Creep on Bulk solder and IMC

In this paper, the creep behaviour of the bulk microstructure was characterized by using nanoindentation as tin based solder alloy are liable to creep. SAC and SAC+Zn samples were subjected to nanoindentation creep. SAC+Al samples were not subjected to nanoindentation creep as its non-uniform bulk microstructure (agglomeration and segregation of hard  $\text{Cu}_3\text{Al}$ ) can cause large variation in the results of creep test. A commonly-used procedure for evaluating the steady state creep stress exponent,  $n$ , from indentation data were not used in this study as it has been shown by Campbell et al. (2017) that it was fundamentally flawed. It was demonstrated that for a genuinely stable velocity, the procedure always leads to the same, constant value for  $n$  (either 1.0 or 0.5, depending on whether the tip shape is spherical or self-similar). This occurs irrespective of the value of the measured velocity, or indeed of any creep characteristic of the material (Campbell et al., 2017). Thus, in this study, creep behaviours were studied by evaluating the creep displacement. Displacement error from thermal drift will be a major issue for creep test, especially when hold durations was long which could be up from several minutes to hours. The Hysitron nanoDMA® III reference creep testing technique can solve this problem by applying a dynamic force all through the test, enabling continuous measurement of contact stiffness. First, the estimation of the modulus of the material (the reference modulus) is performed when error from thermal drift is insignificant. With the knowledge of the modulus, contact stiffness is continuously measured by keeping the quasi-static load as constant. With these data, contact depth and hardness can be computed without any reliance on the quasi-static displacement measurement, thus making background thermal drift irrelevant. In this manner, creep tests can be reliably performed during long duration.

Nanoindentation creep testing on the cross-sectioned bulk solder was done by using Hysitron nanoDMA® III reference creep testing technique for up to 30 indents in the middle of the solder joints. For each indent, creep displacement for every 180 s (total creep time 900 s) was recorded and the average creep displacement was plotted as time-displacement curve. Figure 4.30 shows the time vs displacement curves for the samples. At the initially, the displacement for all samples increase abruptly as the load was increased steadily at loading rate of 1 mN/s until it reaches the maximum load of 10 mN. This displacement is termed instantaneous displacement. As maximum load is reached, it was hold at the peak for 900 s. During this hold period, as the load is kept at constant, the displacement continues to increase with time. This displacement is called time- dependent displacement. Table 4.3 shows the measured instantaneous, time dependent, and total displacement of the samples. Zn addition in the solder does not have any major effects on the instantaneous displacement. As for the time- dependent displacement, it decreases as a function of Zn, where SAC exhibits the highest time-dependent displacement  $\sim 6.1 \mu\text{m}$ , and SAC+0.5 Zn shows the lowest displacement of  $\sim 4.5 \mu\text{m}$ . Thus, the total displacement has been reduced when Zn is added.

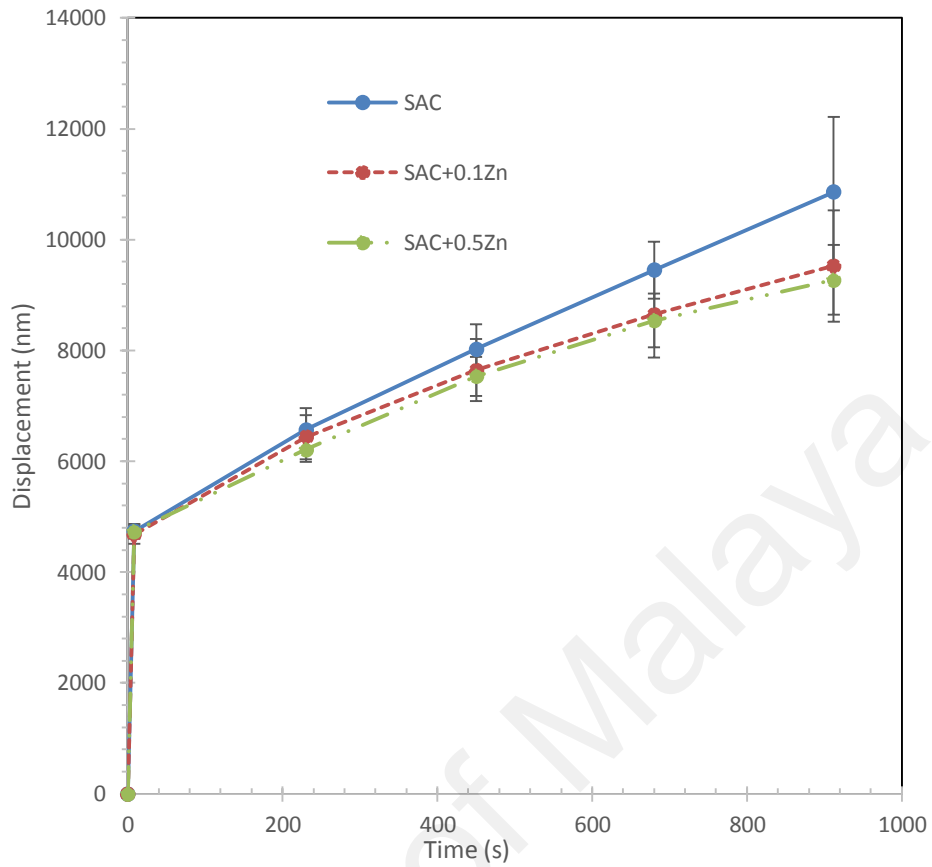


**Fig. 4.30** Average time-displacement curves for SAC, SAC+0.1Zn and SAC+0.5Zn.

**Table 4.3** Instantaneous, total, time-dependent displacement of bulk solder in SAC 105, SAC +0.1Zn and SAC+0.5Zn.

Sample	Instantaneous displacement( $\mu\text{m}$ )	Time dependent displacement ( $\mu\text{m}$ )	Total Displacement ( $\mu\text{m}$ )
SAC 105	$4.74 \pm 0.14$	$6.12 \pm 0.45$	$10.86 \pm 0.59$
SAC+ 0.1Zn	$4.68 \pm 0.19$	$4.85 \pm 0.79$	$9.53 \pm 0.97$
SAC+0.5Zn	$4.73 \pm 0.12$	$4.53 \pm 0.62$	$9.26 \pm 0.73$

#### 4.3.4 Shear strength

Figure 4.31 shows the shear test conducted on the SAC+ X (X=0, 0.1, 0.3, 0.5 % Al, Zn) solder joint after aging at 0 hr, 168 hr and 720 hr. It can be seen that the addition of Al up to 0.3 % and 0.5 % has reduced the shear strength of SAC under all aging conditions. For as-reflowed SAC+ Zn samples, shear strength of SAC+0.1Zn was similar to that of SAC105. With addition of 0.3 % Zn, the shear strength increased, however the addition of 0.5 % Zn reduced the strength. For SAC+0.1Zn and SAC+0.3Zn samples, similar with SAC + Al sample, the shear strength reduced as a function of aging time. While for as-reflowed SAC +0.5Zn, the shear strength dropped significantly when 0.5 % Zn was added. However, unlike other samples, it seems to retain its shear strength as the joints were subjected to thermal aging up to 720hr. The shear value of SAC+ 0.1 Zn, SAC+0.3 Zn and SAC+0.5 are very similar once they are subjected to thermal aging.

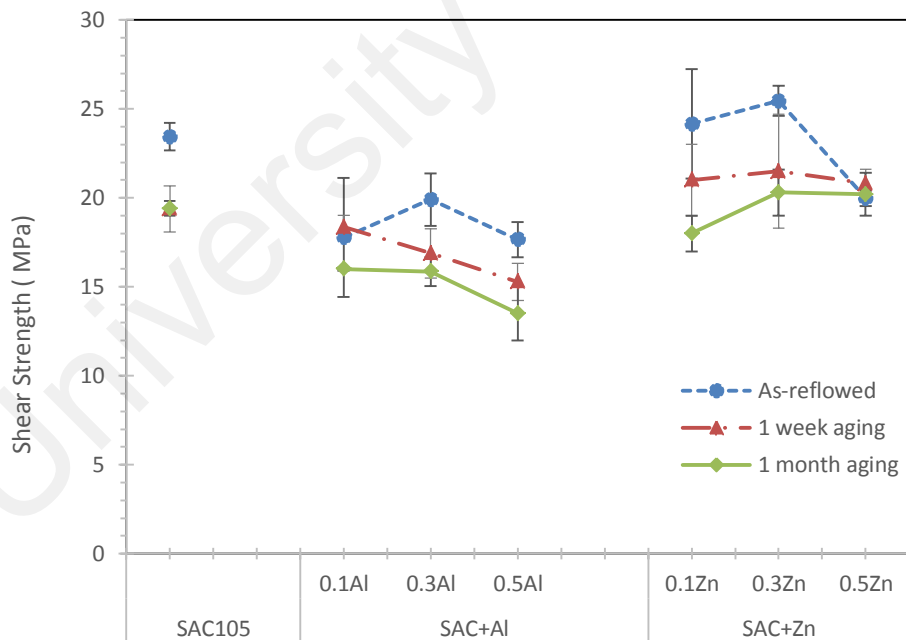


**Figure 4.31** Shear strength of SAC+ X after thermal aging at 150 °C at 0hr (as reflow), 168hr (1 week aging) and 720 hr(1 month aging).

#### 4.3.4.1 Shear Fracture Analysis (as -reflowed sample)

After shear testing on the as- reflowed samples, top fracture surface and cross-sections of the samples were observed under FESEM. In general, there are four types of failure modes: (i) ductile failure mode (ii) quasi- ductile failure mode, (iii) quasi-brittle failure mode and (iv) brittle failure mode (Matsumoto & Mirashi, 2002). Ductile failure mode and brittle failure mode are failure modes which exhibit only ductile fracture and brittle fracture respectively. While quasi-ductile failure mode (ductile fracture dominant) and quasi brittle failure mode (brittle fracture dominant) are both consists mixture of ductile and brittle fracture. Four types of fracture modes were also found in previous studies after shear test on solder balls (Song et al., 2007; Sujan et al., 2015). Thus, a detailed fracture surface analysis was carried out by using FESEM and EDS analyses to identify types of fracture modes for SAC+X solders.

##### (a) SAC105

Figure 4.32 shows the top view and cross sectional of fracture surface of as reflow SAC105. Under FESEM observation, it could be seen that the soft Sn matrix was sheared following the shear direction of the test, and as-reflowed SAC105 exhibits ductile shear. From the cross-sectioned of shear fracture, it further evident that SAC105 exhibit fully ductile shear, as all the cracks propagation occurred at the middle of bulk Sn solder joint or at the Sn region just above the IMC interface (circled in red in Fig 4.32), without exposing the brittle IMC.

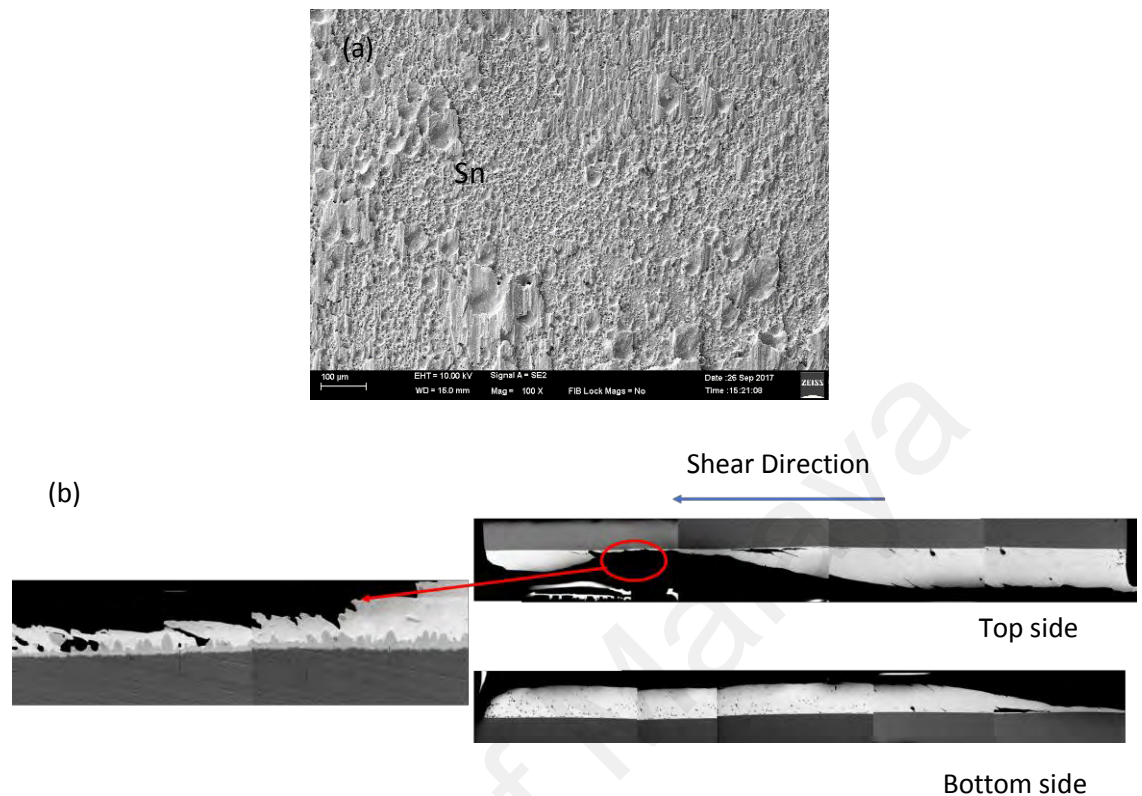
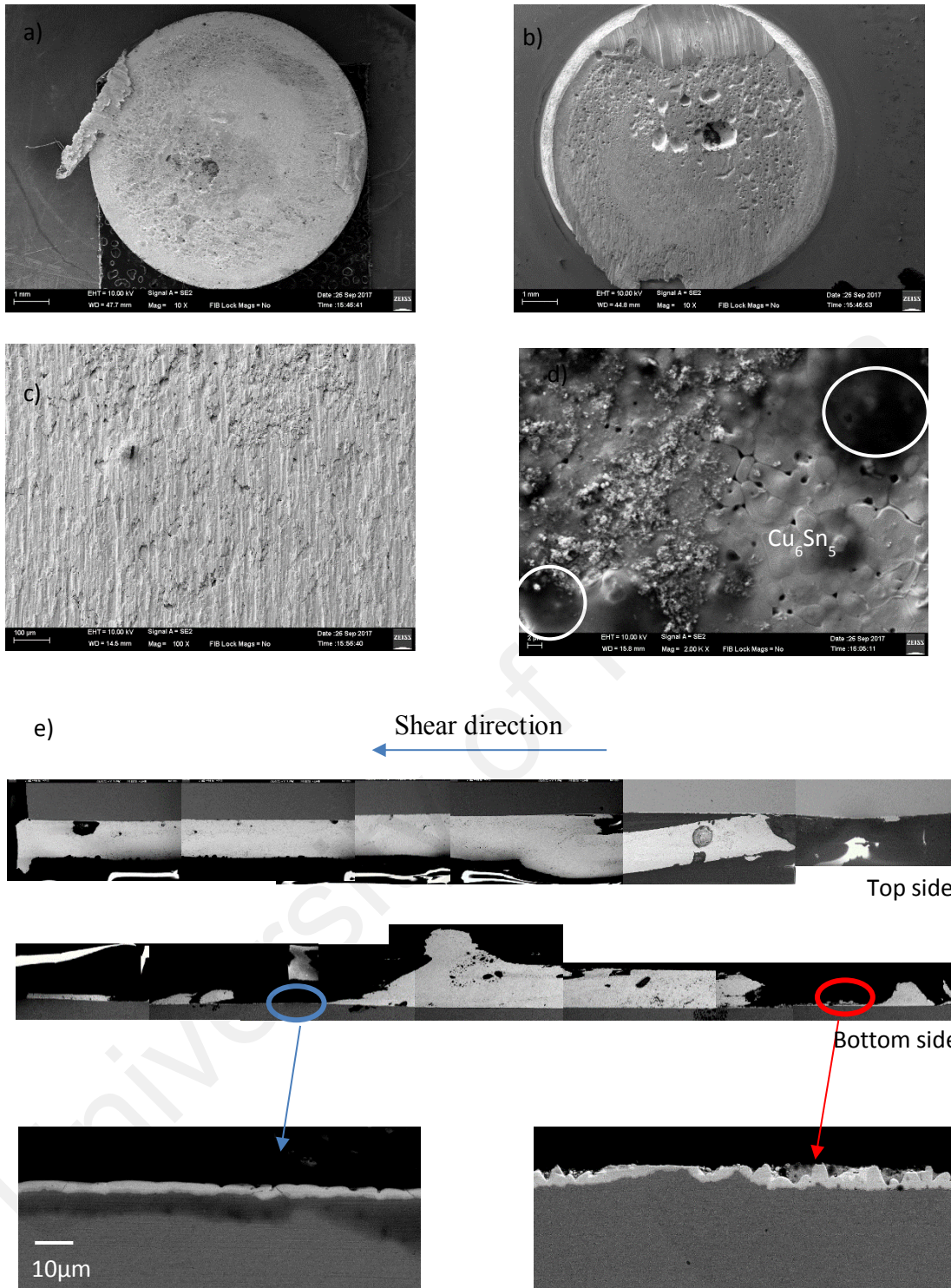


**Figure 4.32** (a) Top view FESEM micrograph of shear fracture of as reflowed SAC; (b) Cross sectional FESEM micrograph of shear fracture of as reflowed SAC105.

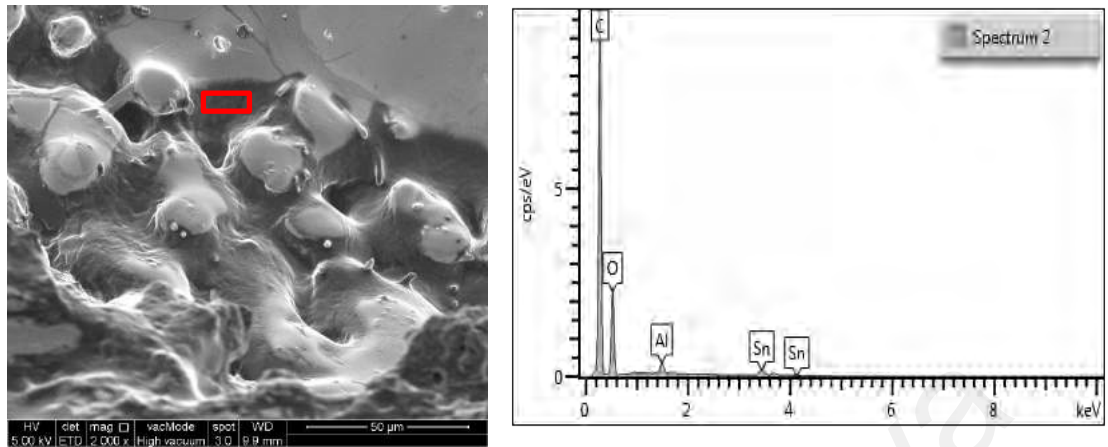
(b) SAC+ Al

Figure 4.33 shows the top view and sideview of the shear fracture of SAC+0.1Al. From the top view of the complement top and bottom fractured sample of SAC 105 (Fig. 4.33 (a&b)), it seems like fracture occurred mainly in the Sn matrix region. Under high magnification, it could be seen that most of the fracture occur on the Sn region (Fig 4.33(c)). Though there are also minor region where fracture occur on the IMC surface and some black substances (circled in white in Fig. 4.33(d)) were found on the exposed IMC. EDX analysis with 10 kV shows that the black substances found on the exposed IMC consists of carbon (~45 %), oxygen (~20 %), Al (~15%) and Cu (~20 %). This result reveals the presence of organic compounds (high % of carbon was found). Since WF 6317 flux used in

this experiment is an organic base water soluble (Senju Metal Industry WF 6317 safety data sheet), it is suspected that the black substances stain found at the fracture surface is a flux residue. Flux residue tends to spread to the outer boundary of solder joints after reflow. EDX analysis was done on the flux residue found at the outer boundary of solder joints. Figure 4.34 shows the EDX results done on the flux residue found at the solder joints' boundary. Both EDX results (EDX analysis on the black substances found on IMC surface and flux residue at the boundary) show high percentage of carbon and oxygen. Besides, both atomic percentage ratio of carbon and oxygen on the black substances and flux residue are very close, which is approximately 3:1. These results support the hypothesis that the origin of the black substances is the flux. Cross sectional view of the shear fracture from side view (Fig, 4.33(e)) further confirmed that SAC+0.1Al has quasi ductile fracture mode. Quasi ductile failure mode consists of mixed failure modes where the crack propagation occurs through both solder matrix (majority) and brittle interfacial IMC (minority). In SAC+0.1Al sample, most of the fracture occur at the Sn matrix region with some of the fracture occur at the brittle  $\text{Cu}_6\text{Sn}_5$ /Sn interface (circled in red) and some fracture occur across the  $\text{Cu}_6\text{Sn}_5$  IMC (circled in blue). As 0.5 % Al was added to SAC105, shear fracture surface of SAC+0.5Al solder joints appeared to be slightly different from that of SAC+0.1Al, where a 'ring' pattern was seen at the fracture surface (Figure 4.35). Detailed examination on the fracture surface shows that SAC+0.5Al also has quasi-ductile fracture mode, where fracture occur at Sn region, Sn/ IMC interface and across IMC region. Besides that, more Al organic black substances were seen on the fracture surface as compared to SAC+0.1Al.



**Figure 4.33** Top view FESEM micrograph of shear fracture of (a) top sample, (b) bottom sample; (c) shear fracture on Sn region; (d) fracture region exposing interfacial IMC region and (e) Cross sectional FESEM micrograph of shear fracture of as-reflowed SAC+0.1Al.



Element	Atomic %
C	75.20
O	22.80
Al	0.85
Sn	1.16

**Figure 4.34** EDX analysis on the flux residue at the boundary of SAC+0.5Al solders joints.

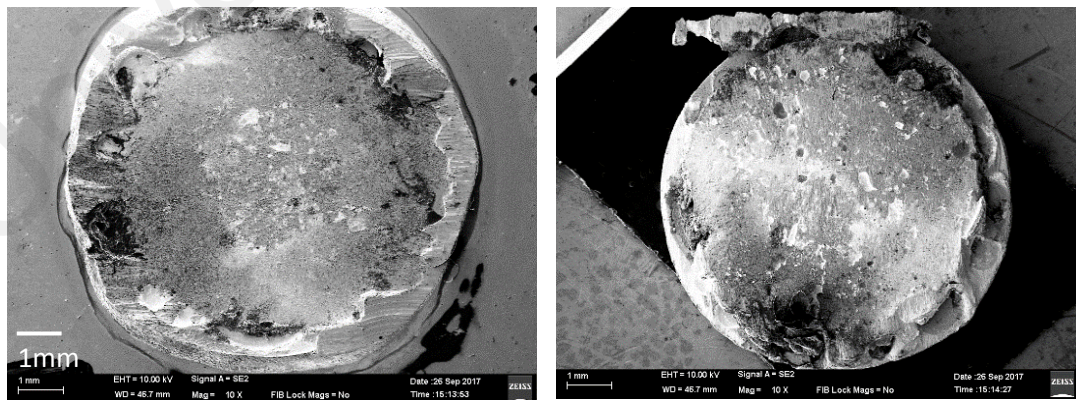


**Figure 4.35** Top view FESEM micrograph of shear fracture of SAC+0.5Al.

c) SAC+ Zn

Figure 4.36 shows cross-sectioned view of the fracture surface of SAC+0.1Zn. It is seen that the fracture occurred at the  $\text{Cu}_6\text{Sn}_5/\text{Sn}$  interface and through the brittle IMC at the bottom side of the sample at the initial stage of shearing. The crack then propagates through the Sn region and reaches the top side of IMC/Sn interface during shearing. The crack continues to propagate along the  $\text{Cu}_6\text{Sn}_5/\text{Sn}$  interface and through the  $\text{Cu}_6\text{Sn}_5$  IMC at the top side of the sample. Thus, based on the fracture from the side view, SAC+0.1Zn as-reflowed solder joints has a quasi-brittle fracture mode. Similar fracture mode was also seen in the SAC+0.5Zn solder joints.

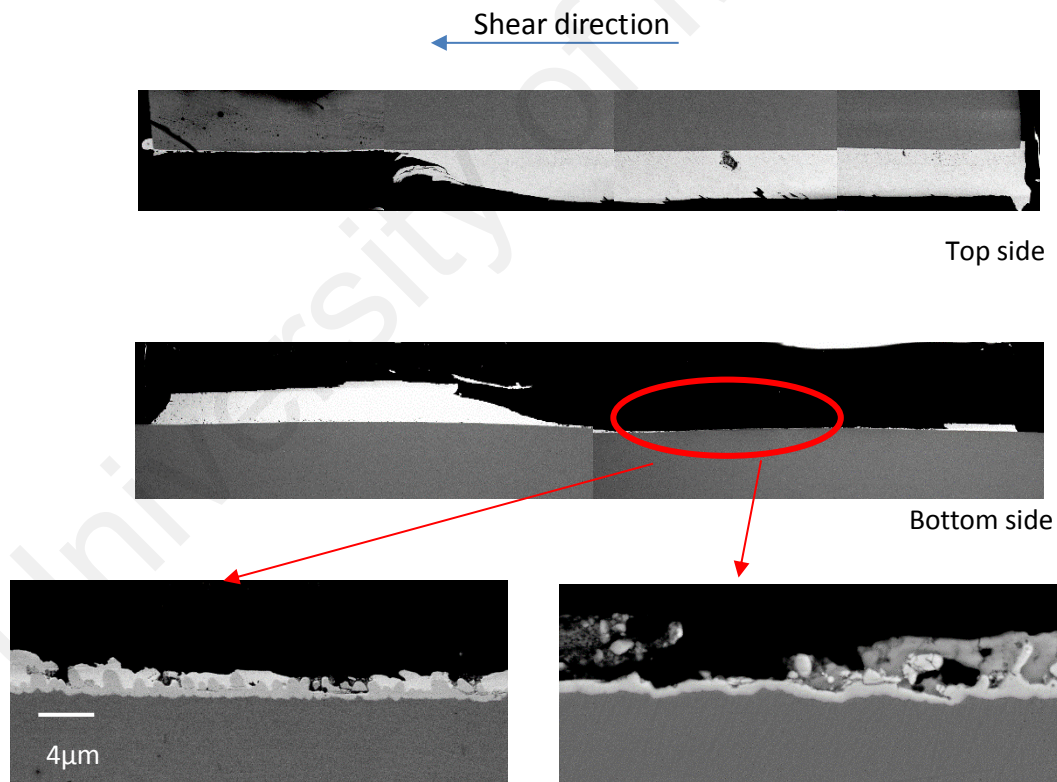


**Figure 4.36** Cross sectional FESEM micrograph of shear fracture of as-reflowed SAC+0.1Zn.

#### 4.3.4.2 Shear Fracture Analysis (Aging at 150 °C up to 1 month)

After shear testing, detailed fracture surface analysis was also carried out on the one month aging solder joints samples to identify various types of failure modes by using FESEM and EDS.

##### a) SAC105

After SAC105 samples were aged for 1 month, the shear fracture mode did not changed and it still exhibited ductile fracture mode. Figure 4.37 shows the top view of the shear fracture of SAC105 after 1 month aging. Ductile fracture on the middle region of Sn matrix (Fig. 4.37a) was dominantly seen throughout the whole fracture surface and some voids (Fig. 4.37b) were also found in some region. No brittle fracture surface was found. Thus, SAC105 solder joints after 1 month aging was categorized as ductile failure modes.

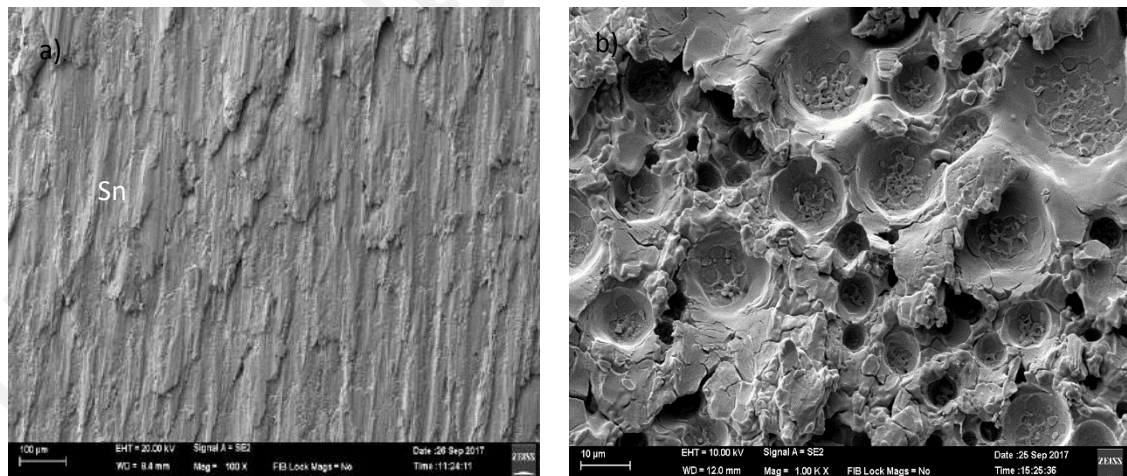


**Figure 4.37** Top view FESEM micrograph of shear fracture of (a)Sn region and (b)voids after 1 month aging.

## b) SAC + Al

After subjected to 1 month thermal aging, SAC+0.1Al solder joints have the same shear fracture mode as SAC+0.1 Al after reflow. Shear fracture surface of SAC+0.1Al after thermal aging, shows combination of ductile shear (majority) and brittle shear and thus categorized as quasi-ductile fracture mode. Figure 4.38 shows the fracture surface of SAC+0.5 Al after 1 month aging from top view. It could be seen that SAC+0.5Al after thermal aging have the same 'ring' fracture pattern as SAC+0.5Al as reflow sample. Similarly, many black substances were seen near the ring fracture surface and EDX analysis shows that they are same as those found in Fig 4.33(b). Elemental mapping shows that this organic compound consist of metallic element such as Al and Cu with no trace of Sn in it. The shear fracture mode of SAC+0.5Al changed when it was subjected to one month aging, where more brittle IMC were exposed throughout the fracture surface and crack propagation occurred at the IMC/ Sn interface. SAC+0.5Al shear fracture has changed from quasi-ductile fracture mode to quasi brittle mode after 1 month thermal aging.

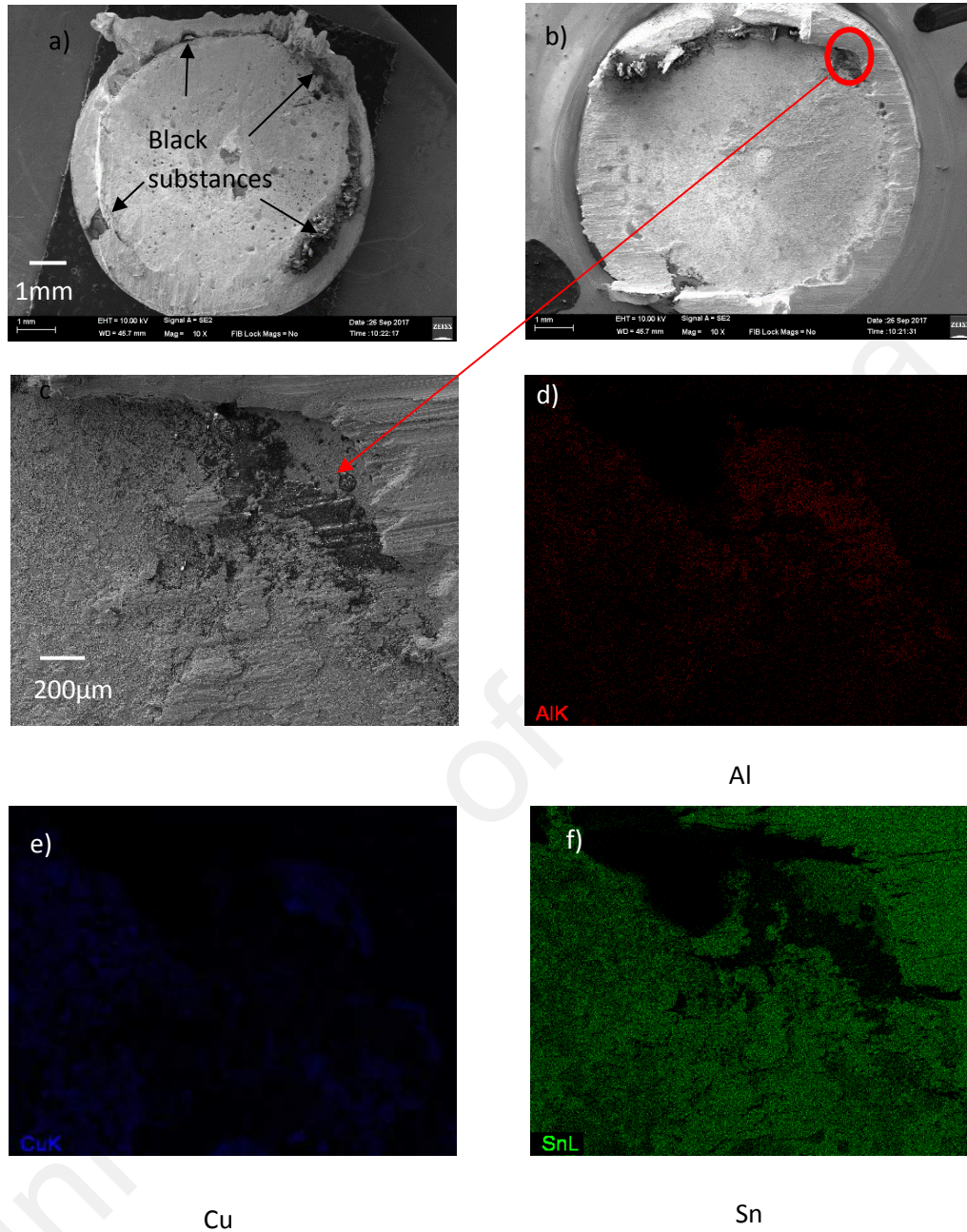


**Figure 4.38** (a,b) Top view FESEM micrograph of shear fracture of SAC+0.5Al after 1 month aging. (c) Magnified FESEM image of red circled area and elemental maps for the constituent elements: (d) Al; (e) Cu; (f) Sn.

### c) SAC + Zn

Figure 4.39 shows the top view and sideview shear fracture of SAC+0.1 Zn after one month aging. The top view fracture surface shows quasi brittle fracture mode where many IMC is exposed and some ductile Sn shear is on the fracture surface. EDX analysis on the exposed IMC (Figure 4.39(a&b)) confirmed the IMCs were consist of  $\text{Cu}_6(\text{Sn,Zn})_5$  and  $\text{Cu}_3(\text{Sn,Zn})$ . This shows that the cracks propagate along the Sn matrix,  $\text{Cu}_6\text{Sn}_5/\text{Sn}$  and  $\text{Cu}_6\text{Sn}_5/\text{Cu}_3\text{Sn}$  IMC. From Figure 4.39(d)), it could be seen that during the beginning of shearing, crack initiated and propagated along the Sn matrix (circled in blue), the crack was then further propagated to the Sn/  $\text{Cu}_6\text{Sn}_5$  IMC and  $\text{Cu}_6\text{Sn}_5/\text{Cu}_3\text{Sn}$  IMC. Similar fracture surface was seen in SAC+0.5 Zn after 1 month aging, thus addition of Zn from 0.1Zn to 0.5 Zn did not changed the fracture mode of the solder joints, where both exhibits quasi brittle fracture mode.

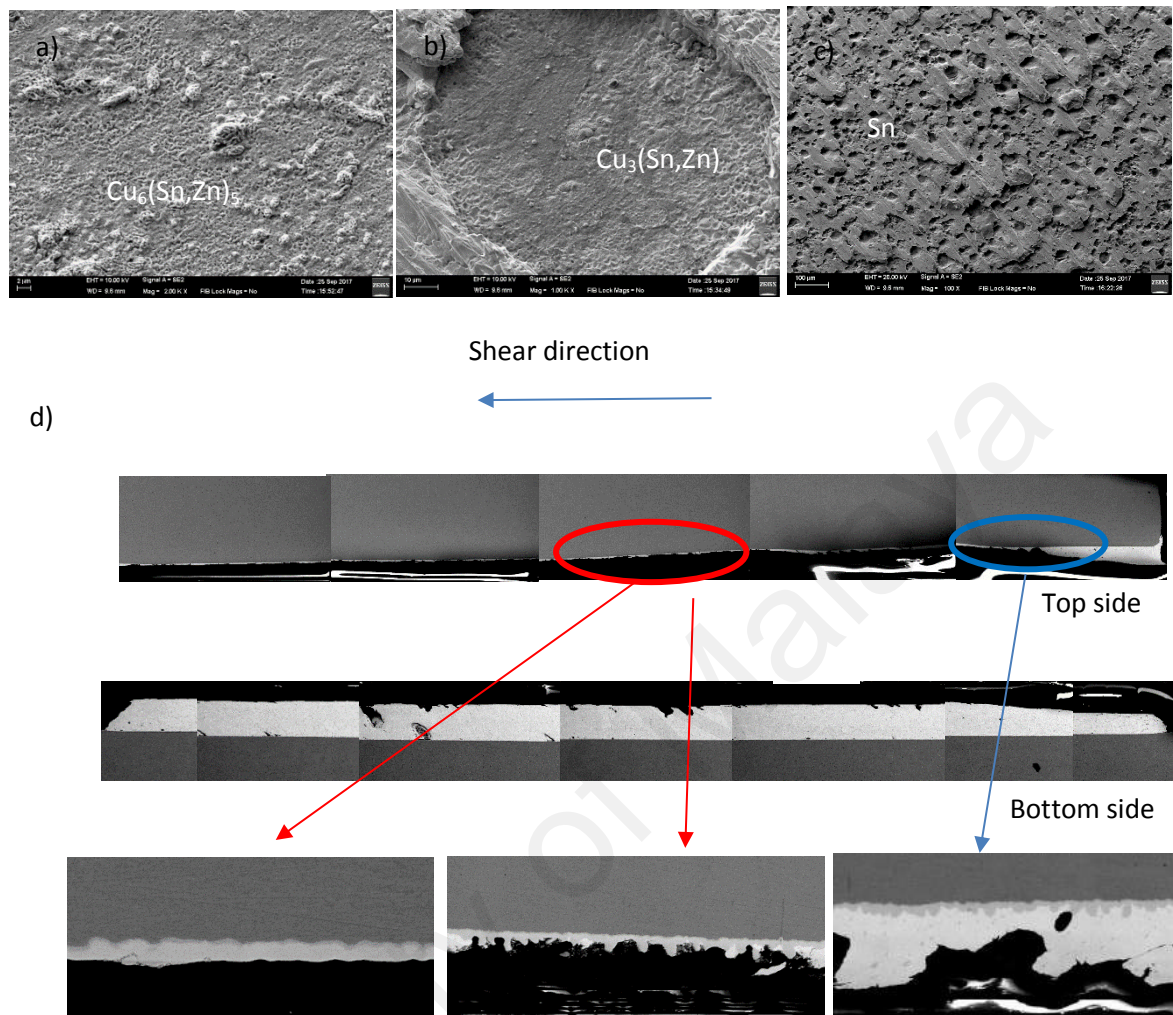


**Figure 4.39** Top view FESEM micrograph of shear fracture of (a)  $\text{Cu}_6(\text{Sn}, \text{Zn})_5$ , (b)  $\text{Cu}_3(\text{Sn}, \text{Zn})$ , (c) Sn region and (d) Cross sectional FESEM micrograph of shear fracture SAC+0.1Zn after aging for 720hr.

#### 4.3.5 Discussions of Mechanical Properties of SAC + X

According to ISO 14577: Metallic Materials—Instrumented Indentation Test for Hardness and Materials Parameters. International Organization for Standardization, type of indentation test eg, macro, micro or nano-indentation tests are characterized by indentations loads,  $L$ , and penetration,  $h$ , (ISO 14577, 2002). Ranges of loads and penetrations for

determining the indentation hardness at the three scale definitions given by ISO are as shown in Table 4.4. Based on the ISO standard, the indentation test that we have done in Chapter 4.3 could be defined as: macrohardness on bulk solder (Vickers test), micro indentation on eutectic region, and nanoindentation on interfacial IMC ( $\text{Cu}_6\text{Sn}_5$  and  $\text{Cu}_3\text{Al}$ )

**Table 4.4** Hardness testing scales defined by ISO 14577-1.

	<b>Load Range (N)</b>	<b>Penetration range (<math>\mu\text{m}</math>)</b>
Macroscale	$2 < L < 30,000$	Not specified
Microscale	$L < 2$	$h > 0.2$
Nanoscale	Not specified	$h < 0.2$

The addition of Al or Zn has different effects on the Vickers hardness of the as received bulk solder. Addition of Zn seems to have slight effect on the hardness of the solder even when Zn was added up to 0.5 % (slight increment for all 0.1-0.5 % Zn samples, Fig. 4.26). While addition of Al has significant effect on the hardness of SAC solder, where the hardness increased as a function of Al %. Significant microstructural refinements were seen in SAC+ Al and SAC+ Zn solders as compared to SAC solder (Fig. 4.3). Both addition of Al or Zn has similar magnitude in refining the microstructure of SAC. Since the obvious increase of hardness was only seen in SAC+ Al solders, thus the main effect of hardness increase was not due to the microstructure refinement. This could be due to the presence of  $\text{Cu}_3\text{Al}$  IMC particles in the bulk solder of all SAC+Al (Fig. 4.3b-d). It should be noted that, no Cu-Zn compound was found in the bulk microstructure of all SAC+Zn solders by EDX. From nanoindentation,  $\text{Cu}_3\text{Al}$  found in all SAC exhibits higher hardness ( $H_{\text{Cu}_3\text{Al}} \sim 10.5\text{GPa}$ ) than other phases ( $H_{\text{Sn}} \sim 0.13\text{GPa}$ ,  $H_{\text{Cu}_6\text{Sn}_5} \sim 6.5\text{GPa}$ ) in SAC + Al. This could be the reason

the hardness of SAC+ Al increase as a function of Al, as more  $\text{Cu}_3\text{Al}$  was found in the bulk solder when Al% was increased. Although the addition of Al seems promising in strengthening the solder joints, the agglomeration of  $\text{Cu}_3\text{Al}$  (as Al was added up to 0.3 and 0.5 % (Fig. 4.4(c,d); Fig. 4.5(a)) should be taken into consideration as well, as it might cause embrittlement of solder joints.

On the other hand, when the bulk solder region of the solder joints was subjected to micro-indentation, it could be seen that the results vary from that of Vickers hardness (macro-indentation). In micro-indentation, addition of Al increased the micro-hardness up to 0.3 % Al while the microhardness increased as a function of Zn addition up to 0.5%. Figure 4.40 and Figure 4.41 illustrate the macroscale and microscale indentation on SAC+ X samples. In the case of a macroscale indentation, such a Vickers shown in Fig. 4.40, the test creates a large indent size which will average the sample inhomogeneity (eg, for SAC+Al, indent will covered  $\beta\text{Sn}$ , eutectic phase, and  $\text{Cu}_3\text{Al}$ ), and a mean bulk hardness value is obtained. In the case of a micro indentation (Fig. 4.41), using high load nanoindentation (Load = 10 mN) at the bulk solder as in this test, a mean hardness will be measured but variations in small areas can also be assessed. Macro tests yield a material average hardness, while micro- and nanoscale tests indicate variations in different parts of the sample microstructure (Broitman, 2017). From this study, when macro test (Vickers hardness) was done on the bulk microstructure, the hardness was seem to be predominantly determined by the area ratio of soft Sn region to hard precipitates. By comparing Figure 4.41 a&b, Sn grain and microstructure (precipitate) refinement was seen in SAC+0.5Zn samples.  $\text{Cu}_6\text{Sn}_5$  precipitates are larger and spread further apart in SAC105 while  $\text{Cu}_6\text{Sn}_5$  precipitates are much refined and spread closely to each other in SAC+0.5Zn. However, the area of Sn to  $\text{Cu}_6\text{Sn}_5$  ratio that was covered in the indent seems similar in that of SAC105

and SAC+0.5Zn. Thus, there is only slight increase of macro-hardness is observed when Zn is added (Figure 4.26). Macro-hardness of SAC +Al increase as the indentations covered the segregated and agglomerated hard  $\text{Cu}_3\text{Al}$  particles which is  $\sim 70\%$  harder than  $\text{Cu}_6\text{Sn}_5$  (Figure 4.40b). On the other hand, when micro-scale test was conducted on SAC+ Al and SAC + Zn, microstructural refinement will play a significant role in determining the hardness of the small area. Since the spread of  $\text{Cu}_6\text{Sn}_5$  precipitates are further apart in SAC105, thus during microhardness test, there would be less hard  $\text{Cu}_6\text{Sn}_5$  precipitates covered by the small indent (Figure 4.41). Thus, the microhardness of bulk microstructure of SAC +Al and SAC +Zn increase since addition of Al and Zn has significantly refined the IMC ( $\text{Cu}_6\text{Sn}_5$ ,  $\text{Ag}_3\text{Sn}$ ) particles.



**Figure 4.40** Illustration of Vickers hardness indentation on (a) SAC, (b) SAC+0.5Al and (c) SAC+0.5Zn.

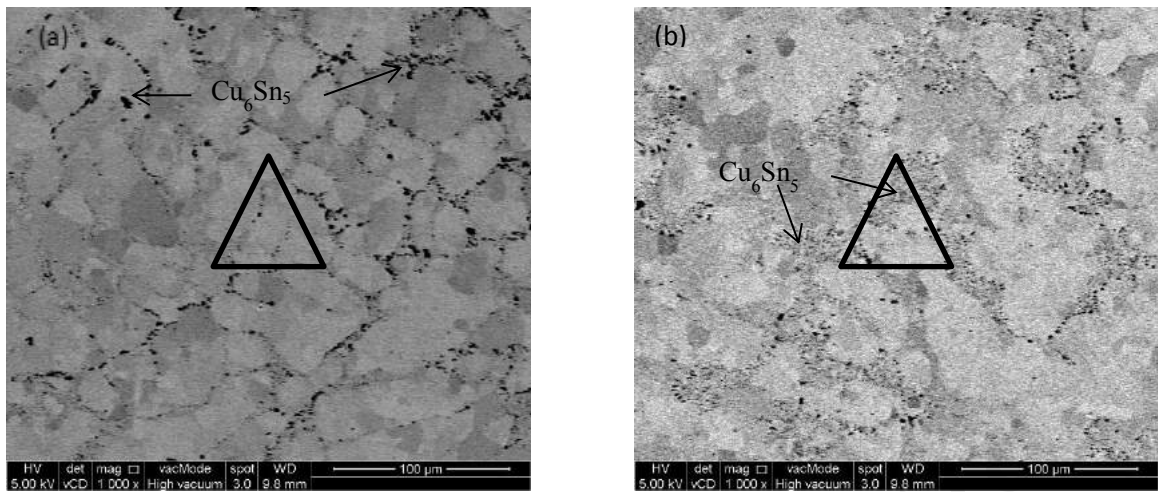


**Figure 4.41** Illustration of microhardness indentation on (a) SAC and (b) SAC+0.5Zn.

Besides, the addition of Zn has improved the creep behaviour of SAC as well, where it has lowered the time dependent displacement. Instantaneous displacement is related to plasticity whereas time dependent displacement is related to creep phenomenon (Fischer, 2004). For deformation at low temperature, low-temperature plasticity by dislocation glide is determined by (a) lattice resistance, (b) discrete obstacles, (c) phonon or other drags and (d) influenced by adiabatic heating (Frost & Ashby, 1982). Based on the Sn-Zn phase diagram, the maximum solubility of Zn in solid Sn is 0.6 % (Moser et al., 1985). Since Zn has such low solubility in Sn and based on the results in Section 4.3.2 (Sn has same hardness in SAC and SAC+Zn sample), solid solution effect was expected to play a minimal/ negligible role in the bulk microstructure. The increase of hardness and improving of creep in the bulk solder with addition of Zn is believed mainly due to the microstructural refinement of the eutectic region and IMC as mentioned above. The hardness of  $\text{Cu}_6\text{Sn}_5$  increased as a function of Zn solubility in  $\text{Cu}_6\text{Sn}_5$  (Table 4.2). It is suggested that the incorporation of Zn in the IMC lattice has increased the lattice resistance. This is in good agreement with studies done by Chen et al. (2015), where they have calculated that the

binding energy in the  $\eta$ -Cu<sub>6</sub>Zn<sub>0.5</sub>Sn<sub>4.5</sub> to be stronger than that of  $\eta$ -Cu<sub>6</sub>Sn<sub>5</sub>. They also found that the hardness of  $\eta$ -Cu<sub>6</sub>Zn<sub>0.5</sub>Sn<sub>4.5</sub> ( $6.44 \pm 0.14$  GPa) increased slightly as compared to that of  $\eta$ -Cu<sub>6</sub>Sn<sub>5</sub> ( $6.25 \pm 0.18$  GPa). With the presence of Zn atom in Cu<sub>6</sub>(Sn, Zn)<sub>5</sub>, it would be more effective in pinning of the dislocation under stress (Riehle et al., 2000). Thus, Cu<sub>6</sub>(Sn, Zn)<sub>5</sub> is more resistant to deformation than Cu<sub>6</sub>Sn<sub>5</sub>, which is the dominant factor in improving the hardness Cu<sub>6</sub>Sn<sub>5</sub>.

Although the minor addition of Al and Zn to SAC seems to have positive effects on the hardness of solder joints and creep behaviour of IMC (Zn addition), the shear test shows an adverse effect with addition of Al and Zn. Table 4.5 shows the summary of the shear fracture analysis of SAC+ X after reflow and after aging for 1 month. After reflow, the shear strength was reduced with the addition of Al, while addition of Zn up to 0.1 and 0.3 % slightly increased the shear strength of SAC, but the shear strength dropped significantly as Zn was added up to 0.5 % (Figure 4.31) Fracture analysis also shows that it has changed the ductile shear of SAC 105 into quasi ductile (SAC+Al) and quasi brittle (SAC+ Zn). All SAC+Al samples and SAC+Zn (0.1 & 0.3 %) reduced as function of aging time, while SAC+0.5Zn retained its shear strength after underwent thermal aging for 1 month. Overall, SAC+Al and SAC+Zn exhibit more tendency towards brittle fracture than SAC105 after reflow and after 1 month aging.

**Table 4.5** Summary of the shear fracture analysis of SAC+ X after reflow and after 1 month aging.

	<b>As reflow</b>	<b>1 month aging</b>
SAC105	<ul style="list-style-type: none"> <li>* Ductile Shear</li> <li>* Fracture occur at bulk Sn or Sn region just above IMC</li> <li>* Ductile fracture with cup consist of bulk IMC</li> </ul>	<ul style="list-style-type: none"> <li>* Ductile shear</li> <li>* Fracture occur at Sn just above IMC / at IMC</li> <li>* Ductile fracture with cup consist of bulk IMC</li> </ul>
SAC+ 0.1Al	<ul style="list-style-type: none"> <li>* Quasi Ductile Shear</li> <li>* Flux residue found at fracture sites</li> </ul>	<ul style="list-style-type: none"> <li>* Quasi Ductile Shear</li> <li>* Flux residue found at fracture sites</li> </ul>
SAC+ 0.5Al	<ul style="list-style-type: none"> <li>* Quasi ductile shear</li> <li>* Many large voids</li> <li>* More flux residues found as compared to SAC+0.1Al</li> <li>* Fracture occur at a 'Ring' pattern, where black substances were found</li> </ul>	<ul style="list-style-type: none"> <li>* Quasi Brittle</li> <li>* Many large voids</li> <li>* More flux residues found as compared to SAC+0.1Al</li> <li>* Fracture occur at a 'Ring' pattern, where black substances were found</li> </ul>
SAC+ 0.1Zn	<ul style="list-style-type: none"> <li>* Quasi Brittle</li> <li>* Fracture occur at mainly at Cu<sub>6</sub>Sn<sub>5</sub>/ Sn region, partially occur at Sn matrix above IMC</li> </ul>	<ul style="list-style-type: none"> <li>* Quasi Brittle</li> <li>* Fracture initiated at Sn matrix and soon propagate to Cu<sub>6</sub>Sn<sub>5</sub>/ Sn and Cu<sub>6</sub>Sn<sub>5</sub>/ Cu<sub>3</sub>Sn</li> </ul>
SAC+ 0.5Zn	<ul style="list-style-type: none"> <li>* Quasi Brittle</li> <li>* Fracture occur at mainly at Cu<sub>6</sub>Sn<sub>5</sub>/ Sn region, partially occur at Sn matrix above IMC</li> </ul>	<ul style="list-style-type: none"> <li>* Quasi Brittle</li> <li>* Fracture initiated at Sn matrix and soon propagate to Cu<sub>6</sub>Sn<sub>5</sub>/ Sn and Cu<sub>6</sub>Sn<sub>5</sub>/ Cu<sub>3</sub>Sn</li> </ul>

Anderson et al. (2009) has studied the effect of alloying element on the shear strength of Sn-3.5Ag-0.95Cu. Addition of 0.21 % Zn and 0.05 % Al were selected as the subject of studies and the solders were reflowed at a peak temperature of 255 °C for 30 s and cooled at 1 °C/s to 3 °C/s to simulate typical surface mount. They found that 0.21Zn and 0.05Al

additions reduced the strength of SAC, but did not change significantly with thermal aging at 150 °C for up to 1,000 h. This is in good agreement with our studies. However, they have found localized ductile shear failure in SAC+ Zn and SAC+ Al in all aging conditions which is different from what we have found in our study.

Black residue was found in the all shear fracture of SAC + Al solder joints in this study. No black organic compound (flux residue) was found in the shear fracture surface of SAC+ Al in Anderson's study (they did not report which type of flux was used in their study). Thus, it was likely the difference in shear fracture mode most was due to the presence of flux residue. From the fracture surface, black organic compounds that found on  $\text{Cu}_6\text{Sn}_5/\text{Sn}$  interface was likely to be accounted for the shear brittle fracture of SAC+ Al. Based on the EDX composition, this black organic compounds believed to be flux residue that react with Al compound and failed to escape from the solder during reflow, however further analysis need to done to confirm such hypothesis. Al was reactive and easily oxidized to form aluminium oxide, it was believed that some Al was oxidized when added to the SAC and during reflow, it reacts with the water-soluble flux which in attempt to remove the oxides and bring it out of the solder. Thus, most of the flux residue (containing Al and Cu) was found near the edge of the fracture surface of solder joints. Segregation and agglomeration of this flux residue at the  $\text{Cu}_6\text{Sn}_5/\text{Sn}$  interface makes it susceptible to crack propagations along the interface. During the shearing process, crack initiated at Sn and quickly propagated along the interface which consists of the flux residue (near the edge of solder joints). Thus, it forms a 'ring' structure fracture (ductile fracture occurred at the outer circle while brittle fracture occurred in the inner circle) where the flux residues are agglomerated.

SAC + Zn solder joints have quasi-brittle fracture at all Zn composition and conditions in this study. As mentioned above, Anderson et al. (2009) reported that addition of Zn has

reduced the shear strength of SAC, which is in good agreement with this study. However, it was reported to exhibit ductile shear failure where they found localized ductile shear through the Sn matrix region adjacent to the  $\text{Cu}_6\text{Sn}_5$  interfacial (Anderson et. al, 2009). While in this study, mixture of ductile shear (fracture at Sn matrix adjacent  $\text{Cu}_6\text{Sn}_5$  interfacial) and brittle shear (fracture at IMC/Sn interface and across the IMC) was found. Brittle fracture found in SAC+Zn could be attributed to the Zn distribution in the IMC (Fig 4.20). From Fig 4.20, Zn atom tends to accumulate at  $\text{Cu}_6\text{Sn}_5$  /Sn and IMC/Cu interface. This accumulation of Zn atom would cause inhomogeneity at the interface and thus making it susceptible to crack propagation. Thus, crack tends to propagate along the  $\text{Cu}_6\text{Sn}_5$  /Sn and IMC/Cu interface. Besides, a study on addition of 1% Zn in Sn-0.7Cu (SnCu) shows that the addition of Zn increased the shear strength of the solder alloys (Gao et al., 2011). However, they noticed that the addition of Zn in solder joint samples had an adverse effect, where SC+Zn/Cu solder joint has lower shear strength than SC/Cu solder joints. It was suggested that this was due to the presence of  $\text{Cu}_5\text{Zn}_8$  particles form at the solder/Cu interface after reflow of the solder joints. This shows that the strength of the bulk solder can be very different than the strength of solder joints. The mechanical properties of solder alloy were determined by its bulk microstructure, however, at solder joint configuration, the mechanical properties were dictates by its interface properties. This is similar to this study. Although addition of Al and Zn increased the hardness and creep resistance (only for SAC+Zn) of the bulk microstructure, both SAC+ X/Cu solder joints lowered the shear strength of SAC. Thus, it could be said that the properties of the solder joint's interface plays a major role in determining the mechanical properties of solder joint.

## CHAPTER 5: CONCLUSION AND RECOMMENDATION

### 5.1 Conclusion

In this work, Al or Zn is added as the fourth micro-alloying element in SAC solders. Investigations in this thesis on the effects of Al or Zn addition to SAC 105 focused on three main aspects: (i) Thermal analysis (ii) Microstructure properties, and (iii) Mechanical properties. The conclusions drawn from this work for each of the elements are listed in the following sections.

#### 5.1.1 Effect of minor addition of Al on SAC105

- Minor additions of Al have reduced the undercooling of SAC105 solder significantly.
- The addition of 0.1–0.5 wt. % Al to SAC105 leads to the formation of  $\text{Cu}_3\text{Al}$  IMC.  $\text{Cu}_3\text{Al}$  IMC segregated near the surface of solder upon reflow, particularly at higher concentration of Al.
- Al additions have reduced the thickness of interfacial  $\text{Cu}_6\text{Sn}_5$  IMC significantly but did not alter its morphology.
- Al additions do not have any significant effect on the thickness of  $\text{Cu}_3\text{Sn}$ .
- It is suggested that Al exerts its influence on the interfacial reaction by hindering the flow of reacting species at the interface during reflow.
- $\text{Cu}_3\text{Al}$  IMC has higher hardness and elastic modulus than other microstructural phases in the SAC105+Al system. The presence of high hardness  $\text{Cu}_3\text{Al}$  IMC is accounted for the increase in the hardness of the bulk solder.
- The addition of Al reduced the shear strength of SAC+105 after reflow and thermal aging. All SAC+ Al solder joints exhibited quasi-brittle fracture mode. A black residue was found on the shear fracture surface of SAC+Al.

### 5.1.2 Effect of minor addition of Zn on SAC105

- Minor additions of Zn have reduced the undercooling of SAC105 solder significantly.
- Zn atoms tend to segregate at the Sn/  $\text{Cu}_6\text{Sn}_5$  and  $\text{Cu}_6\text{Sn}_5$ /  $\text{Cu}_3\text{Sn}$  interface after reflow.
- Zn additions have increased the number of  $\text{Cu}_6\text{Sn}_5$  grains at the interface significantly. It is suggested that accumulation of Zn at the Cu interface act as a preferential site to promote heterogeneous nucleation of  $\text{Cu}_6\text{Sn}_5$ .
- Additions of Zn have reduced the thickness of  $\text{Cu}_6\text{Sn}_5$  during reflow and hindered the formation of  $\text{Cu}_3\text{Sn}$  layer at the interface significantly during isothermal aging.
- It is suggested that Zn impart its influence on the interfacial reaction by stabilizing  $\text{Cu}_6(\text{Sn,Zn})_5$  and hindering the flow of reacting species by accumulating at the solder/IMC and IMC/Cu interface.
- Additions of Zn as minor alloying element have increased the hardness and improved the creep resistance of bulk microstructure. Besides that, the hardness of  $\text{Cu}_6(\text{Sn,Zn})_5$  is increased as a function of Zn content in  $\text{Cu}_6(\text{Sn,Zn})_5$ .
- Zn additions reduced the shear strength of SAC105 after reflow and thermal aging. All SAC+ Zn solder joints exhibited quasi-brittle fracture mode. Accumulation of Zn atom at the solder/ IMC and IMC/Cu interface would cause inhomogeneity and thus making it susceptible to brittle fracture.

## 5.2 Recommendation

The results obtained from this work point out numerous interesting directions, which can be investigated in the future. Some of the future research directions are mentioned below.

- Minor alloying addition of Zn to SAC solder resulted in the dissolution of Zn atoms into  $\text{Cu}_6\text{Sn}_5$  crystal IMC and replaced some of the Sn atoms to form  $\text{Cu}_6(\text{Sn}, \text{Zn})_5$ . From this study, it is seen that Zn are likely to accumulate at the Sn/ $\text{Cu}_6\text{Sn}_5$  interface and  $\text{Cu}_6\text{Sn}_5/\text{Cu}$  interface. Calculation of Phase Diagrams (CALPHAD) method is a semi-empirical technique based on evaluation of experimental data, and theoretical estimates related to the thermodynamic properties of materials. In future, CALPHAD can be used to perform thermodynamic and kinetic studies on Zn atomic mobility in  $\text{Cu}_6\text{Sn}_5$ , and thus understand the accumulation of Zn atoms at the interface.
- By using nanoindentation, it is observed that addition of Zn has increased the hardness of solder matrix and  $\text{Cu}_6\text{Sn}_5$  as a function of Zn% at room temperature. It also improved the creep resistance of bulk microstructure. In the future, study of hardness, creep and deformation mechanisms as a function of temperature can be carried out. It is expected that the deformation mechanism would be different under high temperature.
- Addition of Al or Zn has altered the microstructure of SAC105 (grain refinement, new  $\text{Cu}_3\text{Al}$  IMC in bulk microstructure, segregation of  $\text{Cu}_3\text{Al}$  IMC, reduction in interfacial IMC). In future, study of stress distribution in the solder joints by using simulations can be carried out. It is expected that all the modifications in

microstructure could change the stress distribution of solder joints and thus affected the mechanical behaviour of solder joints.

- The quality of the solder joints can be improved by conducting the reflow process under controlled atmosphere in forming gas. Forming gas used in soldering is usually a mixture of 10 % hydrogen ( $H_2$ ) and 90 % nitrogen  $N_2$ . It is used to improve wetting of the higher temperature solder alloys and reduce oxidation during reflow.

University of Malaya

## REFERENCES

- Ahmad, A. (2013). Evolution of microstructure, thermal and creep properties of Ni-doped Sn-0.5Ag-0.7Cu low-Ag solder alloys for electronic applications. *Materials Designs*, 663-670.
- Ahmed, S., Basit, M., Suhling, J.C. and Lall, P., (2016). Effects of aging on SAC-Bi solder materials. *15th IEEE Intersociety Conference on Thermal and Thermomechanical Phenomena in Electronic Systems (ITherm), Las Vegas, NV, 2016*, 746-754.
- Amagai, M., Toyoda, Y., Ohnishi, T., and Akita, S. (2004). High drop test reliability: lead-free solders. *Proceedings 54th Electronic Components and Technology Conference*
- Amagai, M. (2008). A study of nanoparticles in Sn-Ag based lead free solders. *Microelectronics Reliability*, 1-16.
- Anderson, I.E., Haringa, J.L. (2004) Elevated temperature aging of solder joints based on Sn-Ag-Cu: Effects on joint microstructure and shear strength. *Journal of Electronic Material*, 33, 1485-1496.
- Anderson I.E. (2006) Development of Sn-Ag-Cu and Sn-Ag-Cu-X alloys for Pb-free electronic solder applications. *Lead-Free Electronic Solders*. Springer, Boston, MA.
- Anderson, I.E., Walleiser, J., Haringa, J., Laabs, F., and Kracher, A. (2009). Nucleation Control and Thermal Aging Resistance of Near-Eutectic Sn-Ag-Cu-X Solder Joints by Alloy Design. *Journal of Electronic Materials*. 38(12). 2770-2779.
- Bader, W. (1969). Dissolution of Au, Ag, Pd, Pt, Cu and Ni in a molten tin-lead solder. *Welding Journal*, 551.
- Bakhtiar, Ali (2017). Effect of iron and bismuth addition on the microstructure and mechanical properties of sac105 solder under severe thermal environment. Masters thesis, University of Malaya.
- Bashir, N., Haseeb, A. S. M. A., Rahman, A.Z., Fazal, M.A. (2016). Effect of Cobalt Doping on the Microstructure and Tensile Properties of Lead Free Solder Joint Subjected to Electromigration. *Journal of Materials Science & Technology*. 32.

- Bastow, E. and Jensen, T. (2009). The proliferation of lead-free alloys. *SMTA International Conference*, October, 2009.
- Bath, J. (2007). *Lead Free Soldering*. Springer US.
- Boesenberg, A. J. (2011). Development of Al, Mn, & Zn doped Sn-Ag-Cu-X solders for electronic assembly. Graduate Theses and Dissertations. University of Iowa States.
- Boettinger, W.J., Kattner, U.R., Moon, K.W. (2006). DTA and Heat-flux DSC Measurements of Alloy Melting and Freezing. Special Publication , 960-15. *Special Publication*, 960.
- Bradley, E., Handwerker, C.A., Bath, J., Parker, R.D., and Gedney, R.W. (2007) *Lead-Free Electronics: iNEMI Projects Lead to Successful Manufacturing*. Wiley US.
- Biocca, P. (2006). Lead-Free Reliability – Building it Right the First Time. *Lead-Free Connection*.
- Brook, S. and Lasky R.C. (2011). *Choosing a Low-Cost Alternative to SAC Alloys for PCB Assembly*. Indium Corporation.
- Bull, J. (2005). Nanoindentation of coating. *Applied Physics*, 393.
- Campbell, J., Dean, J. & Clyne, T.W. (2017). Limit case analysis of the “stable indenter velocity” method for obtaining creep stress exponents from constant load indentation creep tests. *Mech Time-Depend Mater*, 21, 31–43.
- Chen, S., Zhou, W. and Wu, P. (2015). Effect of Zn Additions on the Mechanical Properties of Cu<sub>6</sub>Sn<sub>5</sub>-Based IMCs: Theoretical and Experimental Investigations. *Journal of Elec Materi* 44, 3920–3926.
- Cheng, F., Nishikawa, H. and Takemoto, T. (2008) Microstructural and mechanical properties of Sn–Ag–Cu lead-free solders with minor addition of Ni and/or Co. *J Mater Sci* 43, 3643–3648.
- Chou, C.Y. & Chen, S.W. (2006). Phase equilibria of the Sn-Zn-Cu ternary system. *Acta Materialia*, 54, 2393.
- Cho, M., Kang, S., Seo, S., Shih, D., & Lee, H. (2009). Effects of under bump metallization and nickel alloying element on the undercooling behavior of Sn-based, Pb-free solders. *Journal of Materials Research* , 24. 534-543.
- Choi, S., Bieler T. R., Lucas J. P. and Subramanian, K. N. (1999) Characterization of the growth of intermetallic interfacial layers of Sn-Ag and Sn-Pb eutectic solders and their composite solders on Cu substrate during isothermal long-term aging. *Journal of Electronic Materials*. 28(11).1209–1215.

- Chuang, C., Tsao, L., Lin, H. and Feng, L. (2012) Effects of small amount of active Ti element additions on microstructure and property of Sn<sub>3.5</sub>Ag<sub>0.5</sub>Cu solder. *Materials Science and Engineering: A*, 558, 478-484.
- Deng, X., Koopman, M., Chawla, N., and Chawla, K. (2004). Young's modulus of (Cu, Ag)-Sn intermetallics measured by nanoindentation. *Materials Science and Engineering: A*. 364. 240-243.
- Dudek, M. & Chawla, N. (2010) Effect of Rare-Earth (La, Ce, and Y) Additions on the Microstructure and Mechanical Behavior of Sn-3.9Ag-0.7Cu Solder Alloy. *Metall and Mat Trans A* 41, 610–620 (2010).
- Dušek, M., Szendiuch, I., Bulva, J. and Zelinka, M. (2016), Wettability – SnPb and Lead-free. pp. 2-6, available at: [www.umel.feec.vutbr.cz/szend/novinky/wettability.pdf](http://www.umel.feec.vutbr.cz/szend/novinky/wettability.pdf)
- El-Daly A.A. & El-Taher, A.M. (2013) Improved strength of Ni and Zn-doped Sn-2.0Ag- 0.5Cu lead-free solder alloys under controlled processing parameters,” *Materials & Design*, vol. 47, pp. 607–614, 2013.
- El-Daly A.A, Hammad, A.E., Fawzy, A., Nasrallah, D. (2012). Microstructure, mechanical properties, and deformation behavior of Sn-1.0Ag-0.5Cu solder after Ni and Sb additions. *Materials and Design*. 43. 40–49.
- Fallahi, H., Nurulakmal.S., Fallahi, A.A., and Jamaluddin,A. (2012). Effect of iron and indium on IMC formation and mechanical properties of lead-free solder. *Materials Science and Engineering: A*. 553. 22-31.
- Fecht, H. Z., Zhang, X., Chang, Y.A., and Perepezko, J.H. (1989). Metastable phase equilibria in the lead-tin alloy system: Part II. Thermodynamic modeling. *Metallurgical Transaction A*, 795-803.
- Frear, D.R., Jang, J.W., and Lin, J.K.(2011). Pb-free solders for flip-chip interconnects. *JOM* 53, 28–33.
- Frost, H.J., Ashby M.F.,(1982). Deformation-mechanism maps. *Oxford: Pergamon Press*.
- Gabbott, Ian (2007) Designer granules : beating the trade-off between granule strength and dissolution time. PhD thesis, University of Sheffield.
- Gagliano, R.A., Ghosh, G. and Fine, M.E. (2002). Nucleation kinetics of Cu<sub>6</sub>Sn<sub>5</sub> by reaction of molten tin with a copper substrate. *Journal of Electronic Materials*, 31, 1195–1202.

- Gao, Y., Hui, J., Sun, X., Zhao, F., Zhao, J., Cheng, C., Luo, Z., and Wang, L. (2011). Role of Zinc on Shear Property Evolution between Sn-0.7Cu Solder and Joints. *Procedia Engineering*. 16. 807-811.
- Garcia, L., Osorio, W., Garcia, A. (2011). The effect of cooling rate on the dendritic spacing and morphology of Ag<sub>3</sub>Sn intermetallic particles of a SnAg solder alloy. *Materials & Design*. 32. 3008-3012.
- Gebhardt, E. & Petzow, G. (1959)The Constitution of the System Ag-Cu-Sn. (in German), *Z. Metallkd.*, 50, 597-605.
- Günther, E., Mehling, Ha., Hiebler, S.(2007). Modeling of subcooling and solidification of phase change materials. *Modelling and Simulation in Materials Science and Engineering*. 15, 879.
- Handwerker, C. (2003), “NEMI Pb-free solder project”, Proceedings of the SMTA International Conference, Chicago, IL, September, pp. 25-31.
- Handwerker, C., Kattner, U. and Moon, K.W. (2007). Fundamental Properties of Pb-Free Solder Alloys, New York: Springer.
- Haseeb, A. S. M. A., Leong, Y.M. and M., Arafat. (2014). In-situ alloying of Sn–3.5Ag solder during reflow through Zn nanoparticle addition and its effects on interfacial intermetallic layers. *Intermetallics*. 54. 86–94.
- Hayes, F.H., Lukas, H.L., Effenberg, G. and Petzow, G. (1986). A Thermodynamic Optimisation of the Cu-Ag-Pb System, *Z Metallkde.*, 77(11), 749–754
- Henderson, D., Gosselin, T., Sarkhel, A., Kang, S., Choi, W., Shih, D., Goldsmith, C., and Puttlitz, K.j. (2002). Ag<sub>3</sub>Sn plate formation in the solidification of near ternary eutectic Sn-Ag-Cu alloys. *Journal of Materials Research*, 17. 2775-2778.
- Huang, H. W., Winchester, K., Suvorova, A., Lawn, B, Liu, Y., Dell, J.M. and Faraone, L.. (2006). Effect of deposition conditions on mechanical properties of low-temperature PECVD silicon nitride films. *Materials Science and Engineering A*, 425, 453-459.
- Huang, M.L., Wang, L. (2005). Effects of Cu, Bi, and In on microstructure and tensile properties of Sn-Ag-X(Cu, Bi, In) solders. *Metallurgical and Materials Transactions A*. 36. 1439-1446
- Huang, Z. (2013). Fracture of Lead-Free Solder Joints for Electronic Applications: Effect of Material, Processing and Loading Conditions. Wsulibs. [https://research.wsulibs.wsu.edu/xmlui/bitstream/handle/2376/4709/Huang\\_wsu\\_0251E\\_10629.pdf?sequence=1](https://research.wsulibs.wsu.edu/xmlui/bitstream/handle/2376/4709/Huang_wsu_0251E_10629.pdf?sequence=1)
- Hodúlová, E., Hong, Li., Šimeková, B., Kovaříková, I. (2018). Structural analysis of SAC solder with Bi addition. *Welding in the World*. 62.1-2.

- Ipser H., Flandorfer H., Luef C., Schmetterer C., and Saeed U. (2006) Thermodynamics and phase diagrams of lead-free solder materials. In: *Lead-Free Electronic Solders*. Springer, Boston, MA.
- International Organization for Standardization. (2002). Metallic materials — Instrumented indentation test for hardness and materials parameters — Part 1: Test method. ISO 14577-1:2002
- International Organization for Standardization. (2002). Metallic materials — Instrumented indentation test for hardness and materials parameters — Part 2: Verification and calibration of testing machines. ISO 14577-2:2002.
- Jiang, L. C., Jiang, H., Chawla, N.(2010). Mechanical properties of Cu<sub>6</sub>Sn<sub>5</sub> intermetallics by micropillar compression testing. *Journal of Electronic Materials*, 480-483.
- Kang, S. K. (2004). Controlling Ag<sub>3</sub>Sn plate formation in near-ternary-eutectic Sn-Ag-Cu solder by minor Zn alloying. *Journal of Mineral, Metal and Materials*, 34- 38.
- Kang, S.K. (2012). *Lead-Free Solders: Materials Reliability for Electronics*.119-159.
- Kang, S.K., Lauro,P., Shih, D.Y., Henderson, D., and Puttlitz, K. (2005). Microstructure and mechanical properties of lead-free solders and solder joints used in microelectronic application. *IBM Journal of Research and Development*. 49(4.5), 607 – 620.
- Kang, S.K., Leonard, D., Shih, D.Y., Gignac, L., Henderson, D., Cho, S., and Yu, J. (2006). Interfacial Reactions of Sn-Ag-Cu Solders Modified by Minor Zn Alloying Addition. *Journal of Electronic Materials*. 35(3). 479-485.
- Kang, S., Cho, M., Lauro, P., and Shih, Da. (2007). Critical Factors Affecting the Undercooling of Pb-Free, Flip-Chip Solder Bumps and In-Situ Observation of Solidification Process. *Proceedings - Electronic Components and Technology Conference*. 1597 - 1603.
- Kantarcıoğlu, A., & Kalay, Y.E. (2014). Effects of Al and Fe additions on microstructure and mechanical properties of SnAgCu eutectic lead-free solders. *Materials Science and Engineering A, Structural Materials: Properties, Microstructure and Processing*, 79-84.
- Kanlayasiri, K., Mongkolwongrojn, M., and Ariga, T. (2009). Influence of indium addition on characteristics of Sn-0.3Ag-0.7Cu solder alloy. *Journal of Alloys and Compounds*. 485. 225-230.
- Karakaya I. &Thompson W.T. (1987). The Ag-Sn system. *Bull. Alloy Phase Diagr*, 8:340-341.

- Kashchiev, D. (2000): Nucleation: Basic Theory with Applications. *Butterworth-Heinemann, Oxford*.
- Karlya, Y., Gagg, C., and Plumbridge, W.J. (2000). Tin pest in lead-free solders. *Soldering and Surface Mount Technology*, 13(1), 39-40.
- Keller, J., Baither, D., Wilke, U. and Schmitz, G. (2011). Mechanical properties Pb-free SnAg solder joints. *Acta Materialia* , Vol. 59 No. 7, pp. 2731-2741.
- Koo, J., Lee, C., Hong, S., Kim, K., and Lee, H. (2015). Microstructural discovery of Al addition on Sn-0.5Cu-based Pb-free solder design. *Journal of Alloys and Compounds*. 650.
- Kotadia, H. R., Mokhtari, O., M. Bottrill, M.P. Clode, M. A. Green, S.H. Mannan (2010)., Reactions of Sn-3.5Ag-Based Solders Containing Zn and Al Additions on Cu and Ni(P) Substrates, J. Electron. Mater. 39 (2010) 2720 - 2731. *Journal of Electronic Materials*, 39, 2720-2731.
- Kotadia, H. R., Mokhtari, O., Pannerselvam, A., M. A. Green, S.H. Mannan (2012). , Massive spalling of Cu-Zn and Cu-Al intermetallic compounds at the interface between solders and Cu substrate during liquid state reaction. *Journal of Applied Physics*, 0749021-0749026.
- Kotadia, H. R., Rahnama, A., Das, A., Sridhar, S. and Mannan, S. (2017). Role of Zinc Content on Solidification and Interfacial Nucleation of Sn-Cu Solder Alloy by Experiments and Phase-field Simulation. *Conference: 6th Decennial International Conference on Solidification Processing, At Old Windsor*.
- Kumar, K. & Kubaschewski, O. (2007). Ag-Cu-Sn (Silver-Copper-Tin). *Non-Ferrous Metal Systems. Part 3*. SpringerMaterials
- Lasky, R.C. (2005). Tin Pest: A Forgotten Issue in Lead-free Soldering? *SMTA International 2004 Proceedings*.
- Laurila, T., Vuorinen, V., and Kivilahti, J. (2005). Interfacial Reactions Between Lead-Free Solders and Common Base Materials. *Materials Science and Engineering R Reports*. 37,1-60.
- Laurila, T., Vuorinen, V., and Kivilahti, J. (2010). Impurity and alloying effects on interfacial reaction layers in Pb-free soldering. *Material Science and Engineering R*, 68, 1-38.
- Li, J. A., P.A., Johnson, C.M. (2012). Effect of trace Al on growth rates of intermetallic compound layers between Sn-based solders and Cu substrate. *Journal of Alloys and Compound*, 70-79.

- Li, G.Y., Chen, B., Shi, X., Wong, C.K., and Wang, Z.F.. (2006). Effects of Sb addition on tensile strength of Sn–3.5Ag–0.7Cu solder alloy and joint. *Thin Solid Films*, 504, 421-425.
- Li, S., Liu, Y., Zhang, H., Cai, H., Sun, F., Zhang, G.Q. (2018). Microstructure and hardness of SAC305 and SAC305-0.3Ni solder on Cu, high temperature treated Cu, and graphene-coated Cu substrates. *Results in Physics*. 11.
- Liu, P., Yao, P. and Liu, J. (2009). Effects of multiple reflows on interfacial reaction and shear strength of SnAgCu and SnPb solder joints with different PCB surface finishes. *Journal of Alloys and Compounds*, 470, 188-194.
- Liu, Weiping & Lee, Ning-Cheng. (2007). The effects of additives to SnAgCu alloys on microstructure and drop impact reliability of solder joints. *JOM*. 59. 26-31.
- Liu, Y., Li, S., Zhang, H. (2018) et al. Microstructure and hardness of SAC305-xNi solder on Cu and graphene-coated Cu substrates. *J Mater Sci: Mater Electron* 29, 13167–13175.
- Loomans, M.E. & Fine, M.E. (2000). Tin-Silver-Copper Eutectic Temperature and Composition”, *Metall. Mater. Trans.*, 31A, 1155-1162.
- Luo, D., Xue, S. & Li, Z.( 2014). Effects of Ga addition on microstructure and properties of Sn–0.5Ag–0.7Cu solder. *J Mater Sci: Mater Electron*, 25, 3566–3571
- Ma, Z. L., Belyakov, S. A. & Gourlay, C. M. (2016). Effects of cobalt on the nucleation and grain refinement of Sn-3Ag-0.5Cu solders. *J. Alloys Compd*. 682, 326–337.
- Marques, V.M.F., Johnston, C. and Grant, P. (2013). Nanomechanical characterization of Sn-Ag-Cu/Cu Joints- Part 1: Young's Modulus , hardness and deformation mechanisms as a function of temperature. *Acta Materialia*, 61, 2460-2470.
- Marques, V.M.F., Johnston, C. and Grant, P. (2013). Nanomechanical characterization of Sn-Ag-Cu/Cu Joints- Part 2: Nanoindentation creep and its relationship with uniaxial creep as a function of temperature. *Acta Materialia*, 61, 2471-2480.
- Matsumoto, T. and Mihashi, H. (2002). “JCI-DFRCC summary report on DFRCC terminologies and application concepts.” *Proceedings of the JCI International Workshop on Ductile Fiber Reinforced Cementitious Composites*, 59-66.
- Mattila, T., Vuorinen, V., & Kivilahti, J. (2004). Impact of printed wiring board coatings on the reliability of lead-free chip-scale package interconnections. *Journal of Materials Research*, 19(11), 3214-3223.
- Massalski, T.B.(1980) The Al–Cu (Aluminum-Copper) system. *Bulletin of Alloy Phase Diagrams*, 1, 27–33. <https://doi.org/10.1007/BF02883281>.

- McKeown, J.T., Zwiack, K., Liu, C. (2016). Time-Resolved In Situ Measurements During Rapid Alloy Solidification: Experimental Insight for Additive Manufacturing. *JOM* 68, 985–999 (2016).
- Meyers, M., & Chawla, K. (2008). Mechanical Behavior of Materials. *Cambridge: Cambridge University Press.*
- Miller, C.M., Anderson, I.E. and Smith, J.F. (2004). A viable tin-lead solder substitute: Sn-Ag-Cu. *Journal of Electronic Materials*, 23, 595–601.
- Moon, K. B., Boettinger, W. J., Kattner, U. R., Biancaniello, F. S., Handwerker, C. A. (2000). *Experimental and thermodynamic assessment of Sn-Ag-Cu solder alloys*. *Journal of Electronic Materials*: 1122-1136.
- Moser, Z., Dutkiewicz, J., Gasior, W. (1985) The Sn–Zn (Tin-Zinc) system. *Bulletin of Alloy Phase Diagrams*, 6, 330–334.
- Mu, D. H., Huang H. and Nogita, K. (2012). Anisotropic mechanical properties of Cu<sub>6</sub>Sn<sub>5</sub> and (Cu,Ni)<sub>6</sub>Sn<sub>5</sub>. *Materials Letters*, 86, 46-49.
- Mu, D. H., Huang H., McDonald, S. and Nogita, K. (2013). Creep and Mechanical Properties of Cu<sub>6</sub>Sn<sub>5</sub> and (Cu,Ni)<sub>6</sub>Sn<sub>5</sub>. *Journal of Electronic Materials*, 304-311.
- Murray, J.L.(1985). The aluminium-copper system. *Int Met Rev*, 30, 211.
- Newbury, D., & Ritchie, N. (2015). Performing elemental microanalysis with high accuracy and high precision by scanning electron microscopy/silicon drift detector energy-dispersive X-ray spectrometry (SEM/SDD-EDS). *Journal of Materials Science*. 50,493–518.
- Nogita, K. (2010). Stabilisation of Cu<sub>6</sub>Sn<sub>5</sub> by Ni in Sn-0.7Cu-0.05Ni lead-free solder alloys. *Intermetallics*, 18(1), 145-149.
- Nogita, K., Gourlay, C., McDonald, S., Suenaga, S., Read, J., Zeng, G., and Gu, Q.. (2013). Characteristics of Beta/Alpha transformations in high purity tin. *Phase Stability, Phase Transformations, and Reactive Phase Formation in Electronic Materials*.
- Noor, Mhd., Nasir, N. F., Idris, S. R. A. (2016). A review: lead free solder and its wettability properties. *Soldering & Surface Mount Technology*, 28(3), 125–132.
- Oh, C.S., Shim, J.H., Lee, B.J., and Lee, D.N. (1996). A thermodynamic study on the Ag-Sb-Sn system, *Journal of Alloys and Compounds*, 238(1–2), 155-166,
- Oh, M. (1994). Growth Kinetics of Intermetallic Phases in the Cu-Sn Binary and the Cu-Ni-Sn ternary system at low temperature. *Doctoral Dissertation*.

- Oliver, W.C. and Pharr, G.M. (2004) Measurement of Hardness and Elastic Modulus by Instrumented Indentation: Advances in Understanding and Refinements to Methodology. *J. Mater. Res*, 19, 3-20.
- Riehle M., Simmchen E. (2000) Grundlagen der Werkstofftechnik, *Deutscher Verlag für Grundstoffindustrie*, Stuttgart. Retrieved from: <https://www.giessereilexikon.com/en/foundrylexicon/Encyclopedia/show/strengthening-mechanisms-4698/?cHash=a1de8b3f251a87d649ec6d341ee39d8d>
- Sayyadi, R. & Naffakh-Moosavy, H. (2019). The Role of Intermetallic Compounds in Controlling the Microstructural, Physical and Mechanical Properties of Cu-[Sn-Ag-Cu-Bi]-Cu Solder Joints. *Sci Rep*, 9, 8389.
- Seo, S., Cho, M., Kang, S., Jang, J., and Lee, H. (2011). Minor Alloying Effects of Ni or Zn on Microstructure and Microhardness of Pb-free Solders, *Proc. 2011 ECTC, Orlando, FL*. 84-89, June.
- Shnawah, D. S., Sabri, M., Faizul, M., Irfan, B., Said, M., and Che, F.X.. (2012). , The bulk alloy microstructure and mechanical properties of Sn–1Ag–0.5Cu–xAl solders (x =0, 0.1 and 0.2 wt. %). *Journal of Material Science: Materials Electronics*, 23, 1988-1997.
- Shi, Y. W., Tian, J., Hao, H., Xia, Z. D., Lei, Y. P., Guo, F. (2008) Effects of small amount addition of rare earth Er on microstructure and property of SnAgCu solder. *Journal of Alloys and Compounds*, 453(1-2): 180.
- Song, F., Lee, S. W. R., Newman, K., Sykes, B. and Clark, S. (2007). Brittle Failure Mechanism of SnAgCu and SnPb Solder Balls during High Speed Ball Shear and Cold Ball Pull Tests. *Proceedings 57th Electronic Components and Technology Conference, Reno*, 364-372.
- Song, J.M., Lin, J., Huang, C. & Chuang, W. (2007). Crystallization, morphology and distribution of Ag<sub>3</sub>Sn in Sn-Ag-Cu alloys and their influence on the vibration fracture properties. *Materials Science and Engineering a-Structural Materials Properties Microstructure and Processing*. 466(1-2) 9-17.
- Song, J.M., Liu, Y., Lai, Y., Chiu, Y., & Lee, N. C. (2012). Influence of trace alloying elements on the ball impact test reliability of SnAgCu solder joints. *Microelectronics Reliability*, 52, 180-189.
- Subramaniam, K. (2012). *Lead-free Solders: Materials Reliability for Electronics*. Wiley US.

- Sujan, G.K., Haseeb, A., & Afifi, A.M. (2014). Effects of metallic nanoparticle doped flux on the interfacial intermetallic compounds between lead-free solder ball and copper substrate. *Materials characterization*, 97, 199-209.
- Sujan, G. K., Haseeb, A. S. M. A., Amalina, M.A., Nishikawa, H. (2015). Ball Shear Strength and Fracture Modes of Lead-Free Solder Joints Prepared Using Nickel Nanoparticle Doped Flux. *Electronic Materials Letters*. 11. 452-456. 10.1007/s13391-015-4377-6.
- Sun, Lei & Zhang, Liang. (2015). Properties and Microstructures of Sn-Ag-Cu-X Lead-Free Solder Joints in Electronic Packaging. *Advances in Materials Science and Engineering*. 2015. 1-16.
- Swenson, D. (2007). The effects of suppressed beta tin nucleation on the microstructural evolution of lead-free solder joints. *J Mater Sci: Mater Electron*, 18, 39–54 .
- Syed, Ahmer & Kim, Tae & Cho, Young & Kim, Chang & Yoo, Min. (2007). Alloying effect of Ni, Co, and Sb in SAC solder for improved drop performance of chip scale packages with Cu OSP pad finish. *Proceedings of the Electronic Packaging Technology Conference, EPTC*. 404 – 411.
- Szurdán,S., Medgyes,B., Mende, T., Berényi, R., and Gál, L., Harsányi, G.(2019) Reliability Tests on SAC-xMn Solder Alloys. *IEEE 25th International Symposium for Design and Technology in Electronic Packaging*.
- Tay, S., Haseeb, A. S. M. A., Johan, M., Munroe, P., and Quadir, Md. (2013). Influence of Ni nanoparticle on the morphology and growth of interfacial intermetallic compounds between Sn-3.8Ag-0.7Cu lead-free solder and copper substrate.
- Tsukamoto. H, D. Z., Dong, Z., Huang, H., Nishimura, T., and Nogita, K. (2009). Nanoindentation characterizaition of intermetallic compounds formed between Sn-Cu-Ni ball grid arrays and Cu substrates. *Materials Science and Engineering B*, 164, 44-50.
- Tsukamoto. H., Dong, Z., Huang, H., Nishimura, T., and Nogita, K. 2010). Nanoindentation characterization of intermetallics formed at the lead-free solder/Cu substrate interface. *Material Sciences Forum*, 2446-2449.
- Tu, K. (1973). Interdiffusion and reaction in bimetallic Cu-Sn thin films. *Acta Metallurgica*, 21(4), 347–354. doi:10.1016/0001-6160(73)90190-9.
- Tu, K.N. & Thompson, R. (1982). Kinetics of interfacial reaction in bimetallic CuSn thin films. *Acta Metallurgica*. 30(5), 947-952.
- Qin, H., Zhang, X.P., Zhou, M.B., & Li, X.P., Mai, Y.-W. (2015). Geometry effect on mechanical performance and fracture behavior of micro-scale ball grid array

structure Cu/Sn–3.0Ag–0.5Cu/Cu solder joints. *Microelectronics Reliability*, 55(8) :1214-1225.

- Xia, Y. J., Jee, Y. K., Yu, J., and Lee, T. Y. (2008). , Effect of aluminum concentration on the interfacial reactions of sn-3.0ag-xal solders with copper and ENIG metallizations. *Journal of Electronic Materials*, 1858-1862.
- Yu, C.Y & Duh, J.G. (2011). Stabilization of hexagonal  $\text{Cu}_6(\text{Sn,Zn})_5$  by minor Zn doping of Sn-based solder joints. *Scripta Materialia* , 65. 783-786.
- H. Yu and J. K. Kivilahti. (2006). Nucleation Kinetics and Solidification Temperatures of SnAgCu Interconnections During Reflow Process, in IEEE Transactions on Components and Packaging Technologies, 29(4) ,778-786.
- Zeng, G., McDonald, S. D., Mu, D., Terada, Y., Yasuda, H., Gu, Q., & Nogita, K. (2014). Ni segregation in the interfacial  $(\text{Cu,Ni})_6\text{Sn}_5$  intermetallic layer of Sn-0.7Cu-0.05Ni/Cu ball grid array (BGA) joints. *Intermetallics*, 54, 20-27.
- Zeng, K. & Tu, K.N. (2002) Six cases of reliability study of Pb-free solder joints in electronic packaging technology. *Mater Sci Eng R Rep*. 38(2):55–105.
- Zhao,X.Y., Zhao,M.Q., Cui,X.Q., Tong,M.X. (2007) Effect of cerium on microstructure and mechanical properties of Sn-Ag-Cu system lead-free solder alloys. *Transactions of Nonferrous Metals Society of China*. 17(4), 805–810.
- Zhang, Q.K., Long, W.M., Yu, X.Q., Pei, Y.Y., and Qiao, P.X.. (2015). Effects of Ga addition on microstructure and properties of Sn–Ag–Cu/Cu solder joints. *Journal of Alloys and Compounds*. 622. 973-978.
- Zhang, L., Xue, S., Gao, L. (2009). Effects of trace amount addition of rare earth on properties and microstructure of Sn–Ag–Cu alloys. *J Mater Sci: Mater Electron*, 20, 1193.
- Zhang, P., Xue, S., Wang, J., Xue, P., Zhong, S., Long, W. (2019). Effect of Nanoparticles Addition on the Microstructure and Properties of Lead-Free Solders: A Review. *Applied Sciences*. 9. 2044.
- Zhou, S., Mokhtari, O., Rafique, M. G., Shunmugasamy, V. C., Mansoor, B., & Nishikawa, H. (2018). Improvement in the mechanical properties of eutectic Sn58Bi alloy by 0.5 and 1 wt% Zn addition before and after thermal aging. *Journal of Alloys and Compounds*, 765, 1243-1252.
- Zobac, O., Kroupa, A., Zemanova, A., Richter, K. (2019). Experimental Description of the Al-Cu Binary Phase Diagram. *Metallurgical and Materials Transactions* ,50, 3805–3815.

## LIST OF PUBLICATIONS AND PAPERS PRESENTED

### Publications

- Haseeb, A. S. M. A., Leong, Y.M. and M., Arafat. (2014). In-situ alloying of Sn–3.5Ag solder during reflow through Zn nanoparticle addition and its effects on interfacial intermetallic layers. *Intermetallics*. 54. 86–94.
- Leong, Y.M. & Haseeb, A. S. M. A. (2016). Soldering Characteristics and Mechanical Properties of Sn-1.0Ag-0.5Cu Solder with Minor Aluminum Addition. *Materials*. 9(7):522.
- Haseeb, A. S. M. A., M., Arafat, Tay, S., and Leong, Y.M. (2017). Effects of Metallic Nanoparticles on Interfacial Intermetallic Compounds in Tin-Based Solders for Microelectronic Packaging. *Journal of Electronic Materials*, 46, 5503–5518.
- Leong, Y. & Haseeb, A. S. M. A & Nishikawa, Hiroshi & Mokhtari, Omid. (2019). Microstructure and mechanical properties of Sn–1.0Ag–0.5Cu solder with minor Zn additions. *Journal of Materials Science: Materials in Electronics*. 30, 11914–11922.

### Conference Proceedings

- Leong, Y.M., Haseeb, A. S. M. A. and Arafat. M.M. (2012). Soldering And Interfacial Characteristics of Sn-3.5Ag Solder Containing Zinc Nanoparticles. *35th IEEE/CPMT International Electronics Manufacturing Technology Conference (IEMT)*, 1-6. DOI:10.1109/IEMT.2012.6521748
- Leong, Y.M. & Haseeb, A. S. M. A. (2014). Soldering and interfacial Characteristics of Sn-1.0Ag-0.5Cu solder with minor Aluminium addition. Paper presented at the *The International Symposium on Visualization in Joining & Welding Science*
- Leong, Y.M. & Haseeb, A. S. M. A. (2014). Soldering characteristics and mechanical properties of Sn-1.0Ag-0.5Cu solder with minor Aluminium addition. Paper presented at the *International Union of Materials Research Societies – International Conference on Electronic Materials, Taipei, Taiwan*.